Regulation of adipogenesis and fat storage by IRX3 and IRX5

Jan-Inge Bjune

Thesis for the degree of Philosophiae Doctor (PhD)
University of Bergen, Norway
2020

UNIVERSITY OF BERGEN

Regulation of adipogenesis and fat storage by IRX3 and IRX5

Jan-Inge Bjune

Thesis for the degree of Philosophiae Doctor (PhD)
at the University of Bergen

Date of defense: 24.04.2020

Year: 2020

Title: Regulation of adipogenesis and fat storage by IRX3 and IRX5

Name: Jan-Inge Bjune

Print: Skipnes Kommunikasjon / University of Bergen

Scientific environment

This study was conducted from October 2015 to December 2019 at the Hormone Laboratory Research Group, Department of Medical Biochemistry and Pharmacology, Haukeland University Hospital and Department of Clinical Science, University of Bergen, Bergen, Norway. Parts of the study was conducted in collaboration with the MRC Harwell Institute, Oxfordshire, UK.

During this period, the Hormone Laboratory Research Group has been part of the KG Jebsen Center for Diabetes Research and the Mohn Nutrition Research Laboratory, which both have contributed to funding of this study. Additional financial support was provided by Personalized Medicine for Children and Adults with Diabetes Mellitus (PERSON-MED-DIA), the Western Norway Regional Health Authority, the Novo Nordisk Foundation Award, the Research Council of Norway, and travel grants from the Meltzer Research Fund, the Research School of Clinical Medical Research, the KG Jebsen Center for Diabetes Research, the Norwegian Association for the Study of Obesity (NFFF) and the European Association for the Study of Obesity (EASO) Research School for New Investigators.

Acknowledgements

I would like to express my sincere gratitude to my main supervisor and head of the research group, Gunnar Mellgren, for believing in me, providing me with the opportunity to work in the Hormone Laboratory Research Group and for guiding me safely through the joys and perils of the PhD journey. I truly appreciate your calm and friendly nature and approach to any challenge that may arise. Your office has always been hospitable and open to me. I would also like to thank the Faculty of Medicine and the Department of Clinical Science (K2) at the University of Bergen for accepting me to the PhD program and allowing me to be your proud representative.

I would like to direct a special thanks to my co-supervisor Simon Dankel for your profound commitment to this project way beyond what could be expected from a co-supervisor. You have been instrumental in the planning and execution of many experiments, not to mention the invaluable help in interpreting data and writing manuscripts. I have learned a lot from you!

I'm also deeply grateful for my co-supervisor and co-head of the research group Jørn Sagen, the fatherly figure who wanders the corridors late at night with a friendly word of encouragement. You were my PI even before I started this project and invested a lot of time and effort in training me to be an independent researcher whilst I was still working as a technician. I would also in this regard thank André Madsen for patiently training me in the lab in this period.

I would also like to express my deep gratitude to my co-supervisor Pål Rasmus Njølstad for all your expert advice, help with scientific writing, and for introducing me to your friends at the Joslin Diabetes Center, Harvard Medical School, Boston, MA, USA. You inspire me to always push on further.

I wish to thank all my wonderful colleagues, including fellow PhD candidates, technicians, master students, exchange students and other members of the research group and the routine lab for making the Hormone Laboratory a fantastic and fun place to be.

There are many people involved in making a lab run smoothly, many who have spent countless hours autoclaving, cleaning, organizing, ordering, purifying plasmids, seeding cells or baby-sitting carry-ons, the list goes on indefinitely… Thank you very much Carol Cook, Margit Solsvik, Linn Skartveit, Olivera Bozickovic, Alba Kaci, Divya Sri Priyanka Tallapragada, Maren Hoff Austgulen, André Madsen, Regine Åsen Jersin, Mona Nilsen, Thomas Helland, Elise Grytten, Kristina Strand, Martha Haugstøyl, Linn-Jeanette Waagbø and Karen Toska.

I also want to thank my co-authors, especially Christine Haugen and Oddrun Gudbrandsen for doing all the mouse work, Laurence Dyer for pioneering the bioinformatics, Hans Jørgen Nielsen and Villy Våge for surgical procedures and collection of biopsies, Gro Vatne Røsland and Karl Johan Tronstad for work on Seahorse and ICC, Ole Petter Nordbø, whom I had the pleasure of co-supervising, for all the hard work on generating the CRISPR-Cas9 cell lines, and our collaborators Samantha Laber, Roger Cox and Melina Claussnitzer for sharing their data and expertise.

I would like to thank other current and former colleagues, including Johan Fernø, Kristin Amundsen, Marianne Flågeng, Jessica Svärd, Therese Halvorsen Røst, Lise Bjørkhaug Gundersen, Ingvild Fenne, Anita Ivarsflaten, Anne Sellevold, Hege Skavøy, Tone Myhra, Øyvind Eng, Iren Hjellestad, Eirik Søfteland, Camilla Tunes, Kristin Aakre and Kristin Visste. Many thanks as well to master and medical students Ida Martinsen, Kaya Cetin, Lorentze Hornnes, Victoria Langhelle, Elise Moltzau Wanderås, Magdalena Keindl, Aaron Willems and Camilla Nergård for keeping the morale more up during long evenings in the lab.

Many thanks to Rita Holdhus and Tomasz Stokowy at the Genomics Core Facility and Brith Bergum at the Flow Cytometry Core Facility, University of Bergen.

I also wish to thank Johan Fernø for valuable feedback to my oral presentations, and also for pushing it down the ski slopes. It's always fun travelling with you and Gunnar.

Thanks to members of the legendary Jern & Betong weight lifting community; Thomas “Posøren” Helland, Alexander “Sir Alex" Hellesen, Lars “Baronen” Breivik and Tore “the Russian” Lillebø. Legend has it that a championship once was held, although no one really knows who participated, and each member claims to have won the championship at least once…

Finally, I want to express my deepest gratitude to my family; my parents, Janne & Knut and my siblings, Per-Anders & Katrine. You have always supported me in every way and are the foundation in my life. Last, but not least, I want to thank my beautiful girlfriend Mona for being so patient and understanding when I needed to work long hours in the lab (which I always needed).

“Alt makter jeg i ham som gjør meg sterk.” Fil 4:13

Bergen, December 2019

Jan-Inge Bjune

Abbreviations

Aβ	Amyloid beta
AGE	Advanced glycation end products
APP	Amyloid beta precursor protein
ATAC-seq	Assay for transposase-accessible chromatin using sequencing
ATP	Adenosine triphosphate
BAT	Brown adipose tissue
BBS	Bardet-Biedl Syndrome
BLAST	Basic local alignment search tool
BMI	Body mass index
CaSR	Calcium-sensing receptor
ChIP	Chromatin immunoprecipitation
CRM	*Cis*-regulatory module
CVD	Cardiovascular disease
DAG	diacyl glyceride
DEG	Differentially expressed gene
DN	dominant negative
DNA	Deoxyribonucleic acid
ECM	Extracellular matrix
eQTL	Expression quantitative trait loci
ES	Embryonic stem
eWAT	Epididymal white adipose tissue
FABP4	Fatty acid-binding protein 4
FACS	Fluorescence-activated cell sorting
FFA	Free fatty acid
FPG	Fasting plasma glucose
FTO	Fat mass and obesity-associated protein or gene
GWAS	genome-wide association study
gWAT	Gonadal white adipose tissue
HD	Homeodomain
HDL	High-density lipoprotein
HDR	homology directed repair
HOX	Homeobox
HUNT4	Helseundersøkelsen i Nord-Trøndelag 4
IR	Insulin receptor
IRO	Iroquois homeobox factor domain
IRX	Iroquois homeobox factor
IRX3	Iroquois homeobox factor 3
IRX5	Iroquois homeobox factor 5
ISO	Isoproterenol
iWAT	Inguinal white adipose tissue

KD	Knock down
KDM3A	Lysine demethylase 3a
KO	Knock out
LEP	Leptin
LEPR	Leptin receptor
MC4R	Melanocortin-4 receptor
MCE	Mitotic clonal expansion
ME3	Mouse embryonic fibroblast with RB-KO cell line 3
MR	Magnetic resonance
MRI	Magnetic resonance imaging
mRNA	Messenger RNA
NAFLD	Non-alcoholic fatty liver disease
NASH	Non-alcoholic steatohepatitis
NHEJ	nonhomologous end joining
OGTT	Oral glucose tolerance test
PAM	Protospacer adjacent Motif
PG	Plasma glucose
PGC-1A	Peroxisome proliferator-activated receptor gamma coactivator 1-alpha
PHB2	Prohibitin 2
PMCA	Phylogenetic module complexity analysis
PPARG	Peroxisome proliferator-activated receptor gamma
PPARGC1A	See "PGC-1A"
PPARγ	See "PPARG"
pRB1	Retinoblastoma protein 1
qPCR	Quantitative polymerase chain reaction
REK	Regional committee for Medical Research Ethics
RNA	Ribonucleic acid
ROS	Reactive oxygen species
rWAT	Renal white adipose tissue
SNP	Single nucleotide polymorphism
SVF	Stromovascular fraction
T2D	Type 2 diabetes
TAG	Triacyl glycerides
TALE	Three amino acid loop extension
TF	Transcription factor
TSS	Transcription start site
UCP1	Uncoupling protein 1
WC	Waist circumference
WHO	World Health Organization
WHR	Waist-hip ratio
WT	Wild type

Abstract

Obesity is a highly prevalent disease underlying several chronic diseases including Type 2 diabetes (T2D) and cardiovascular diseases (CVDs). Thus, increasing levels of obesity is associated with a series of co-morbidities and elevated risk of premature death. Obesity results from a chronic positive energy balance, causing white adipose tissue dysfunction, which in turn promotes dyslipidemia, systemic lipotoxicity and insulin resistance, eventually leading to ectopic fat accumulation and chronic diseases in multiple organs, including the heart, liver, arteries and kidneys.

Unlike white adipocytes, beige fat cells are capable of disposing of excess energy by heat dissipation, thus protecting against obesity-related disease. Recently, two developmental transcription factors, IRX3 and IRX5, were shown to inhibit beige adipogenesis via an obesity associated risk genotype-dependent activation in preadipocytes. The aim of this study was therefore to investigate whether reducing *IRX3* or *IRX5* expression in adipose tissue offers protection from obesity, and if so, by which mechanisms.

In paper I, we randomized wild type (WT) and *Irx5* knock-out (KO) mice to a control or high-fat diet, and measured body weight, fat mass and global gene expression in adipose tissue. We found *Irx5*-KO mice to be lean and completely protected from diet-induced obesity. This was found to be partially attributable to increased mitochondrial respiration and thermogenesis due to reduction of Irx5 and App specifically in adipocytes.

In papers II and III, we investigated the role of Irx3 in transcriptional regulation of adipogenesis, using WT and CRISPR-Cas9 mediated KO of *Irx3* in preadipocytes, followed by RNA-, ATAC- and ChIP-sequencing. We found Irx3 to be critical for adipogenic identity and the ability of precursor cells to differentiate into mature adipocytes. Moreover, this lineage control was found to be mediated by direct transcriptional regulation of chromatin remodeling factors by Irx3.

In conclusion, genetic repression of *Irx3* or *Irx5* offers strong protection against obesity, and reduces adipose tissue mass partially by increasing thermogenesis and improving mitochondrial respiration in existing adipocytes, and partially by preventing the formation of new adipocytes.

This work has implications for identifying patients with genetic predisposition to obesity, who could benefit from potential therapeutic intervention targeting IRX3 or IRX5.

List of publications

Bjune JI*, Haugen C*, Gudbrandsen O, Nordbø OP, Nielsen HJ, Våge V, Njølstad PR, Sagen JV, Dankel SN and Mellgren G. *IRX5 regulates adipocyte amyloid precursor protein and mitochondrial respiration in obesity*. **Int J Obes 2019;43: 2151-62.**

Bjune JI, Dyer L, Røsland GV, Tronstad KJ, Njølstad PR, Sagen JV, Dankel SN and Mellgren G. *The homeobox factor Irx3 maintains adipogenic identity*. **Metabolism 2020;103: In press. Available online November 2019.**

Bjune JI*, Laber S*, Dyer L, Njølstad PR, Sagen JV, Claussnitzer M, Mellgren G, Cox R and Dankel SN. *Epigenetic control of adipogenesis by Irx3*. **To be submitted.**

* contributed equally

Related papers not included in the thesis

Visscher TL, Lakerveld J, Olsen N, Küpers L, Ramalho S, Keaver L, Brei C, **Bjune JI**, Ezquerro S, Yumuk V. *Perceived Health Status: Is Obesity Perceived as a Risk Factor and Disease?* **Obes Facts. 2017;10(1):52-60**

Madsen A*, **Bjune JI***, Bjørkhaug L, Mellgren G, Sagen JV. *The cAMP-dependent protein kinase downregulates glucose-6-phosphatase expression through RORα and SRC-2 coactivator transcriptional activity.* **Mol Cell Endocrinol. 2016 Jan 5;419:92-101**

Madsen A, Bozickovic O, **Bjune JI,** Mellgren G, Sagen JV. *Metformin inhibits hepatocellular glucose, lipid and cholesterol biosynthetic pathways by transcriptionally suppressing steroid receptor coactivator 2 (SRC-2).* **Sci Rep. 2015 Nov 9;5:16430**

* contributed equally

Table of contents

1. Introduction

1.1 Obesity

1.1.1 Body composition and fat storage

Overweight and obesity are defined by the World Health Organization (WHO) as excessive fat accumulation that increases health risk [1]. The most widely used population-level measure of body composition is the body mass index (BMI), defined as a person's weight in kg divided by the square of the height in meters (kg/m^2). WHO defines the following BMI categories of body composition (Table 1):

Table 1: Definitions of BMI categories[a]

Category	BMI (kg/m^2)
Underweight	< 18.5
Normal weight	18.5-24.9
Overweight	≥ 25
Obesity	≥ 30
Obesity class I	30-34.9
Obesity class II	35-39.9
Obesity class III	≥ 40

[a] According to WHO guidelines [2].

Although useful to estimate body composition on the population level, BMI does not take into account lean mass, making it less accurate on the individual level. Moreover, BMI does not consider the distribution of body fat, which has a profound impact on health risk and can broadly be divided into two main depots (Figure 1); fat stored in the trunk (visceral intraabdominal, or omental adipose tissue), which is associated with increased mortality and elevated risk of a range of metabolic diseases including T2D, hypertension and heart disease, and fat stored under the skin (subcutaneous adipose tissue), which is considered less harmful [3–10]. Disease-associated visceral adipose tissue normally constitutes only about 10-20% of total body fat in men and 5-10% in women [11], but this ratio may vary greatly in different individuals. Thus, subjects with

matched BMI and total fat mass may have large variations in visceral adiposity, and thereby also in disease risk [5,12].

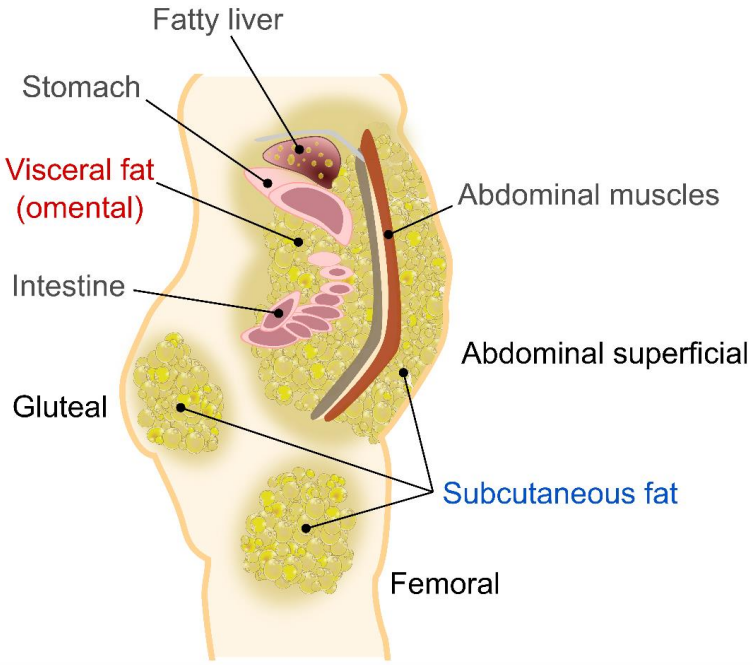

Figure 1: Main human adipose tissue depots

Human adipose tissue is distributed into different depots with distinct properties and associations with disease risk. Subcutaneous depots include gluteal, femoral and abdominal subcutaneous adipose tissues located just below the skin. Visceral depots, also known as omental fat, surrounds the intestines and other inner organs deep within the abdomen. Figure adapted with permission from [11]. Copyright Elsevier.

To better evaluate visceral adiposity and predict disease risk, measuring waist-hip-ratio (WHR) or waist circumference (WC) alone is more accurate than BMI and far more feasible than imaging modalities like computed tomography (CT) and magnetic resonance (MR) [5–7,13–16]. Sex-specific WC and metabolic risk categories are shown in Table 2, although these thresholds are debated [15] and do not take into account, i.e., Asian populations that tend to have increased visceral adiposity at lower BMI [2,8]. Moreover, WHR and WC fail to distinguish subcutaneous fat in the abdominal region from visceral fat [5,8]. Despite these arguable shortcomings, WC is

widely used as one of five parameters used to define “metabolic syndrome”, together with levels of circulating triglycerides, high-density lipoprotein (HDL)-cholesterol, fasting glycaemia and blood pressure [8].

Table 2: Waist circumference and metabolic risk[a,b,c]

Metabolic risk	Waist circumference (cm)	
	Men	**Women**
Increased	≥ 94	≥ 80
Substantially increased	≥ 102	≥ 88

[a] Categories suggested by Lean et al. [13].
[b] Risk assessment by Han et al. [17].
[c] Adapted from [2].

1.1.2 Prevalence and impact of obesity

Global prevalence of overweight and obesity has increased with near pandemic proportions during the past four decades. Since 1974, the global prevalence of overweight in adults has almost doubled from 22% to 39%, and the prevalence of obesity nearly tripled from 4.7% to 13% [18,19]. Thus in the world today, more than 2.1 billion adult individuals are in the overweight BMI range and 650 million have obesity [1]. In the USA, 35% of men and 40% of women were classified as obese in 2014 [20]. In comparison, preliminary data from the most recent Norwegian epidemiological study, The Nord-Trøndelag Health Study (HUNT4), suggest that 23.5% of men and 22.5% of women in Norway were obese in 2018 [21]. These figures are supported by WHO estimates for 2016 [22].

Given the high prevalence of overweight and obesity, what is the impact on affected individuals and on the society? Elevated BMI is a well-known risk factor for several noncommunicable and chronic diseases, including T2D, osteoarthritis, cancer, microvascular diseases (retinopathy, nephropathy, neuropathy) and macrovascular diseases like heart disease and stroke, which were the leading cause of death in 2012 [1].

Large epidemiological studies have clearly shown that increases in BMI above 30 is, on the population level, associated with an exponential increase in mortality risk [23–25]. Although the association is indisputable for obesity, it has been debated whether the same association also holds for overweight (BMI 25-29.9) as, for instance, a large meta study found little evidence for increased mortality risk in this category [26]. Clarifying this issue was important owing to the large number of overweight individuals that would potentially be at risk. Adams et al. [23] initially made the same observations, but when limiting the analysis to non-smokers, the increased mortality rate was apparent already in overweight subjects, and this finding was even stronger in people 50 years of age (Figure 2). In this subgroup, the risk of death increased by 20-40% with overweight and 200-300% with obesity [23]. These findings were supported by more recent meta-analyses, including 1.5 million people of European ancestry [27] and 239 prospective studies from four continents, which both found similar hazard ratios [25].

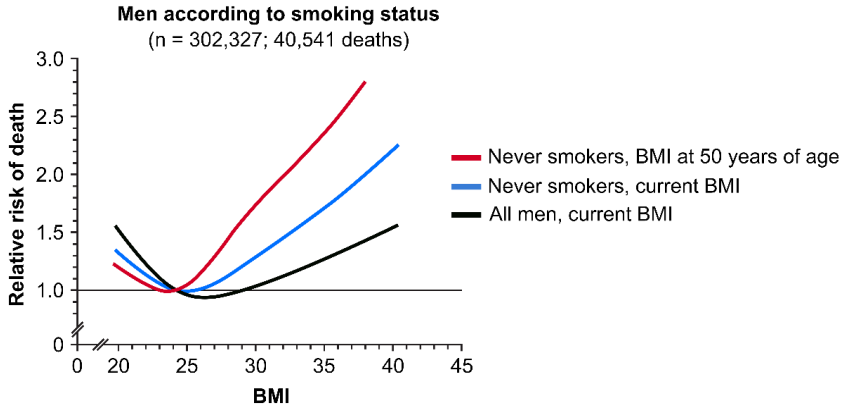

Figure 2: Relative risk of death according to BMI

Dose-response curve for mortality according to BMI in men, adjusted for age, ethnicity, education, alcohol consumption and physical activity. The "All men" category includes smokers and is adjusted for number of smoked cigarettes per day. The reference point (relative risk of 1.0) is the midpoint of a reference group with BMI between 23.5-24.9. Similar results were obtained for women. The figure is adapted with permission from [23], Copyright Massachusetts Medical Society.

Apart from increasing the risk of premature death, the abovementioned chronic diseases associated with obesity, like CVD, cancer and T2D, are also major causes of disabilities and economic burden on health care systems [15]. In European countries, overweight and obesity was found to be responsible for 80% of cases of T2D, 35% of ischemic heart disease and 55% of hypertensive disease among adults [28,29]. The cost for heart disease survivors is large, both in terms of disabilities and requirement for costly drugs [15]. However, the far most expensive public health consequence of obesity is diabetes, which in the USA alone has tripled, from a yearly cost of 99 to 327 billion dollars between 1995 and 2017 [30,31]. Patients with diabetes now accounts for 25% of the entire US health care budget [31]. In Norway, the prevalence of T2D increased from 4.9% to 6.1% between 2009 and 2014, but the incidence was reduced by about 30% [32], indicating that the disease prevalence is now starting to level out. Overall, however, obesity poses a great personal health- and societal economic burden [15,33].

1.1.3 Mechanisms underlying co-morbidities of obesity

Adipose tissue dysfunction

The mechanisms underlying the co-morbidities of obesity are complex, involving a range of metabolic, cellular and physiological pathways that converge on cardiovascular diseases, as shown in Figure 3. Chronic excess energy is converted into triacyl glycerides (TAG) and stored as lipid droplets in adipocytes, providing a reservoir to buffer day-to-day variations in energy balance [34]. However, with a constant energy surplus, the demand for lipid-storing capacity increases, promoting an increase in both adipocyte size and numbers, resulting in enlargement of adipose tissue depots [35]. The ability of such adipocyte expansion depends on the plasticity of the extracellular matrix (ECM), a mesh of proteins that maintains the structure of the adipose depot. At some point, however, the enlarged adipocytes have no more room to expand, leading to a series of pathological effects, including ECM fibrosis, adipocyte lipid leakage, hypoxia, inflammation, cell death and changes in secreted adipokines,

all promoting local and systemic insulin resistance [35,36]. Recruitment and polarization of immune cells to pro-inflammatory M1 macrophages further exacerbates the insulin resistance in adipocytes [35,36].

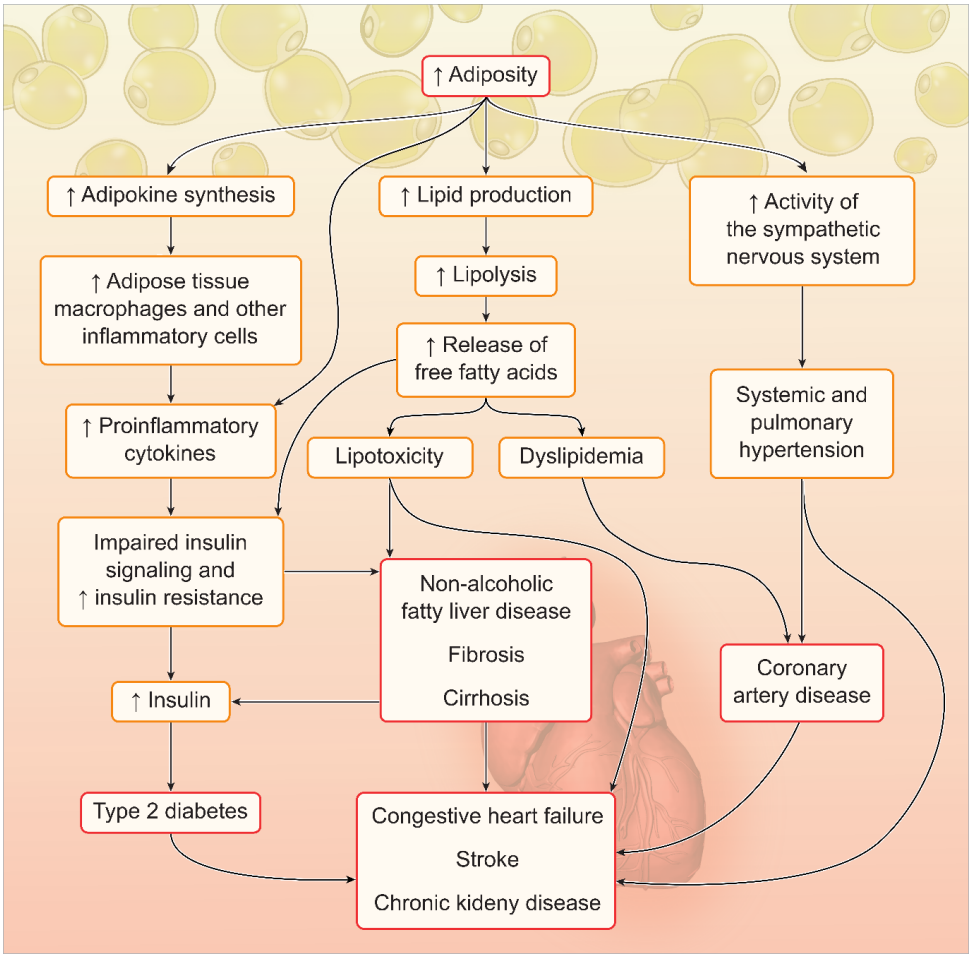

Figure 3: Pathways mediating the effect of adiposity on disease and mortality risk

Chronic energy surplus and adipose expansion leads to adipose tissue dysfunction, which increases the risk of chronic diseases (red boxes) and premature death via multiple pathways, including insulin resistance, lipotoxicity and dyslipidemia. Adapted with permission from [36], Copyright Massachusetts Medical Society.

Insulin resistance and ectopic fat accumulation

Insulin is a strong suppressor of lipolysis [35,37], thus insulin resistance in adipocytes results in increased lipolysis, involving hydrolysis of TAG to free fatty acids (FFAs) and glycerol, which are released into the bloodstream [36,37]. Subsequent elevation of circulating FFAs is a major contributor to the systemic insulin resistance observed in people with obesity [36] (Figure 3). One mechanism mediating this effect is hepatic lipotoxicity [37]. Adipocyte-derived FFAs and glycerol are taken up by the liver, promoting β-oxidation and increased gluconeogenesis, as well as hepatic insulin resistance and insulin-independent hepatic TAG accumulation [37]. This mechanism serves a protective role in glucose homeostasis during starvation, where its temporary activation in response to depleted glycogen stores helps maintain normoglycemia [37]. However, with chronic overnutrition, this process turns pathogenic when locked in a positive feedback loop with chronic insulin resistance in adipose tissue and in the liver, leading to lasting elevated glucose output from the liver.

In addition to promoting glucose production via β-oxidation, excess FFAs and glycerol taken up by the liver can be esterified to TAG, resulting in ectopic lipid accumulation in the liver (Figure 3). This process, also known as steatosis, results in non-alcoholic fatty liver disease (NAFLD). Prolonged steatosis can lead to immune cell infiltration and inflammation, a condition characterized as non-alcoholic steatohepatitis (NASH), which in turn can progress into fibrosis and cirrhosis, characterized by impaired liver function due to cell death and excessive scarring of the hepatic tissue [38].

A second detrimental effect of chronic elevation of circulating FFAs is insulin resistance in skeletal muscles, the major site of glucose disposal. Here, increased uptake of FFAs promotes esterification to diacyl- and triacyl glycerides (DAG and TAG, respectively). DAG has been shown to translocate to the plasma membrane and inhibit the phosphorylation cascade of the insulin receptor (IR) signaling pathway. Additionally, other FA intermediates, including ceramides, serve similar inhibitory roles on the IR. The resulting impaired insulin sensitivity leads to reduced glucose

uptake and glycogen storage in the skeletal muscles, thus further elevating blood glucose [37].

Type 2 diabetes

Taken together, chronic overnutrition leads to adipose dysfunction, systemic insulin resistance, elevated hepatic glucose secretion and reduced glucose uptake in skeletal muscles, which together promotes hyperglycemia [37] (Figure 3). In response, pancreatic β-cells secrete more insulin to achieve normoglycemia, until eventually β-cells exhaustion occurs, leading to impaired insulin output and manifested hyperglycemia, a condition referred to as glucose intolerance or prediabetes. With progressively deteriorating β-cell function, T2D will eventually develop [39–42]. Table 3 summarizes the clinical thresholds for prediabetes and T2D by the oral glucose tolerance test (OGTT) or the HbA1c test. In the OGTT test, the fasting plasma glucose (FPG) of the patient is measured, followed by oral administration of 75 gram glucose and measurement of the plasma glucose after 2 hours [43]. Although commonly used, this test only reflects the blood glucose levels at the time of testing, and is therefore susceptible to day-to-day variations. Therefore, glycated hemoglobin (HbA1c), which reflects the average plasma glucose levels over the past 3 months, is now the recommended mean to diagnose diabetes [44]. For both tests, however, a value above the diagnostic threshold should be confirmed in a second test on a different day before a diagnosis can be made.

Table 3: Diagnostic thresholds for prediabetes and T2D

Category	**OGTT[a,b]**				**HbA1c[e]**	
	Baseline (FPG[c])		2h (PG[d])		Average past 3 months	
	mM	mg/dL	mM	mg/dL	mmol/mol	%
Normal	< 5.6	< 100	< 7.8	< 140	< 39	< 5.7
Prediabetes	5.6 – 6.9	100 – 125	7.8 – 10.9	140 – 199	39 – 47	5.7 – 6.4
T2D	≥ 7.0	≥ 126	≥ 11.0	≥ 200	≥ 48	≥ 6.5

[a] Oral glucose tolerance test.

[b] Defined by the Expert Committee on the Diagnosis and Classification of Diabetes Mellitus [43].

[c] Fasting plasma glucose.

[d] Plasma glucose.

[e] According to WHO guidelines [44].

Vascular complications of obesity and T2D

Chronic hyperglycaemia, particularly in conjunction with insulin resistance, dyslipidaemia, hypertension and obesity, promotes both microvascular as well as macrovascular diseases with detrimental effects on multiple organs, including the heart, brain, kidneys, skin and eyes, as reviewed in [45].

Diabetic microvascular complications, involving small blood vessels (capillaries), include retinopathy, neuropathy and nephropathy. Retinopathy is characterized by visual disabilities and blindness, mediated by loss of the protective pericytes that surround endothelial cells of the capillaries, leading to abnormal capillary constriction, proliferation and weakening of vessel walls [45]. In the advanced stage of the disease, excessive compensatory proliferation of new abnormal blood vessels may lead to detachment of the retina, resulting in blindness [45]. Neuropathy affects about 50% of diabetic patients [46] and includes peripheral neuropathy, which often manifests as lower-limb pain, loss of sensation and foot ulcers, as well as autonomic neuropathy, leading to abnormal heart rate [45]. Finally, about 25% of diabetic patients have some

degree of elevated albumin levels in the urine, indicating renal dysfunction, or nephropathy, which can eventually progress to renal failure [45,47].

CVDs include macrovascular complications of the large blood vessels (arteries and veins), leading to coronary and peripheral arterial diseases and cerebrovascular disease, and is the major cause of death, both in the general population, and particularly in people with T2D [1,45,48]. A common etiology for these diseases is atherosclerosis, the narrowing of arteries due to plaque formation, mainly consisting of accumulated cholesterol, calcium and immune cells within the arterial walls [49]. Over time, these plaques may obstruct blood flow, causing local heart attack or peripheral arterial disease, depending on the affected artery. Moreover, plaques may burst and release blood clots, which in turn can block the blood flow elsewhere, including the brain and heart, causing stroke and heart attack, respectively [45,49].

The risk of vascular diseases is exacerbated with increased severity and duration of diabetes, through multiple mechanisms (reviewed in [45]). Common for both micro- and macrovascular diseases is the accumulation of advanced glycation end products (AGE), which have a wide range of adverse effects, including overproduction of endothelial growth factors, induction of apoptosis, changes in extracellular matrix proteins and inhibition of blood vessel relaxation due to blocked nitrous oxide production [45]. Chronic hyperglycaemia also induces abnormal PKC and RAS signalling pathways, smooth muscle cell dysfunction, platelet aggregation and promotes chronic inflammation, which further promotes vascular disease [45].

Ectopic fat deposition in obesity further contributes to CVD. Accumulation in the liver and skeletal muscles contribute to local and systemic insulin resistance and lipid dysregulation, as described above. Ectopic fat surrounding the heart, coronary and peripheral arteries promotes atherosclerosis, and negatively affects cardiac function via paracrine signalling, whereas fat in and around the kidneys contribute to increased blood pressure and albuminuria [50]. Finally, fat deposition in and around the pancreas promotes β-cell dysfunction and impaired insulin secretion [51,52].

1.2 The causes of overweight and obesity

In its simplest terms, obesity is caused by a chronic positive energy balance where the energy intake and/or absorption outweighs the energy expenditure. The aspects influencing this energy balance, however, include a complex interplay between environmental, genetic and epigenetic factors [36].

1.2.1 Environmental and lifestyle factors

During the past 7 decades, the per capita food availability and consumption has increased steadily [53], with a particular rise in energy-dense, processed and palatable foods, including sugar-sweetened beverages [36,54]. These types of food tend to circumvents normal appetite regulation, leading to further elevated energy intake [33,55]. The importance of energy intake is highlighted by clinical trials that clearly demonstrate the benefit of caloric restriction [56,57]. Coincidingly with increased energy intake, the overall energy expenditure has dropped as time spent on physical activities at home, work and during leisure has been replaced with time filled with sedentary activities [33,36,58,59].

There is also a range of other environmental, personal and societal factors that contribute to obesity, including sleep patterns, socioeconomic status, education, city planning/design, gut microbiota and even social networks, as reviewed in [57], as well as more frequent use of medicines that have weight gain as a side effect [36].

1.2.2 Genetic contribution to obesity

Despite exposure to the same environment as obese individuals, many people appear resistant to developing obesity, suggestive of protective genetic factors. The heritability of obesity was reported already in 1894 [60], and genetic factors have since been demonstrated, through family, adoption and twin studies, to explain 70-80% of variation in observed BMI [61–64]. Therefore, genetic factors can be considered powerful modulators of susceptibility to an obesogenic environment. Evidence for this

hypothesis was provided by overfeeding and exercise intervention studies in twins, where weight change, and particularly body fat distribution, was strongly correlated within twin pairs, but not between pairs [65,66]. Therefore, identifying causal obesity genes would be immensely valuable to identify individuals at risk, and ultimately provide therapeutic targets.

Monogenic obesity

Pinpointing the genes that influence obesity has proved challenging, as only eleven rare forms of monogenic obesity have been identified [36]. This form of obesity is typically caused by protein-altering mutations in single genes with high penetrance, meaning that loss-of-function of these genes almost invariably leads to obesity. The most well-studied examples include deficiency in the leptin (*LEP*), leptin receptor (*LEPR*) and melanocortin-4 receptor (*MC4R*) signaling axis, key components in hypothalamic regulation of appetite and energy expenditure [36,67]. Among these, and all the other monogenic obesity genes, heterozygous mutations in *MC4R* are by far the most common, occurring in 2-5% of obese children in Europe [34,67–69]. Collectively, these monogenic obesity disorders are classified as *non*-syndromic. In addition, there exists about a dozen extremely rare *syndromic* forms of monogenic obesity [67]. These are characterized by mental retardation, dysmorphia and various organ abnormalities, with obesity as a secondary feature [67]. Prader-Willi´s syndrome is the most studied obesity syndrome, and is mainly caused by genetic deletions in the paternal allele of *MKRN3*. As the maternal allele is usually epigenetically silenced, only truncated protein from the paternal allele is expressed, leading to disease [67]. Other examples include Bardet-Biedl´s (BBS) and Alström´s syndromes, both caused by mutations leading to dysfunctional cilia [67]. Taken together, monogenic obesity accounts for only about 5% of total obesity, suggesting that more complex genetic interactions explain the majority of genetic contribution to obesity.

1.2.3 GWAS – The hunt for elusive obesity gene variants

Identification of gene variants associated with obesity were long hampered simply because most variants in the human genome were unknown. However, the advent of large biobanks [70], combined with new genome-wide genotyping technologies and the identification of the most prevalent human single-nucleotide polymorphisms (SNPs) through the 2003 HapMap project [71], paved way for genome-wide association studies (GWAS) of a range of diseases and traits [72], including T2D [73–76] and obesity [77]. In GWAS, the SNPs of a large number of individuals with a specific phenotype, i.e. obesity, are compared with a similarly sized control group with a different phenotype, for example normal BMI. If a specific variant is found more frequently in case versus control, it is associated with disease. This method revolutionized the field of medical genetics and enabled the identification of hundreds to thousands of variants associated with obesity and T2D [72,78–81].

The missing heritability

In contrast to the rare, high-impact variants causing monogenic disease, the vast majority of variants detected by early GWAS studies were common variants, with minor allele frequencies of more than 5%, and typically moderate effect sizes, with odds ratios between 1.1 and 1.5 [34]. These early GWAS analyses were often underpowered and were still only able to explain less than 5% of variations in BMI [34,72], which is far from the expected 70-80% that was estimated from the twin studies [82]. It was believed that this "missing heritability" was due to missing high-impact rare variants [83], but with the tremendous increase in GWAS sample sizes in recent years, it became clear that there is a very long tail of genetic variants with moderate to diminishing allele effects that constitute the genetic predisposition to late-onset obesity [72,84,85].

Limitations of GWAS

The main challenge today is to make sense out of this newfound knowledge and link variants to biological mechanisms [86]. There are a number of challenges and limitations with GWAS data, as reviewed in [72,87]. Firstly, 90-95% of the associated SNPs are typically located in noncoding regions [88,89], thus not affecting protein

sequence, but rather gene regulation through promoter and enhancer elements [72,87]. This greatly complicates interpretation of the SNP function, particularly for SNPs in enhancers, because most enhancers as well as their target genes are usually unknown. Therefore, the effect of each SNP on the expression of nearby genes must be computationally predicted and experimentally tested [72]. For variants in promoters and some enhancers, this test is straightforward as the closest gene usually is the target. However, many enhancers have a regulatory range of hundreds of kilobases, some reaching up to 1.5 million, due to chromatin folding [90,91]. In this range, there may be tens to hundreds of candidate target genes. Consequently, each of the thousands of obesity-associated SNPs may in turn regulate up to hundreds of genes, making mechanistic follow-up a daunting task. Chromosome conformation capture techniques may give clues as to what chromosome regions interact, but these methods generally have low resolution and cannot establish causality [72].

Secondly, the reported trait-associated SNP may not be the causal variant, but rather merely a tag marking the genomic area associated with the causal variant [72,87]. This results from humans being a young species, with many genomic regions in high linkage disequilibrium, meaning that despite overall variations in the genome, some stretches of DNA always contain the same set of SNPs, so-called haploblocks [72]. For each trait-associated SNP, there may therefore be one or several nearby causal variants [92,93]. Without knowing the precise genomic location of the associated variant, one cannot predict the affected binding site for DNA-binding proteins, thereby hindering elucidation of the cis-regulatory mechanism.

Finally, because GWAS data only point at the *genomic location* of a trait-associated variant, they reveal little about which cells and tissues that are relevant, or when in a person's embryonal and postnatal life the variant has an effect. Taken together, these challenges have led to a disappointing progression towards the discovery of novel genes and molecular pathways regulating obesity.

1.3 The obesity-associated *FTO* locus

The *FTO* locus provides a prime example of the challenges faced when interpreting GWAS data, but also how these challenges can be overcome. The locus, harboring 89 common variants in intron 1 of the *FTO* gene, shows the strongest GWAS association with obesity across age and ethnicity [77,94–98]. Adults homozygous for this risk variant alone have an 1.7-fold increased odds of obesity and an average additional weight of 3 kg compared to non-risk carriers [77]. Initial analyses focused on regulation of *FTO* itself, which was found to have DNA demethylase activity, be highly expressed in hypothalamic regions and be crucial for control of energy balance [99] through promoting energy intake [100–106]. Overexpression and knockout studies in mice subsequently demonstrated that FTO promoted obesity and glucose intolerance, suggesting that *FTO* itself could be the target gene of the *FTO* intronic obesity-associated SNPs [87,96,107–109]. However, human subjects homozygous for a coding mutation that inactivates the FTO enzymatic activity did not develop obesity [110], suggesting that *FTO* is not the primary target of these obesity-associated variants [96]. Instead, investigators turned to the nearby genes, *FTS*, *RPGRIP1L*, *IRX3*, *IRX5* and *IRX6*.

1.3.1 Target genes of the *FTO* locus

The *RPGRIP1L* gene was comprehensively investigated by the Leibel group who proposed, through a series of publications, that *FTO* and *RPGRIP1L* are co-regulated by binding of the homeobox factor CUX1 (also known as CUTL1) to the *FTO* variant locus, leading to modulations of the leptin receptor in hypothalamic cilia, as reviewed in [96]. Although interesting, as dysfunctional cilia are already implicated in syndromic obesity (refer to section 1.2.2 and [111,112]), conclusive evidence for the causality of common obesity is lacking as *FTO* locus risk alleles have not been correlated with changes in expression of neither *FTO* nor *RPGRIP1L* [96].

In parallel with the Leibel group, Ragvin et al. identified a block of highly conserved, noncoding regulatory elements in the *FTO* locus, and used a zebrafish reporter system

to demonstrate that this noncoding region regulated the expression of the distant neighbor *IRX3* [90]. These findings were confirmed by Smemo et al, who showed, by chromatin conformation capture in mice embryonic and adult brain tissue, that the *FTO* locus physically and strongly interacts with the promoter of *IRX3* [113]. Moreover, a mouse reporter system clearly demonstrated that the *IRX3* expression depends on *FTO* locus variants, and expression quantitative trait loci (eQTL) data from the cerebellum of the human brain revealed that the obesity-linked SNPs correlated (weakly) with *IRX3* expression, but not with expression of *FTO* [113]. Finally, Smemo et al. showed that global *Irx3* knock-out (KO) mice were protected from obesity compared to wild-type (WT) mice, with reduced body weight, adipose tissue, and increased expression of thermogenic markers. Moreover, hypothalamic overexpression of dominant-negative (DN) *Irx3*, resulting in dysfunctional Irx3 specifically in the brain, recapitulated the effect by the global KO [113], indicating that the *FTO* locus exerts its effect on obesity through hypothalamic regulation of *Irx3* [96]. This finding was supported by others studies suggesting that most SNPs associated with BMI are primarily active in the brain, controlling appetite and energy balance [79,95]. On the other hand, SNPs associated with fat distribution were found to be active mainly in peripheral tissues like adipocytes, regulating adipogenesis and insulin signaling [114].

1.3.2 A way of identifying causal SNPs

As mentioned earlier, the usefulness of GWAS data has been severely limited by the inability to pinpoint the causal SNP among several variants in any given locus associated with disease. However, in 2014, the field was pushed forward as Claussnitzer et al. developed a computational model that could significantly narrow down the number of candidate nucleotide variants within a GWAS locus. Coupled with functional analyses, the approach can enable the identification of exact causal SNPs [115]. The model relies on the nature of transcription factor (TF) binding to regulatory motifs of target genes, where, despite extensive evolutionary turnover of TF motifs, functionally important motif combinations, i.e., cis-regulatory modules (CRMs), have been repeatedly preserved across humans and other species. Such complex co-

occurring patterns of TF motifs function as enhancers, allowing for combinatorial TF binding and hence robust and redundant control of gene expression [116]. However, genetic variants can influence the architecture and TF binding affinities in such CRMs and thereby modulate basal expression levels of target genes. The method, termed phylogenetic module complexity analysis (PMCA), uses libraries of TF binding motifs to search for similar modules of TF binding motifs in humans and at least two other species, allowing some variation in the distances between motifs and number of motifs. Such modules cannot readily be detected from the linear sequence of binding motifs in a single species. Based on a scoring algorithm for motif and module similarities across species, PMCA classifies any given genomic region as complex or noncomplex [115]. In other words, if a genomic region is enriched with evolutionary conserved *modules* of TF binding sites, it is classified as a complex region, a region of particular biological significance in terms of gene regulation.

Claussnitzer et al. demonstrated how PMCA could be used to assess the immediate surroundings (120 bp) of each potential causal SNP in linkage disequilibrium with a tag-SNP for biological significance, and thereby strongly reduce the number of candidates [115]. The candidate SNPs found to be in complex regions are ranked by the number of TF binding motifs in the module, thereby further reducing the number of variants for functional analyses. Such functional analyses typically involve highly laborious work, including testing the effect of risk versus non-risk variant of the SNP on binding of each TF predicted to bind the module [115]. Claussnitzer et al. proved the usefulness of this approach by revealing a significant enrichment of homeobox family of transcription factors (refer to section 1.5 for further reading on homeobox factors) at 48 T2D-associated risk loci, including that of *PPARG*. The PMCA scoring together with a positional bias analysis were further utilized to identify a SNP in the *PPARG* locus, hitting a motif for the homeobox repressor protein PRRX1 within a CRM, thus inferred to be a strong causal candidate. The specific causal mechanism could then be tested experimentally, which revealed that the homeobox repressor protein PRRX1 inhibited expression of *PPARγ2* in a risk-allele specific manner [115].

1.3.3 An *FTO* locus variant regulates *IRX3* and *IRX5* in adipocytes

Equipped with the PMCA method, Claussnitzer et al. next turned to the *FTO* locus to delineate the causal SNP. The highest PMCA score was obtained for rs1421085, a SNP in perfect LD with the tag-SNP rs1558902 [117]. In parallel, the investigators sought to identify in what tissues and cells the *FTO* variant locus is active by analyzing publicly available data on epigenetic markers in over hundred cell types. In contrast to previous findings suggesting a regulatory role in the brain, Claussnitzer et al. identified a strikingly long enhancer element specifically in mesenchymal adipocyte progenitor cells [117]. Furthermore, by transfecting respective 10 kb subsets of the 50 kb *FTO* locus in adipocyte cultures and performing luciferase reporter assays in a risk versus non-risk haplotype manner, the locus containing the active variant that affected gene expression was narrowed down to a 10 kb window that harbored the rs1421085 candidate SNP, but not the tag-SNP [117]. Moreover, when repeating the reporter assay using a narrow 1 kb tile centered on the rs1421085, a risk-allele specific activation of the enhancer was again observed, and this effect was only seen in adipocytes and not in other cell types, including neurons [117]. Taken together, these data strongly pointed to rs1421085 as causal and active specifically in adipocyte precursor cells.

Having identified the potential causal variant and the cell type in which it acts, the investigators subsequently investigated which genes might be affected by the risk variant. To this end, chromosome conformation capture analysis was performed, which identified potential interaction with eight neighbors of *FTO*, including the previously suggested target genes *IRX3* and *RPGRIP1L* [117]. However, eQTL analyses of these eight genes revealed that only *IRX3*, in addition to the closely related, but further distantly located gene *IRX5*, displayed risk variant-dependent changes in gene expression during early differentiation of preadipocytes [117]. Thus, *IRX3* was confirmed, and *IRX5* established, as long-range targets of the *FTO* locus, with rs1421085 as a likely causal variant (Figure 4, upper panel).

To pinpoint the mechanism by which the causal SNP affected *IRX3* and *IRX5* expression, the team examined the TF binding sites surrounding the causal SNP in greater detail, and found rs1421085 to be situated directly in the binding motif of the

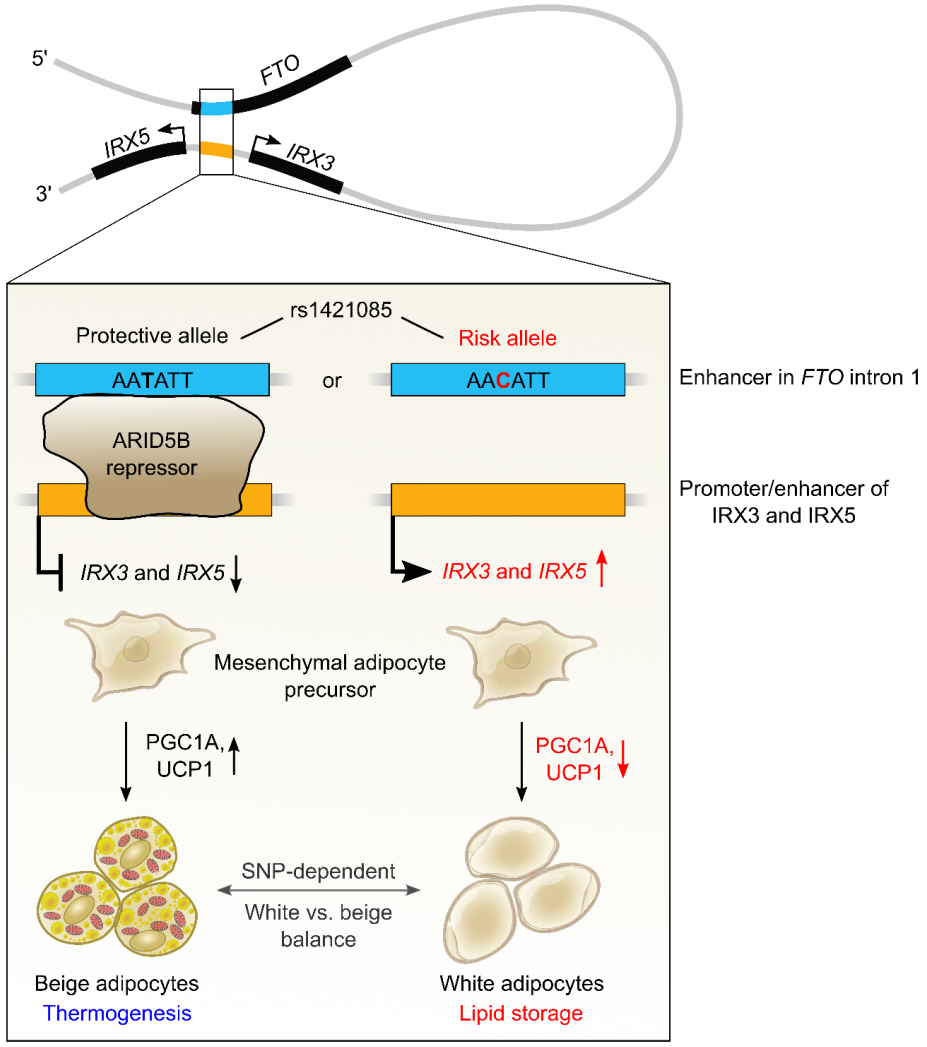

Figure 4: The causal variant in the *FTO* locus regulates *IRX3* and *IRX5*

Top panel, the enhancer in the *FTO* locus forms long-range interactions with local enhancer and promoters of *IRX3* (0,3 MB) and *IRX5* (1.2 MB). Bottom panel, in mesenchymal adipocyte precursor cells, the obesity-associated risk variant (C) at rs1421085 disrupts binding of the ARID5B repressor, leading to increased expression of *IRX3* and *IRX5*, and a resulting repression of thermogenesis and a developmental shift from beige heat-dissipating to white lipid-storing adipocytes. Figure adapted with permission from [117,118], Copyright Cell Press and Massachusetts Medical Society.

TF ARID5B, which showed the highest expression among different members of the ARID family in adipose tissue [117]. EMSA revealed loss of ARID5B binding to this

motif specifically for the risk variant, suggestive of a repressive effect on *IRX3/5* expression. Moreover, knockdown of *ARID5B* in preadipocytes increased *IRX3/5* expression, but only in cells with the protective variant harboring the functional binding site. Importantly, whereas CRISPR-Cas9 editing of the protective allele to the risk variant increased *IRX3/5* expression, a second edit back to protective allele reduced *IRX3/5* levels, but only in the presence of ARID5B, thus establishing causality [117].

Finally, Claussnitzer et al. investigated how increased levels of IRX3 and IRX5 could mediate the effect of the risk variant on obesity risk (Figure 4, lower panel). *IRX3* and *IRX5* mRNA expression was found to correlate positively with mRNA expression of lipid metabolism genes and negatively with mitochondrial function genes like *PGC1A* and *UCP1* in human adipose tissue, and to be more highly expressed in white compared to brown adipocytes [117]. In agreement, primary adipocytes from risk allele carriers (who have higher IRX3/5 levels) had reduced expression of mitochondrial function-related genes, impaired mitochondrial respiration and uncoupling. In contrast, the same cells demonstrated elevated levels of lipid-storing genes and increased adipocyte size, indicating a shift from consuming to storing energy. Importantly, the repressed thermogenic activity could be restored by CRISPR-Cas9 editing of cells with the risk variant back to the protective variant [117].

The anti-thermogenic, pro-lipogenic effect of elevated IRX3 specifically in adipocytes was confirmed on the whole-body level in mice by inactivation of Irx3 solely in the adipose tissue [117]. To this end, overexpression of dominant-negative *Irx3* driven by the adipocyte-specific promoter of *Fabp4* (also known as *Ap2*) was performed. Mice devoid of functional adipose Irx3 weighed less, were resistant to diet-induced weight gain, had reduced adipose tissue and smaller fat cells, and had increased thermogenesis.

In summary, the risk variant in rs1421085 was found to disrupt binding of the ARID5B repressor specifically in adipocyte precursor cells during early adipogenic differentiation, which lead to de-repression of *IRX3* and *IRX5* and subsequent inhibition of thermogenesis and promotion of white adipogenesis at the expense of beige adipocyte formation from mesenchymal precursor cells (Figure 4).

1.4 White, beige and brown adipocytes

Adipose tissue serves as a master regulator of energy balance and maintains homeostasis of key nutrients, including lipids and glucose [35]. There are two main types of adipocytes with opposing functions and different developmental origin that act together to achieve energy homeostasis; white and brown fat cells [35,119]. In addition, there also exists a third, intermediate cell type, termed beige adipocytes, which shares the developmental origin with white adipocytes, but with potential to function like brown adipocytes under certain conditions [35,119], as discussed below.

1.4.1 Opposing metabolic roles of adipocyte types

White and brown adipocytes

White adipocytes constitute most of the total adipocyte mass and specialize in energy storage by taking up glucose and fatty acids from the circulation and converting it to triglycerides which are subsequently stored as large lipid droplets. Conversely, located in small, defined depots, brown adipocytes also take up large amounts of nutrients [120], but rather funnel this energy to heat production (thermogenesis) instead of lipid storage by uncoupling the mitochondrial electron transport chain from ATP production. This process is mainly achieved through the action of uncoupling protein 1 (UCP1), expressed in thermogenic adipocytes and localized to the inner mitochondrial membrane where it short-circuits the membrane potential, leading to free flux of H^+ back into the inner matrix. This process deprives ATP synthase of its driving force, hence preventing production of ATP, while at the same time promoting a compensatory increased substrate demand for the electron transport chain.

Mouse BAT prevents obesity

Brown adipose tissue (BAT) is readily detected in interscapular and perirenal regions in mice, and manipulation of BAT has clearly demonstrated its ability to prevent obesity and metabolic disease [119,121–130]. Consequently, brown adipocytes can be regarded as metabolic sinks capable of disposing of surplus energy. This ability is crucial in preventing white adipocytes from overfilling with lipids, a condition linked

to a series of adverse metabolic events, including adipose tissue inflammation and lipid spillover, both drivers of local and systemic insulin resistance and metabolic syndrome.

Human BAT is associated with improved metabolic health

Human BAT, in contrast, has proved far more elusive. Although well-known to exist in human infants, BAT was thought to disappear with age, and was not unequivocally detected in adults until 2009, when several independent groups demonstrated the presence of functional thermogenic adipocytes in the supraclavicular and spinal region, using [18^{F}]-FDG-PET/CT scans [131–137]. Whether these cells should be considered brown or beige has been debated, and their ability to affect whole-body metabolic homeostasis has been questioned [119]. However, amounting evidence indicates that the activity of thermogenic cells, regardless of their classification, is positively associated with reduced BMI and improved whole-body metabolism and insulin sensitivity in humans [131,133,135,138–146], suggesting an important contribution of these cells also in humans. Thus, understanding and controlling thermogenic cells is therefore of great therapeutic interest [119,147].

Beige adipocytes

Beige adipocytes are capable of thermogenesis despite having a different developmental origin than BAT. While brown fat cells share origin with muscle cells, beige cells are derived from a separate precursor pool shared with white adipocytes residing in WAT [148,149], thus constituting a larger biomass than BAT. However, unlike BAT, which displays high basal expression of *UCP1*, beige adipocytes must be stimulated to express *UCP1*, which is mainly induced by chronic cold-stimulation through adrenalin/β-adrenergic signaling [137]. Once activated, the beige adipocytes possess thermogenic activity comparable to that of BAT [137]. In addition to cold stimulation, a range of other secreted factors, including natriuretic peptides, Vegf, Irisin, and Fgf21, have been found to promote beige and brown adipocyte development and function, as reviewed in [119].

Interestingly, once beige cells have been acquired by cold exposure, they are retained during subsequent warm-exposure, where they temporarily lose *Ucp1* expression until

subsequent cold exposure [150]. This remarkable display of plasticity demonstrates the ability of beige cells to operate as either white or brown-like adipocytes depending on external circumstances and the shifting needs of the affected organism [35,119,137]. However, whether mature beige adipocytes develop by de novo differentiation from precursor cells [137,150–152], or by transdifferentiation from mature white adipocytes [153] is controversial and a subject of ongoing investigation. For instance, as described above and shown in Figure 4, Claussnitzer et al. proposed that the effect of the *FTO* risk allele, and the consequent elevated levels of *IRX3* and *IRX5,* shifts the developmental fate of a common white/beige precursor towards the white lineage by inhibiting *PRDM16* and *PGC-1A*, key transcriptional activators of thermogenic adipocytes. Importantly, this genotype-dependent gene regulatory mechanism appears to exert its effect in a specific window early in adipocyte differentiation. This finding indicates that altered expression of transcriptional regulators in early differentiation can alter epigenetic programs that manifest in persistent metabolic effects in mature adipocytes.

1.4.2 Transcriptional and epigenetic regulation of adipogenesis

Adipogenesis requires two steps, commitment of pluripotent stem cells and precursor cells to preadipocytes, and terminal differentiation to mature adipocytes [35,147]. Both processes involve interactions between lineage-specific TFs and chromatin landscapes. The commitment phase is less studied, but in bone-marrow-derived mesenchymal stem cells, which can develop into either bone, cartilage or adipocytes, the commitment switch is known to involve Wnt and hedgehog signaling pathways. When activated, these pathways inhibit adipogenesis and promote osteogenesis [154]. Conversely, insulin signaling promotes adipogenesis [155]. Moreover, during commitment from pluripotent stem cells to lineage-specific multipotent cells, the expression of pluripotent genes are epigenetically silenced by introduction of repressive tri-methylation marks on H3K9 and H3K27 histone tails [147,156]. Conversely, lineage-specific genes become poised for rapid induction by bivalent H3K4me3 activating and H3K9me3 repressive marks, causing the RNA polymerase to bind, but pause at these

promoters [147,156,157]. During terminal differentiation, these poised regions are resolved to contain either the activating or repressive mark, thereby specifying which lineage is allowed to differentiate [1].

Terminal differentiation has been exhaustively studied, and is controlled by the master regulator PPARγ and C/EBPα/β/δ family members [35,147]. In preadipocytes, the promoter of *PPARγ* is still poised, which keeps PPARγ levels low [156]. The immediate early genes *C/EBPδ* and *C/EBPβ*, on the other hand are expressed, but the resulting proteins are inactive. However, adipogenic stimulation results in phosphorylation and activation of C/EBPδ/β, and at the same time removal of the H3K9me3 repressive marks on the *PPARγ* promoter [147,156]. These two events allow C/EBPδ/β to bind to and initiate expression of *PPARγ*, which in turn forms positive feedback loops with C/EBPα and -β [158–160]. PPARγ subsequently binds to and promotes the expression of virtually all genes related to adipocyte metabolism [35,147].

Of note, C/EBP family members and PPARγ are adipogenic master regulators of all adipocyte types including white, beige and brown [154]. Lineage-specific development occurs by differential binding to various target genes, guided by chromatin availability and other transcription factors and -cofactors [161,162]. Specifically, activating H3K27ac and H3K4me3 marks on target gene enhancers and promoters, respectively, specify what genes are available for activation by PPARγ [147,157,163]. For example, this epigenetic discrimination underlies the difference between adipocytes and macrophages, which both express *PPARγ* [164] and also between white versus beige adipocytes that both require PPARγ, but display differences in available binding sites [147,161,162]. Moreover, in thermogenic adipocytes, Ebf2 directs Pparγ to unique sites like the promoter of *Prdm16*, a co-activator that complexes with chromatin remodeling factors like Ehmt1 to further specify thermogenic-specific adipogenesis [161,165]. Indeed, the difference in transcriptomic profiles between brown and beige adipocytes on one hand and white adipocytes on the other, mainly converges on the activities of PGC-1α and PRDM16, both positive regulators of *UCP1* [35].

PGC-1α is a well-known master regulator of mitochondrial biogenesis and oxidative function in multiple cell types [119], acting as a co-activator of PPARγ, PPARα and a range of other TFs [166,167]. Thermogenic adipocytes rely heavily on mitochondrial activity, and therefore have very high *PGC-1α* expression levels. Additionally, in these cells, PGC-1α acts as an essential inducer of cold-stimulated expression of *UCP1* and other thermogenic genes [167–172]. High *PGC-1α* expression is therefore widely used as a hallmark of thermogenic compared to white adipocytes.

PRDM16 expression is another key marker of brown and beige cells in mice [123,149] and humans [135,173] that has been found to be crucial for maintaining thermogenic identity. Overexpression of *PRDM16* in white adipocytes is sufficient to convert them into beige cells [123,148], and conversely, knock-down of *PRDM16* in brown or beige cells prevents thermogenesis and increases expression of white fat markers [123,148,149,174]. Mechanistically, PRDM16 acts by binding to and modulating the activity of other TFs and co-regulators, including C/EBPβ, PPARγ, PPARα and PGC-1α [148,149,175,176].

Strikingly, most if not all reported regulators of thermogenesis appear to mediate their effect via PRDM16 or PGC-1α [147], including the homeobox factors IRX3 and IRX5 [117], which our group discovered as novel players in obesity a decade ago [177].

1.5 The homeobox factors IRX3 and IRX5

1.5.1 Homeobox transcription factors

Homeobox transcription factors, or Homeoproteins, are key transcription factors in embryonic and adult development [178,179] that share a common conserved DNA-binding domain, the homeodomain (HD) [180,181]. Most vertebrates, including humans, are found to possess around 250 homeobox genes that can be divided into 16 classes with diverse target genes and functional roles [178,182]. Among these, the class I homeobox genes (*HOX*) are most well-known, consisting of 39 genes, organized into 4 clusters (HOX A-D) each located on a different chromosome, [183,184].

During development, temporal and spatial expression of *HOX* genes determines the identity of different regions along the body axis [185]. For instance, during embryogenesis, the *Hox* genes physically located in the 3' end are expressed early and define the anterior regions, whereas other Hox genes located in the 5' end are expressed later and control the posterior regions of the embryo [186]. Following the comprehensive study of *HOX* genes in embryogenesis, an increasing attention was given to the involvement of these genes in adult development [187–189], including metabolism [190] and adipogenesis [191].

Roles of Homeobox transcription factors in obesity

In 2003, the Cillo group reported the use of semi-quantitative PCR to assess the expression of the 39 class I *HOX* genes in adult human white and fetal brown adipose tissue depots. They found the *HOX* gene network in general to be active in adipose tissue, with several *HOX* genes being consistently expressed in all samples and depots [192]. Moreover, a clear depot-specific expression pattern of other *HOX* genes was also observed, particularly for the group 4 paralogs which appeared to confer lineage identity [192]. Specifically, *HOXA4* and *HOXC4* was found to be markers of white and brown adipocytes, respectively, whereas *HOXD4* was expressed in every depot and *HOXB4* in none [192].

With later technological advances, including microarrays and quantitative PCR, the C. Ronald Kahn lab subsequently identified differential expression of several homeobox

genes between visceral and subcutaneous white adipose tissue in mice and humans [193]. HOXA5 and HOXC8 were found to be most highly expressed in the visceral depots, whereas SHOX2 and HOXC9 and were elevated in the subcutaneous compartments. Furthermore, these findings were consistent across whole tissue, stromovascular fraction (SVF), isolated adipocytes and after *in vitro* culture [193]. Of note, the fold changes between depots were greater in humans compared to mice. Finally, the visceral marker HOXA5 was found to be significantly positively correlated with increased BMI and WHR in humans in both genders and both depots, with strongest associations in visceral adipose tissue [193].

In a later follow-up study in mice, where more visceral and subcutaneous white depots, as well as a BAT depot was included, *Shox2* was confirmed as a general subcutaneous marker, and *Hoxa5* was more highly expressed in all white visceral depots, but in fact highest in BAT. The other *Hox* genes analyzed in this study, on the other hand, displayed low expression levels in BAT [194]. Several subsequent studies by various groups have later confirmed depot-specific expression profiles of *HOX* genes in humans [195–198], and found *HOXC9* and *HOXC10* to be associated with obesity, fat distribution and glucose metabolism [198]. This difference in *HOX* expression pattern in WAT and BAT likely reflects the different developmental origin of cells from these two depots. Indeed, several investigators have suggested that HOX genes are likely drivers of the depot-specific differences in adipocyte differentiation and function, although the mechanisms remained to be elucidated [194,198].

Our group identified up-regulation of several homeobox factors in subcutaneous adipose tissue after bariatric surgery, including class I family members *HOXA5*, *HOXA9*, *HOXB5*, *HOXC6* in addition to *EMX2*, *PRRX1* and *IRX3* and *IRX5* [177]. As described in section 1.3.2, we subsequently elucidated a mechanism whereby PRRX1 modulates obesity risk by risk allele-specific binding to, and repression of, an enhancer of *PPARγ2* [115]. We next found adipose *IRX3* and *IRX5* expression to depend on the risk-allele specific abolished binding of another repressor, ARID5B, to the super-enhancer in intron 1 of *FTO*, as described in section 1.3.3 and [117]. The resulting elevation of *IRX* levels repressed thermogenic genes, indicative of a developmental

shift from beige to white adipogenesis from a common precursor, but the exact mechanisms and target genes were not found [117].

1.5.2 The Iroquois homeobox factors

The Iroquois class of homeobox factors (sometimes abbreviated IRO, but herein termed IRX) constitutes, together with four other evolutionary related classes, the Three Amino Acid Loop Extension (TALE) superclass of homeoproteins [178,182,199]. As the name indicates, all TALE type homeoproteins are characterized by additional residues in the loop between helices 1 and 2 of the HD [179–181,200]. The IRX class consists of six family members (IRX1-6) that share a unique and highly conserved 9 aa IRO box C-terminal of the HD [199,201,202]. Until recently, the function of the IRO domain was unknown, but recent evidence from *Drosophila* suggests this domain is involved in protein-protein interactions [203].

Like HOX proteins, the IRX transcription factors are found in all multicellular organisms, ranging from sponges to mammals and play essential roles in developmental patterning formation via spatial and temporal regulation of target genes [201,204–206]. Since their discovery between 1997-2000 [207,208], the *IRX* genes have been implicated in a wide range of developmental processes, including formation of the organizer during gastrulation [209], embryonic neurogenesis [207,208,210,211], and formation of heart [212–218], kidneys [219], eyes [202,220–224], ovaries [225] and the central nervous system [226]. Despite the evident importance of IRX transcription factors, knowledge of their target genes and mechanistic action is limited [227]. IRX proteins have most frequently been shown to mediate transcriptional suppression [204,205,209,218,228–230], although Matsumoto et al. reported Irx2 to also have an activating role depending on phosphorylation status, with MAPK signaling promoting the activating form [230].

In humans, biallelic mutations in *IRX5* leads to defect craniofacial morphogenesis and impaired heart, blood, bone and germ cell development [204]. Employing a *Xenopus* model system, these investigators further demonstrated that Irx5 acted as a

transcriptional repressor of *Sdf1*, which codes for a chemokine vital to migration of cranial neural crest and gonadal primordial germ cells [204]. Correct temporal and spatial repression of *SDF1* signaling by IRX5 therefore seems crucial during human development [204].

Evidence for the involvement of Irx5 and Irx3 during both embryonic and adult development of the same tissue has been provided by KO studies in mice. Whereas constitutive double KO of *Irx3* and *Irx5* is embryonic lethal, accompanied with severe cardiac structural defects [214], constitutively knocking out each factor alone, or conditionally deleting both genes postnatally, results in mice that are viable, but with specific defects in adult cardiac functions [214,231–234]. These results demonstrated that *Irx3* and *Irx5* are functional redundant during embryogenesis, but have partially separate, and sometimes antagonistic roles in adult development [214].

Further, IRX3 and IRX5 have been implicated in adult cellular proliferation. IRX5 promotes cell-cycle progression in human prostate cancer cells [235] and vascular smooth muscle cells [236], and IRX3 has been found to be frequently derepressed in human acute leukemias, leading to changes in cellular identity [237]. Finally, IRX3 has been found to have a proangiogenic effect in human microvascular endothelial cells [238].

Taken together, IRX3 and IRX5 play important roles in both embryonic and adult tissues.

1.5.3 Roles of IRX3 and IRX5 in obesity

As delineated above in chapters 1.3.3 and 1.5.1, one of the adult tissues found to be regulated by IRX3 and IRX5 is the adipose. Briefly, our group found the expression of these factors to increase in subcutaneous human adipose tissue after bariatric surgery [177]. Moreover, the Claussnitzer group, in collaboration with us, found IRX3 and IRX5 to promote white over beige adipocyte development from mesenchymal precursor cells, dictated by a causal risk variant in the obesity-associated *FTO* locus [117]. Recently, several other groups have further investigated the role of IRX3 and IRX5 in adipose biology, and regulation of body weight, as discussed below.

While Claussnitzer et al. measured *IRX* expression in lean adults, Landgraf et al. measured *IRX* expression in lean and obese children, and found higher expression levels of both *IRX3* and *IRX5* in the mature adipocyte fraction compared to the SVF [239]. Interestingly, in the mature adipocytes, *IRX3* expression was higher in lean compared to obese patients. Moreover, an *FTO* locus, rs1421085 risk allele-dependent increase in both *IRX3* and *IRX5* expression was observed, but only in mature adipocytes of lean children [239]. Although *IRX3* mRNA levels were higher in UCP1-negative compared to UCP1-positive adipocytes [239], consistent with its reported inhibitory effect on *UCP1* expression [117], this effect was, again, only seen in lean children [239]. Finally, *IRX3* was negatively associated with adipocyte size, inflammation and insulin resistance. These results appear somewhat counter-intuitive, as one would perhaps expect the pro-adipogenic effect of *IRX3* to be active in obese individuals, as opposed to lean. However, the authors suggest this may be an example of a thrifty allele that, in an evolutionary perspective, has undergone positive selection in environments where food is scarce [240]. Thus, IRX3 may promote weight gain in lean individuals as a protective mechanism against undernutrition [239].

From studies on mice, it was seemingly clear that having intact Irx3 promotes weight gain and increased adipose tissue mass, as global *Irx3*-KO mice, as well as mice with adipocyte- and hypothalamus-specific DN-*Irx3* mutants are protected from diet-induced obesity, displaying reduced body weight, fat mass and increased energy expenditure and thermogenic gene expression [113,117]. However, de Araujo et al.

recently reported the opposite result when reducing Irx3 levels by 50% specifically in the hypothalamus, through lentiviral-mediated knockdown [241]. This effect, however, was only seen in mice fed a high-fat diet. Thus, obese mice became even more obese following *Irx3*-knockdown, and this effect coincided with increased energy intake, reduced energy expenditure and reduced *Ucp1* expression in adipose tissue [241]. Therefore, in contrast to previous findings, a positive correlation between *Irx3* and *Ucp1* expression was found in this study. This discrepancy could perhaps be explained by difference in Irx3 action in the hypothalamus versus adipose tissue, but another study, by Zou et al., made similar observations specifically in adipocytes [242]. Here, *Irx3* and *Ucp1* expression was found to be positively correlated, and moreover, knockdown of *Irx3* inhibited *Ucp1* expression and thermogenesis in beige adipocytes from mice and humans [242].

Of note, in contrast to the debated effects of Irx3 on energy expenditure, fat mass and body weight, no studies have assessed these parameters in *Irx5*-KO mice.

Taken together, although IRX3 (and to a lesser extent, IRX5) have been shown in several studies to promote obesity in mice and humans, these findings have recently been challenged by opposite findings in other studies. The reasons for these discrepancies are unknown, highlighting the need for further elucidating the function and target genes of IRX3 and IRX5 in adipose tissue [243].

2. Aims

Elevated expression of the homeobox transcription factors *IRX3* and *IRX5* has been found to mediate the strong association between genetic risk variants in intron 1 of *FTO* and obesity. However, the mechanisms involved were not fully understood and remained controversial. The overall aim of this study was therefore to elucidate the transcriptional roles of IRX3 and IRX5 in adipose tissue and their implications for body weight and fat mass.

Specific aims included:

1) Characterize the effect of *Irx5*-KO on body weight and fat mass in mice.
2) Identify adipocyte gene networks and cellular functions under control of Irx3 and Irx5.
3) Map genome-wide binding of Irx3 and Irx5 to adipocyte promoters and enhancers to determine direct Irx3/5 target genes.

3. Comments on methods

This work is based on a wide range of materials and methods, as described in detail in each individual paper. An overview of key methods is presented and briefly discussed as follows.

3.1 Mouse Models (Papers I and III)

The studies using mouse models in paper I were conducted at The Laboratory Animal Facility, University of Bergen, Norway. The study was approved by the Norwegian State Board of Biological Experiments with Living animals and carried out in accordance with their guidelines.

Wild-type (WT) and *Irx5*-KO mice of a mixed 129/Sv and CD1 background were a gift from Kyoung-Han Kim and Chi-Chung Hui, The Hospital for Sick Children, and Department of Molecular and Medical Genetics, University of Toronto, Canada. Briefly, the *Irx5*-KO mice were generated by introducing a loss-of-function mutation in *Irx5* [224], in which parts of exon 1 was replaced with a PGK-*neo* cassette in R1 embryonic stem (ES) cells [244]. In Bergen, heterozygous $Irx5^{-/+}$ mice were bred to produce homozygous WT and *Irx5*-KO mice. The mice were kept in a 12h light/dark cycle at 20 ± 3°C and relative humidity of 65 ± 15% with free access to tap water. From the age of 8-10 weeks, the mice were randomized to either a control or high-fat diet (10 and 45 kcal% fat, respectively), containing the same amount of proteins. Body weight was measured every week, feed intake was measured after 3.5 weeks, Magnetic Resonance Imaging (MRI) of renal white adipose tissue (rWAT) was performed after 7 weeks, and the mice were sacrificed after 10 weeks of diet intervention. After euthanasia, epididymal white adipose tissue (eWAT) was dissected out and weighed before RNA isolation.

The mouse studies in paper III were conducted by our collaborators, Roger Cox, Samantha Laber and colleagues, at the MRC Harwell Institute, Oxfordshire, UK, in accordance with the UK Animals Act. Mice with C57BL/6NJ (B6N) background were housed in a 12h light/dark cycle at 21 ± 2°C and relative humidity of 55 ± 10%, fed ad

libitum chow (RM3, 3.6 kcal/g) with free access to water. At 6-10 weeks of age, the mice were euthanized and primary preadipocytes from the stromovascular fraction (SVF) of inguinal and gonadal white adipose tissues (iWAT and gWAT, respectively) were isolated by collagenase treatment and centrifugation, as previously described [245]. The cells were subsequently cultured and stimulated to differentiate by addition of adipogenic cocktails, as described in detail in paper III. These cells were used for ChIP-seq and ATAC-seq analyses.

3.2 Patient samples (Papers I-III)

The human studies were approved by the Western Norway Regional committee for Medical Research Ethics (REK) and each of the subjects gave written informed consent.

In paper I, subcutaneous adipose tissue was collected from 12 severely obese patients undergoing bariatric surgery (average BMI of 46) and 12 healthy lean individuals undergoing hernia repairs (average BMI of 24). Floating mature adipocytes were subsequently isolated from the adipose tissue by collagenase digestion of connective tissue, followed by sieving and filtering, as described before [246]. Because mature adipocytes cannot be maintained in culture, these cells were immediately lysed for RNA purification.

In papers II-III, subcutaneous adipose tissue was collected from liposuction material from 10 patients undergoing plastic surgery. From this material, we isolated the pelleted SVF containing preadipocytes and mesenchymal stem cells, following the same method as above. These primary cells were maintained in culture, induced to differentiate following stimulation by adipogenic cocktails, and treated with siRNA against *IRX3* and *IRX5* before RNA purification.

3.3 Cell cultures (Papers I-III)

Primary preadipocytes were isolated from human and mice white adipose tissue depots as outlined above and cultured *in vitro* in proliferation and differentiation media as described in detail in papers I-III. While primary cells have the advantage of close resemblance to cells *in vivo*, these cells can only be cultured for a limited amount of time, and should thus be used fresh, ideally without expansion, freezing and thawing. Having to isolate cells prior to each downstream analysis is highly costly and laborious, and introduces an additional source of variation in the experiments, making the use of these cells infeasible for many routine assays. Moreover, some experiments, like generation of stable gene KO by CRISPR-Cas9, requires prolonged cultivation unsuitable for primary cells.

Therefore, we have also employed several immortalized cells in this study, including white preadipocytes isolated from iWAT of C57BL/6 mice (paper I), beige preadipocytes isolated from mouse embryonic fibroblasts (ME3, paper I-III), white preadipocytes derived from human subcutaneous adipose tissue (paper III) and simian kidney cells (COS-1, papers I and III). The ME3 and COS-1 and cells were used to provide adipogenic and non-adipogenic environments, respectively, in luciferase reporter assays. Moreover, the iWAT and ME3 cells were subjected to CRISPR-Cas9 mediated knock-down/out of *Irx5* and *Irx3*, respectively.

3.4 CRISPR-Cas9 genome editing (Papers I-III)

The CRISPR-Cas9 genome editing was performed essentially as described previously [247], with the aim of introducing loss-of-function mutations in each target gene. To this end, WT cells were transfected *in vitro* with a plasmid containing both guide RNA and Cas9-GFP. The Cas9 enzyme is an endonuclease that originates from the bacteria *Streptococcus pyogenes* where it serves as a defensive mechanism against foreign DNA [248]. Cas9 requires two small RNA sequences to function. First, a guide-RNA complementary to the genomic target site is necessary to specify the site where Cas9 is allowed to cut. Second, a scaffolding RNA, which base-pairs with the guide-RNA and binds to Cas9, is required for Cas9 complex formation and activation. In addition to the specificity imposed by the guide-RNA, Cas9 must also be directed to a site containing a 3-base pair sequence known as the Protospacer Adjacent Motif (PAM) [249,250]. These short PAM sequences are found densely interspaced throughout the genome. Thus, in genomic engineering, computational methods available online (i.e. https://chopchop.cbu.uib.no/) [251–253] are used to identify these CRISPR-compatible PAM sequences and design guide-RNAs unique to the nearby genomic sequence. Using this tool in combination with basic local alignment search tool (BLAST) [254] and pilot experiments, we identified the best performing guide-RNA out of three constructs each for *Irx3* and *Irx5* which were used for subsequent experiments. For both genes, the best CRISPR-Cas9 site was found to be in the beginning of exon 2, containing the HOX domain.

DNA-cleavage by Cas9 introduces a double-stranded break, which the cell attempts to repair by one of two possible mechanisms; nonhomologous end joining (NHEJ) or homology directed repair (HDR). While HDR is precise when a desired repair template is provided, it is extremely slow and inefficient. NHEJ, on the other hand, occurs within a few minutes and is highly error-prone, often making NHEJ the preferred method, especially for generating KO. The error-prone nature of NHEJ frequently leads to generation of various indel mutations surrounding the Cas9 cut site, leading to frameshift and, in most cases, premature stop codon and truncated protein. In this study, we relied on NHEJ. To isolate clones with truncation of either Irx3 or Irx5 protein,

flow cytometry followed by Fluorescence-Activated Cell Sorting (FACS) was used to identify and seed single cells expressing GFP-tagged Cas9.

Starting from 100-400 single cells, about 10-24 clones were successfully expanded. Sequencing revealed that CRISPR-Cas9 mediated editing had occurred in 90% of the clones, although in most cases the allelic events were unclear. Therefore, the individual alleles of each clone were amplified by PCR, TOPO cloned in *E. coli* and sequenced. While *Irx5* had been edited on one allele only, producing a functional knockdown, *Irx3* was edited to yield frameshift on both alleles, via different indel events, producing a complete knockout. Finally, to verify the knockdown/out, the protein levels of Irx5 and Irx3 was assessed by Wester Blotting using antibodies recognizing the middle or C-terminal part of the proteins. In accordance with the sequencing, Irx5 protein levels were reduced by 50%, whereas the Irx3 protein was undetectable in the CRISPR-edited cells.

3.5 Gene expression analyses (Papers I-III)

All papers in this study include gene expression analyses, each measuring the relative or absolute abundance of mRNA transcribed from a handful to tens of thousands of genes. Accurate and precise quantification of mRNA is affected by multiple factors, from the biological system and study design to tissue handling, RNA purification, conversion to cDNA and finally quantification of the cDNA.

3.5.1 Variation and bias

Simply put, precision refers to variation or the reproducibility of data. The underlying biology of a model system can greatly influence the reproducibility of the data. For example, analyzing gene expression in a pool of cells extracted from the adipose tissue of different humans introduces several layers of potential variation, including genetic and environmental factors, as well as cell composition. For these reasons, working with

genetically identical mouse models and, particularly, cell lines, offers a clear advantage. Moreover, cell lines can also be kept under highly similar conditions, thereby further reducing variation. On the other hand, one must keep in mind that results may vary depending on the selected models.

In paper I, we observed larger variation between individual mice than expected, and this was seen for several parameters, including body weight, fat mass and gene expression, suggesting the influence of an unidentified environmental factor. These observed variations could negatively affect the confidence in the results and make it more challenging to draw conclusions. However, by complementing these results with *Irx5*-manipulation in isolated adipocytes *in vitro*, we were able to identify similar gene expression patterns with low variation.

Accuracy refers to proximity to the true value, or bias, which can be introduced by many factors from choice of model system to technical procedures. For example, because RNA is highly sensitive to degradation from endogenous and exogenous RNases, great efforts were made to preserve and validate RNA integrity in each sample. Extracted tissues were immediately snap-frozen in liquid nitrogen and stored at -80^{0}C until extraction, and during extraction, investigators always wore clean gloves. RNA integrity can be assessed using the Bioanalyzer system, where reported RIN values range from 0-10, representing completely degraded to perfectly intact RNA, respectively. In this study, samples had a RIN value above 9, exceeding the threshold for acceptable quality.

3.5.2 Quantitative polymerase chain reaction (qPCR)

Targeted relative gene expression was quantified by isolation of RNA and reverse transcription to cDNA, followed by real-time qPCR using the Roche LightCycler® 480 system. Briefly, SYBR™ Green, a dye specifically recognizing double-stranded DNA, is quantified by fluorescence following each cycle of DNA duplication, using specific primers to amplify a short region of the gene of interest. Importantly, because SYBR-green detects any double-stranded DNA in the reaction, including primer dimers and

unspecific amplicons, we carefully designed the primers to avoid such errors. Primers were designed using either of the publicly available softwares Roche UPL Assay Design Center or Primer-BLAST with stringent criteria. Each primer was further assessed *in silico* for propensity of self- or cross-dimerization using the Premier Biosoft Beacon Designer software, and tested *in vitro* using melting curve analysis. Only non-dimerizing primers with efficiency above 1.9 were used in subsequent analyses.

In this study, relative quantification was performed using the delta-delta Ct method, where the Ct value of the target gene is first subtracted from the Ct value of the reference gene, producing a ΔCt value for each sample. A control sample is then assigned as normalizer and its ΔCt value subsequently subtracted from each of the other samples, producing normalized ΔΔCt values. Because Ct values are exponentially inversely related to original mRNA levels, the ΔΔCt values can be expressed as 2^{-Ct} or fold change relative to the normalizer. Finally, these fold change values are normalized according to the average of the biological replicates of the control treatment, which are centered around the value 1. We used *Rps13* as reference gene, which shows superior stability across a wide range of cell types and experimental conditions, as demonstrated by [255].

3.5.3 Global gene expression analyses

Global gene expression was mainly measured by RNA sequencing (RNA-seq) in this study, and some experiments were performed with microarrays. While the microarray approach was an established method for measuring "global" gene expression before the advent of modern sequencing technologies, it suffers from the biased use of an *a priori* determined set of probes complementary to mRNA of selected genes [256,257]. Moreover, microarrays also display high background and are prone to signal saturation of highly expressed genes [257].

RNA-seq

RNA-seq relies on deep-sequencing technology where, in this study, the global transcriptome (mRNA) was converted into a library of cDNA fragments and directly

sequenced using the Illumina platform with a depth of about 40 million reads per sample. Importantly, to avoid contamination with DNA, all samples were treated with DNase during isolation of RNA. Once sequenced, each fragment, consisting of 75 bp, was then mapped to a reference genome, counted and normalized to account for library size and transcript length. By directly sequencing all transcripts in a sample, RNA-seq eliminates the bias introduced in microarrays. Moreover, RNA-seq is free from background signals and has an almost unlimited dynamic range [257].

3.6 Luciferase reporter assays

Luciferase reporter, or transactivation assays, are convenient and powerful tools used to investigate the ability of any given protein, most often a TF or coregulator, to modify the expression of any given promoter. First, the promoter to be investigated, for example the *Ucp1* promoter, must be cloned into a reporter vector harboring a luciferase-encoding gene. Next, the reporter is co-expressed with an overexpression-plasmid encoding the TF, for example *IRX5*, hypothesized to transcriptionally modulate the target promoter. These plasmids are often expressed in cells that are easy to transfect and have low endogenous levels of the respective factors to be investigated in order to reduce background. For these reasons, COS-1 kidney cells have been the major host of transactivation assays in this study. However, when the TF has repressive properties, like IRX proteins often have, it can be also be useful to express the reporter in a host containing (other) endogenous factors that promote high basal activation of the reporter. Therefore, ME3 preadipocytes have also been used as a host in this study.

Activated by endogenous or overexpressed factors, the promoter of the reporter plasmids induces expression of the luciferase enzyme, which catalyzes the conversion of luciferin to oxyluciferin, a reaction that releases energy in the form of light that can be detected and quantified. Thus, differences in light production in cells with overexpression of *IRX3* or *IRX5* compared to a negative control (empty plasmid) reveal whether the IRX proteins transcriptionally regulate the given promoter or not.

3.7 ATAC-seq

Global chromatin accessibility can be conveniently assessed by Assay for Transposase-Accessible Chromatin using sequencing (ATAC-seq). This assay relies on the activity of a hyperactive mutant of the Tn5 Transposase, which binds to any accessible chromatin, cleaves it and tags it with sequencing adaptors. These tagged DNA fragments, which only originate from open chromatin, are subsequently purified, sequenced, mapped to a reference genome and quantified. Thus, the number of reads at a specific locus corresponds to degree of chromatin availability.

3.8 ChIP and ChIP-seq

Chromatin Immunoprecipitation (ChIP) is a powerful method used to experimentally map binding sites of any given protein, or protein modification, associated with chromatin, including TFs and histone modifications [258]. The method requires crosslinking to preserve DNA-protein interactions, most commonly achieved by formaldehyde fixation. Further, chromatin is extracted from the nuclei and sheared by sonication to produce fragments of about 200-1000 bp. Then, in a critical next step, antibodies capable of recognizing the target protein in the native and fixated state are used to capture the DNA fragments bound by the target protein. Following reversal of crosslinking, the DNA is purified and quantified in a targeted (ChIP) or global (ChIP-seq) manner. In this study, we performed ChIP-seq to map genome-wide Irx3 and Irx5 binding sites during differentiation of beige ME3 cells and white adipocytes.

Unfortunately, no commercially available ChIP-seq grade Irx5 antibodies are currently available. We tested multiple candidate antibodies for ability to recognize native and crosslinked Irx5, and subjected the best-performing antibody (Cat# SAB2106408, LOT# QC6282) to commercial ChIP-seq. However, in a pilot ChIP-seq experiment, this antibody did not meet the stringent criteria for ChIP-seq and we could therefore not map the direct Irx5 binding sites.

In contrast to Irx5, one commercially available Irx3 antibody is rated as ChIP-seq grade (Cat # ab25703). This antibody passed the ChIP-seq quality control in our samples (commercial service), and full-scale ChIP-seq was therefore performed on ME3, iWAT and gWAT samples. While the signal-to-noise ratio in ME3 cells was too low to defend subsequent analyses, we obtained peaks of sufficient quality in iWAT and gWAT.

Finally, we used ChIP followed by targeted qPCR to assess changes in binding of Kdm3a, one of the discovered Irx3-target genes, to the promoters of *Ucp1* and *Pgc-1α* following *Irx3*-KO in ME3 cells. We also used ChIP to quantify changes in two histone marks on the same loci. In these assays, we enjoyed the benefit of commercially available antibodies of high ChIP-seq quality, providing high enrichment of precipitated DNA over input.

4. Summary of results

4.1 Paper I: "IRX5 regulates adipocyte amyloid precursor protein and mitochondrial respiration in obesity"

In this study, we addressed the lack of reports on *in vivo* effects of Irx5 on body weight and fat storage. We therefore randomized WT and global *Irx5*-KO mice to either control or high-fat diet for 10 weeks, and observed a strong reduction in body weight and fat mass in *Irx5*-KO compared to WT mice. Moreover, the KO mice were resistant to diet-induced weight gain. We next compared the global gene expression in epididymal white adipose tissue (eWAT) between the WT and *Irx5*-KO mice, and found networks of differentially expressed genes (DEGs) to center around the amyloid precursor protein (*App*). We also found the thermogenic genes *Pgc-1α* and *Ucp1* to be upregulated with *Irx5*-KO.

To investigate whether these observed effects could be attributed to lack of Irx5 specifically in adipocytes, we stably knocked down (kd) *Irx5* in immortalized primary white adipocytes isolated from WAT of WT mice. We found that knocking down *Irx5* specifically in adipocytes recapitulated the effects of global *Irx5*-KO on adipose tissue, including reduced *App* expression and elevated expression of *Pgc-1α* and *Ucp1*. Moreover, luciferase reporter assays confirmed that Irx5 transcriptionally activated *App*, and that both Irx5 and App transcriptionally repressed *Pgc-1α* and *Ucp1*. In agreement, we found App and Irx5 to impair mitochondrial respiration and uncoupling. Finally, we found significant enrichment of Irx5-sensitive genes to be differentially expressed between adipocytes from obese and lean humans.

In conclusion, we found *Irx5*-KO mice to be protected from obesity, and this could at least partially be attributed to ablation of Irx5 specifically in adipocytes, which diminished adipocyte App, thereby relieving a dual Irx5/App-mediated inhibition of adipocyte mitochondrial respiration and uncoupling.

4.2 Paper II: “The homeobox factor Irx3 maintains adipogenic identity”

In this study, we sought to investigate the role of Irx3 specifically in adipocytes capable of beiging. To this end, we first performed comprehensive global gene expression profiling at five timepoints during differentiation of the beige ME3 cell line, and found *Irx3* to be co-expressed with genes related to the cell-cycle/mitotic clonal expansion. Hypothesizing that Irx3 might control this process, we stably knocked out *Irx3* in the ME3 cells and assessed the effect on differentiation. We observed a striking lack of adipogenic differentiation in the *Irx3*-KO cells, however, this effect was not attributable to changes in clonal expansion. Instead, global gene expression revealed altered expression of morphogenic genes early in differentiation, accompanied by increased activity of genes related to the extracellular matrix (ECM). *In silico* cell type enrichment analysis suggested loss of preadipocyte identity and gain of chondrocyte-like identity in the *Irx3*-KO cells. This finding was confirmed *in vitro* by stimulation of WT and *Irx3*-KO cells with a chondrogenic cocktail for 19 days, which promoted chondrogenesis specifically in the *Irx3*-KO cells.

Finally, we observed profound reductions in mitochondrial respiration and uncoupling, reactive oxygen species (ROS) generation and proliferation rates in the *Irx3*-KO cells compared to controls, attributable to differential expression of numerous genes involved in these processes.

In conclusion, Irx3 is required for preadipocyte function, identity and ability to differentiate into mature adipocytes.

4.3 Paper III: “Epigenetic control of adipogenesis by Irx3”

Having identified a large number of genes to be affected by manipulation of Irx3 in adipocytes, we next aimed to identify direct target genes. We therefore performed chromatin immunoprecipitation followed by sequencing (ChIP-seq) to map genome-wide Irx3 binding sites on days 0, 1 and 7 during differentiation of the beiging-competent mouse ME3 cell line. Furthermore, through collaboration with the Harwell Institute, we also received ChIP-seq data for Irx3-DNA interactions in two mouse WAT depots on days -1 and 1 of differentiation. In parallel, we performed open chromatin profiling (ATAC-seq) in the same cells.

In WAT we identified over 300 Irx3 binding sites and found virtually all of them to occur in open chromatin specifically on proximal promoters of genes related to chromatin remodeling, mitochondrial translation and mRNA metabolism. In ME3 cells, however, the ChIP-enrichment was insufficient to produce meaningful peaks, preventing a direct comparison with the binding events in WAT. However, ATAC-seq in ME3 revealed that most of the Irx3 binding sites identified in WAT overlapped with open chromatin in the ME3 cells. Therefore, it was conceivable that these loci could be bound by Irx3 in both cell types. Indeed, we identified 63 Irx3 target genes with differential expression between control and *Irx3*-KO in the ME3 cells. Again, these genes were significantly enriched with genes related to chromatin remodeling, mitochondrial translation and mRNA metabolism.

Finally, we performed functional analyses of *Kdm3a*, one of the differentially expressed Irx3 target genes related to chromatin remodeling, that has previously been shown to promote *Ucp1* expression by removal of repressive H3K9me2 histone marks. We found altered protein levels and recruitment of Kdm3a to the *Pgc-1α* and *Ucp1* promoters, followed by corresponding changes in H3K9me2 marks on these loci in *Irx3*-KO versus control cells. We also found differential expression of *KDM3A* and reduced H3K9me2 marks in primary and immortalized cells from human WAT. Furthermore, luciferase reporter assays confirmed transcriptional regulation of *Kdm3a* by Irx3.

In conclusion, we found Irx3 to bind directly to the promoters of genes involved in epigenetic regulation, mitochondrial function and mRNA metabolism, regulating their expression and downstream activities. Collectively, our findings indicate that Irx3 acts as a master regulator that coordinately impacts cell fate and metabolism via genetic and epigenetic regulation of gene expression.

5. General discussion

5.1 Effect of Irx5 ablation in mice

In paper I, we provided the first report of the *in vivo* metabolic effect of *Irx5* ablation in mice. The global *Irx5*-KO mice displayed a profound anti-obesity phenotype compared to WT littermates, with about 40% reduction in body weight, accompanied by nearly 50% and 70% reductions in renal and epididymal adipose tissues, respectively. Moreover, whereas the WT mice gained more weight on a high-fat diet compared to regular chow, this effect was blunted in the *Irx5*-KO mice, meaning they were protected from diet-induced obesity. These changes were accompanied by increased expression of adipose *Pgc-1α* and *Ucp1*. Our results are highly similar to the effects observed by Smemo et al. in global *Irx3*-KO mice [113], although the effects of knocking out *Irx5* in our study appeared to be stronger. Moreover, the phenotype of the global *Irx5*-KO mice closely recapitulated the phenotype of adipose-specific *Irx3*-DN mice reported by Claussnitzer et al. [117].

Taken together with *in vitro* data from human cells, demonstrating similar effects of IRX3 and IRX5 on regulation of fat storage and thermogenesis [117], our data suggest that Irx3 and Irx5 serve cooperative or converging, rather than redundant, roles in regulation of energy homeostasis. Of note, Irx-proteins from *Drosophila* have been shown to physically interact to form heterodimers *in vitro* [205]. Moreover, Irx3 and Irx5 have been demonstrated to act cooperatively on specific target genes in the adult heart of mice [214]. Thus, it is conceivable that binding of either IRX protein to a target gene is stabilized by previous or subsequent dimerization with the other IRX partner. Indeed, in luciferase experiments using various target promoters, we have often seen more pronounced effects on the reporter when overexpressing Irx3 and Irx5 in combination (unpublished data).

We found reduced expression of the amyloid precursor protein (App) in the adipose tissue of the *Irx5*-KO mice *in vivo*, and demonstrated *in vitro* that *App* expression depends on Irx5. Moreover, we provided evidence for both App and Irx5 to reduce

mitochondrial respiration. While App is most known for its contributing role to Alzheimer's disease through plaque formation by its amyloid beta (Aβ) cleavage products in the brain [259–261], several studies have found positive associations between App itself, or its cleavage products, with obesity and adipose tissue function [262–269]. Moreover, *App*-KO mice were recently shown to recapitulate the anti-obesity phenotype observed in the *Irx5*-KO mice, demonstrating a causal role of App in promoting obesity [270].

In neurons, *soluble* Aβ peptides can accumulate in the mitochondria [271], negatively affecting mitochondrial function through a number of mechanisms, including inhibition of electron transport chain complexes III and IV [272–275], disruption of protein transport into mitochondria [276,277], altered mitochondrial permeability [275,278] and inhibition of proton translocation from the mitochondrial matrix to the inter-membrane space [276,277,279]. Additionally, secreted Aβ peptides interact with a wide array of cell surface receptors, including the calcium-sensing receptor (CaSR) [280], which can, through a positive feedback loop, increase intracellular App and Aβ levels. Interestingly, the CaSR has also been reported to stimulate adipogenesis [281,282]. In our study, we did not quantify Aβ peptides in the circulation or adipose tissue of the *Irx5*-KO mice, and we do not know whether these cleavage products contributed to the observed mitochondrial dysfunction. However, full-length App itself has also been shown to be translocated to the mitochondria, where it becomes trapped between the inner and outer mitochondrial membrane, leading to mitochondrial dysfunction [271,283]. Of note, this mechanism was very recently also observed in WAT and found to promote obesity [284]. Thus, the pro-adipogenic role of Irx5 is likely in part mediated by increased expression of *App*. In support of this, we also found App to inhibit the expression of *Pgc-1α* and *Ucp1*, thus negatively targeting both mitochondrial respiration as well as thermogenesis.

Increased thermogenic gene expression following *Irx5*-KO is further in line with the proposed role of IRX3 and IRX5 in promoting white over beige adipocyte development, as suggested by Claussnitzer et al. [117]. However, these findings are in stark contrast to the report by Zou et al. which suggested that Irx3 *promotes*

thermogenesis [242]. Unfortunately, these authors did not reveal any data on *Irx5* manipulation. Intriguingly, although the lentiviral-mediated reduction in Irx3 clearly inhibited transcription of *Ucp1* and *Pgc-1α*, as well as protein levels, at least for Pgc-1α, these changes did not translate into increased lipid accumulation. Instead, *Irx3*-kd significantly *reduced* lipid accumulation and *Pparγ* expression [242], indicating that Irx3 might play a role in regulating adipocyte differentiation, independently of its role on thermogenesis. Indeed, although displaying increased thermogenesis, the adipocyte-specific *Irx3*-DN mice reported by Claussnitzer et al. actually had reduced brown and beige (and white) adipose depot sizes, as shown in the supplementary figures S4D-F in [117].

5.2 Gene networks under control of Irx3

Due to the potential implications of Irx3 in beige adipogenesis, we next focused on Irx3 in paper II. Here, we employed the adipocyte cell line ME3, which are mouse embryonic fibroblasts committed to the beige lineage by ablation of the retinoblastoma (pRb) protein [285,286]. We found these cells to express relatively low levels of *Ucp1* in the basal state, but high levels following β-adrenergic stimulation by isoproterenol (iso), thus confirming a classic hallmark of beige adipocytes [137].

Adipogenic regulators

Strikingly, we found Irx3 to be critical for adipogenic identity. Stable knock-out of *Irx3* strongly suppressed adipogenesis, as evident by reduced lipid accumulation and abolished expression of the adipogenic master regulators *Pparγ* and *C/ebpα* [287]. Consequently, a wide range of other adipogenic markers, both general and brown/beige-specific genes were also downregulated, including *Pgc-1α* and *Ucp1* [287]. Thus, when analyzed in isolation, this result resembled the report by Zou et al., which claimed that Irx3 promotes browning [242]. However, our results clearly demonstrated that Irx3 did not promote browning over white adipogenesis, but rather targeted adipogenesis *per se*¸ as evident by the loss of preadipocyte identity in the

Irx3-KO cells [287]. Loss of Irx3 would therefore affect adipogenesis of both white and beige cells, thus partially reconciling the reported discrepancies on Irx3 function in adipose tissue. In agreement, and as mentioned above, the adipose-specific *Irx3*-DN mice displayed reductions in both white and brown fat depots [117]. Still, some adipocytes did differentiate in the *Irx3*-DN mice, and in *these* cells, *Pgc-1α* and *Ucp1* were likely upregulated due to relieved transcriptional repression by Irx3, independently of its control over adipogenesis. This suggests that there might exist certain populations of precursor cells that are capable of developing into adipocytes without the presence of Irx3. Whether this relies on developmental origin or biological niche is currently unknown.

Overall though, it appears that the timing of *Irx3* (and likely also *Irx5*) suppression is critical for the outcome on adipocyte biology; early repression blocks adipogenesis in general by loss of adipogenic identity, whereas later inhibition dictates whether the adipocyte will acquire white or beige adipocyte identity. The obesity-associated *FTO* variants that affect *IRX3* and *IRX5* expression were found to primarily affect adipocyte development, as the genotype effect was seen specifically during the first two days of adipogenesis of primary human adipose precursor cells from white adipose tissue [117].

Cell-cycle regulation

While Zou et al. reported increased expression levels of *Irx3* during the course of differentiation in their beige cells [242], we have only seen this expression profile during differentiation of white adipocytes, such as 3T3-L1 and primary white adipocytes from mice (unpublished data). In contrast, *Irx3* mRNA and protein levels peaked during early differentiation (days 0-1) in the ME3 cells [287]. During this early phase of differentiation, adipocytes undergo one to two rounds of cell division, a process known as mitotic clonal expansion (MCE), which is critical for the ability of most preadipocytes to undergo terminal differentiation [288]. Accordingly, we observed a spike in cell-cycle gene expression coinciding with peak *Irx3* and *Irx5* expression on day 1 of differentiation in the ME3 cells [287]. This observation caught our attention, as we previously found cell-cycle genes to be significantly

downregulated following siRNA-mediated knock-down of either *IRX3* or *IRX5* in human primary preadipocytes [287,289]. Moreover, other studies have also found IRX3 or IRX5 to be involved in cell-cycle regulation [235,236,290] and proliferation/cancer development [237]. We therefore hypothesized that Irx3 might control adipogenesis via MCE. In support of this hypothesis, we found preadipocytes with *Irx3*-KO to proliferate at a significantly lower rate compared to control cells due to increased G_0/G_1 retention [287]. However, on day 1 of differentiation, cell-cycle genes were significantly depleted among differentially expressed genes in *Irx3*-KO compared to control cells, meaning that these genes were significantly protected from the effect of *Irx3*-KO. These results indicate that MCE occurs independently of Irx3, at least in the ME3 cells.

Metabolic and morphogenic genes

Overall, about 3,500 and 6,700 genes were differentially expressed on days 1 and 7, respectively, in *Irx3*-KO compared to control cells. These genes are involved in a large number of pathways, including various developmental or morphogenic processes, reflecting the role of Irx3 in development and organogenesis. For example, loss of Irx3 lead to altered expression of genes involved in cardiac function, in line with its reported role in this organ [214,232–234]. Moreover, multiple genes with structural or regulatory roles in the extracellular matrix was strongly upregulated in the *Irx3*-KO cells, facilitating chondrogenesis. Finally, a plethora of genes involved in metabolic processes were downregulated on day 7 in the KO cells, including genes related to the TCA cycle, fatty acid metabolism, amino acid biosynthesis and thermogenesis. However, because Irx3 affected adipogenesis *per se*, we could not, based on gene expression data alone, fully establish which genes were directly controlled by Irx3, and which genes changed as a downstream, secondary effect of altered cell identity. Therefore, identifying *direct* target genes was needed to dissect specific actions of Irx proteins in adipose tissue.

5.3 Direct target genes of Irx3 and Irx5

Gene transcription from promoters are modulated by enhancers, which play a major role in dictating when and in which cells a gene is expressed [291–295]. Because different enhancers regulate the same gene at specific developmental stages and tissues, the total number of enhancers (up to 400,000) greatly outnumbers the protein coding genes (~20,000) [291]. We therefore hypothesized that Irx3 would bind to a large number of enhancers to regulate lineage determination. Unexpectedly, we found Irx3 to bind almost exclusively to promoter regions, and these binding sites were strongly enriched at transcription start sites (TSS) [287]. Although surprising, this discovery enabled us to immediately map virtually all Irx3 binding sites directly to a target gene, eliminating the need for complex computational and functional analyses.

We found that the target genes were related to several biological processes, but a particular enrichment was observed for genes involved in chromatin remodeling, mitochondrial translation and mRNA processing [287]. Furthermore, when overlapping the genes bound by Irx3 with differentially expressed genes following *Irx3*-KO, the same categories were enriched. One such target gene was the chromatin remodeler *Lysine demethylase 3a* (*Kdm3a*), which removes methyl groups specifically from repressive H3K9me2 histone tails. Intriguingly, Kdm3a has previously been shown to promote beiging and thermogenesis by removal of this repressive mark from the promoter of *Ucp1* [284,285]. We observed changes in both mRNA and protein levels, as well as catalytic activity of Kdm3a on the *Ucp1* promoter in response to knockout or knockdown of *Irx3* in mouse and human cells, respectively, illustrating how Irx3 may exert control over *Ucp1*, and likely other genes, via epigenetic remodeling.

Irx3 thus appears to indirectly control gene expression and translation at multiple levels; first, by manipulation of chromatin remodelers, Irx3 exerts influence over the global genetic landscape, potentially dictating lineage specification by determining which promoters are available for transcription. Second, by regulating levels of transcriptional co-regulators and genes controlling RNA stability, Irx3 appears to fine-

tune the expression and translation of genes in the open chromatin. Taken together, this may explain why perturbation of a relatively low number of direct Irx3 target genes (~300) following *Irx3*-KO could change the expression of more than 6,000 downstream genes, resulting in altered cell identity. Moreover, our findings provide compelling evidence for Irx3-mediated epigenetic remodeling as a likely explanation for how the activity of the enhancer in intron 1 of *FTO*, which affects IRX3 and IRX5 expression only at an early stage of adipogenesis, can lead to altered adipocyte identity and thermogenesis specifically in the mature state.

Additionally, many of the direct Irx3 target genes serve multiple roles. For example, the *Prohibitin 2* (*Phb2*) gene encodes a coordinator protein that can translocate between different cellular compartments, serving multiple, distinct roles [296]. While *Phb2* located in mitochondrial are crucial for mitochondrial stability and function, this protein can translocate to the nucleus following estrogen signaling to block estrogen-receptor-mediated transcription by recruitment of epigenetic repressors [296–300]. Indeed, *Phb2* has been found to mediate cross-talk between different compartments and thereby regulate multiple cellular processes, including metabolism, mitochondrial biogenesis and function, cell division and survival [297]. Interestingly, *Phb2* also promotes *Pparγ* expression, and *Phb2* ablation leads to loss of mitochondrial function, changes in ROS generation and inhibition of adipogenesis [296], a phenotype highly similar to *Irx3*-KO cells that exhibit reduced *Phb2* levels.

6. Conclusions

In the present study, we have found Irx3 and Irx5 to have a profound impact on adipocyte biology and whole-body metabolism:

Mice with global knock-out of *Irx5* were lean, with profound fat loss and protection from diet-induced obesity. This was partially attributable to improved mitochondrial respiration and thermogenesis specifically in adipocytes following changes in gene networks centered on *App*.

Adipocyte precursor cells with stable knock-out of *Irx3* lost their preadipocyte identity, were incapable of adipogenic differentiation, and displayed altered cell-cycle progression, ROS generation and mitochondrial respiration. More than 6,000 genes, enriched in genes with GO terms related to metabolism, ECM regulation, chondrocyte differentiation and morphogenic processes, were differentially expressed following *Irx3*-KO. These changes could be attributed to altered expression of about 300 direct Irx3 target genes controlling several biological pathways. Among these, chromatin remodeling, transcription and translation were most strongly and significantly enriched.

Overall, genetic repression of *Irx3* or *Irx5* offered strong protection against obesity, reducing adipose tissue mass partially by increasing thermogenesis and improving mitochondrial respiration in existing adipocytes, and partially by preventing the formation of new adipocytes.

7. Future perspectives

While we have shed new light on the functions of Irx3 and Irx5 in adipose tissue and whole-body homeostasis in this study, reconciling some of the reported discrepancies, further questions remain. Particularly, how some adipocytes depend on Irx3 or Irx5 to maintain their identity, whereas others apparently do not, is not clear, although different developmental origin of precursor cells might be an explanation. Thus, lineage tracing studies in mice could aid in clarifying the context-dependent effects of perturbed *Irx3* and *Irx5* expression.

Moreover, data from additional KO mouse models would be valuable, particularly adipose-specific *Irx5*-KO, and ideally adipose-specific *inducible* KO of *Irx3* and *Irx5* alone or in combination. While embryonic double KO is lethal, inducible double KO postnatally results in viable mice. Finally, to better understand the mechanisms underlying the enhancer-mediated regulation of *Irx3* and *Irx5*, as well as the effect on adipocytes in different depots and whole-body energy homeostasis, generating mouse lines that recapitulate the human risk and non-risk genotype at rs1421085 would be valuable.

Identifying the direct target genes of Irx5 has proved challenging due to lack of antibodies of sufficient quality. As an alternative, one may use CRISPR-Cas9 to tag endogenous *Irx5* with, for example, the myk-ddk/FLAG tag for which ChIP-seq grade antibodies are available. However, despite the small size of a FLAG tag, it may still interfere with protein folding or function, thus careful considerations must be made prior to this approach.

Finally, analyzing more histone marks and chromatin remodeling enzymes by Western Blotting, ELISA and ChIP, as well as investigating higher-order chromatin by promoter capture Hi-C in multiple adipocyte cell lines with and without *Irx3*-KO, would further substantiate our findings in paper III.

8. References

1. WHO. Obesity and overweight Key facts. Fact Sheet No 311 2015.

2. WHO. Obesity: preventing and managing the global epidemic. Report of a WHO consultation. World Heal Organ - Tech Rep Ser 2000;894:1–253.

3. Despres JP, Nadeau A, Tremblay A, Ferland M, Moorjani S, Lupien PJ, et al. Role of deep abdominal fat in the association between regional adipose tissue distribution and glucose tolerance in obese women. Diabetes 1989;38:304–9.

4. Pouliot MC, Després JP, Nadeau A, Moorjani S, Prud'Homme D, Lupien PJ, et al. Visceral obesity in men: Associations with glucose tolerance, plasma insulin, and lipoprotein levels. Diabetes 1992;41:826–34.

5. Wajchenberg BL. Subcutaneous and visceral adipose tissue: Their relation to the metabolic syndrome. Endocr Rev 2000;21:697–738.

6. Janssen I, Katzmarzyk PT, Ross R. Waist circumference and not body mass index explains obesity-related health risk. Am J Clin Nutr 2004;79:379–84.

7. Zhang C, Rexrode KM, Van Dam RM, Li TY, Hu FB. Abdominal obesity and the risk of all-cause, cardiovascular, and cancer mortality: Sixteen years of follow-up in US women. Circulation 2008;117:1658–67.

8. Després JP, Lemieux I. Abdominal obesity and metabolic syndrome. Nature 2006;444:881–7.

9. Balkau B, Deanfield JE, Després JP, Bassand JP, Fox KAA, Smith SC, et al. International day for the evaluation of abdominal obesity (IDEA): A study of waist circumference, cardiovascular disease, and diabetes mellitus in 168 000 primary care patients in 63 countries. Circulation 2007;116:1942–51.

10. Krotkiewski M, Bjorntorp P, Sjostrom L, Smith U. Impact of obesity on metabolism in men and women. Importance of regional adipose tissue distribution. J Clin Invest 1983;72:1150–62.

11. Lee MJ, Wu Y, Fried SK. Adipose tissue heterogeneity: Implication of depot differences in adipose tissue for obesity complications. Mol Aspects Med 2013;34:1–11.

12. Bouchard C, Despreis JP, Maurieige P. Genetic and nongenetic determinants of regional fat distribution. Endocr Rev 1993;14:72–93.

13. Lean MEJ, Han TS, Morrison CE. Waist circumference as a measure for indicating need for weight management. BMJ 1995;311:158–61.

14. Shungin D, Winkler TW, Croteau-Chonka DC, Ferreira T, Locke AE, Mägi R,

et al. New genetic loci link adipose and insulin biology to body fat distribution. Nature 2015;518:187–96.

15. Visscher TL, Seidell JC. The Public Health Impact of Obesity. Annu Rev Public Health 2001;22:355–75.

16. Pouliot MC, Després JP, Lemieux S, Moorjani S, Bouchard C, Tremblay A, et al. Waist circumference and abdominal sagittal diameter: Best simple anthropometric indexes of abdominal visceral adipose tissue accumulation and related cardiovascular risk in men and women. Am J Cardiol 1994;73:460–8.

17. Han TS, Van Leer EM, Seidell JC, Lean MEJ. Waist circumference action levels in the identification of cardiovascular risk factors: Prevalence study in a random sample. BMJ 1995;311:1401–5.

18. Di Cesare M, Bentham J, Stevens GA, Zhou B, Danaei G, Lu Y, et al. Trends in adult body-mass index in 200 countries from 1975 to 2014: A pooled analysis of 1698 population-based measurement studies with 19.2 million participants. Lancet 2016;387:1377–96.

19. Ng M, Fleming T, Robinson M, Thomson B, Graetz N, Margono C, et al. Global, regional, and national prevalence of overweight and obesity in children and adults during 1980-2013: A systematic analysis for the Global Burden of Disease Study 2013. Lancet 2014;383:766–81.

20. Flegal KM, Kruszon-Moran D, Carroll MD, Fryar CD, Ogden CL. Trends in Obesity Among Adults in the United States, 2005 to 2014. Jama 2016;315:2284.

21. HUNT4 2019. https://www.ntnu.no/hunt/hunt4 (accessed November 6, 2019).

22. WHO. Prevalence of obesity among adults, BMI ≥ 30, age-standardized Estimates by country 2017. http://apps.who.int (accessed November 5, 2019).

23. Adams KF, Schatzkin A, Harris TB, Kipnis V, Mouw T, Ballard-Barbash R, et al. Overweight, obesity, and mortality in a large prospective cohort of persons 50 to 71 years old. N Engl J Med 2006;355:763–78.

24. Katzmarzyk PT, Janssen I, Ardern CI. Physical inactivity, excess adiposity and premature mortality. Obes Rev 2003;4:257–90.

25. Di Angelantonio E. Body-mass index and all-cause mortality: individual-participant-data meta-analysis of 239 prospective studies in four continents. Lancet 2016;388:776–86.

26. McGee DL. Body mass index and mortality: A meta-analysis based on person-level data from twenty-six observational studies. Ann Epidemiol 2005;15:87–97.

27. De Gonzalez AB, Hartge P, Cerhan JR, Flint AJ, Hannan L, MacInnis RJ, et al. Body-mass index and mortality among 1.46 million white adults. N Engl J Med

2010;363:2211–9.

28. Tsigos C, Hainer V, Basdevant A, Finer N, Mathus-Vliegen E, Micic D, et al. Criteria for EASO-Collaborating Centres for Obesity Management. Obes Facts 2011;4:329–33.

29. Frühbeck G, Toplak H, Woodward E, Yumuk V, Maislos M, Oppert JM. Obesity: The gateway to ill health - An EASO position statement on a rising public health, clinical and scientific challenge in Europe. Obes Facts 2013;6:117–20.

30. Wolf A, Colditz GA. Current estimates of the economic cost of obesity in the United States. Obes Res 1998;6:97–106.

31. Yang W, Dall TM, Beronjia K, Lin J, Semilla AP, Chakrabarti R, et al. Economic costs of diabetes in the U.S. in 2017. Diabetes Care 2018;41:917–28.

32. Ruiz PLD, Stene LC, Bakken IJ, Håberg SE, Birkeland KI, Gulseth HL. Decreasing incidence of pharmacologically and non-pharmacologically treated type 2 diabetes in Norway: a nationwide study. Diabetologia 2018;61:2310–8.

33. Haslam D, James WP. Seminar - Obesity. Lancet 2005;366:1197–209.

34. Van Der Klaauw AA, Farooqi IS. The hunger genes: Pathways to obesity. Cell 2015;161:119–32.

35. Rosen ED, Spiegelman BM. What we talk about when we talk about fat. Cell 2014;156:20–44.

36. Heymsfield SB, Wadden TA. Mechanisms, Pathophysiology, and Management of Obesity. N Engl J Med 2017;376:254–66.

37. Roden M, Shulman GI. The integrative biology of type 2 diabetes. Nature 2019;576:51–60.

38. Polyzos SA, Kountouras J, Mantzoros CS. Obesity and nonalcoholic fatty liver disease: From pathophysiology to therapeutics. Metabolism 2019;92:82–97.

39. Kahn SE, Cooper ME, Del Prato S. Pathophysiology and treatment of type 2 diabetes: Perspectives on the past, present, and future. Lancet 2014;383:22–8.

40. Stăácaková A, Javorský M, Kuulasmaa T, Haffner SM, Kuusisto J, Laakso M. Changes in insulin sensitivity and insulin release in relation to glycemia and glucose tolerance in 6,414 finnish men. Diabetes 2009;58:1212–21.

41. Weyer C, Bogardus C, Mott DM, Pratley RE. The natural history of insulin secretory dysfunction and insulin resistance in the pathogenesis of type 2 diabetes mellitus. J Clin Invest 1999;104:787–94.

42. Kahn SE, Lachin JM, Zinman B, Haffner SM, Aftring RP, Paul G, et al. Effects of rosiglitazone, glyburide, and metformin on β-cell function and insulin sensitivity in ADOPT. Diabetes 2011;60:1552–60.

43. Genuth S, Alberti KGMM, Bennett P, Buse J, DeFronzo R, Kahn R, et al. Follow-up Report on the Diagnosis of Diabetes Mellitus. Diabetes Care 2003;26:3160–7.

44. WHO. Use of Glycated Haemoglobin (HbA1c) in the Diagnosis of Diabetes Mellitus. Geneva: 2011.

45. Cade WT. Diabetes-Related Microvascular and Macrovascular Diseases in the Physical Therapy Setting. Phys Ther 2008;88:1322–35.

46. Dyck PJ, Kratz KM, Karnes JL, Litchy WJ, Klein R, Pach JM, et al. The prevalence by staged severity of various types of diabetic neuropathy, retinopathy, and nephropathy in a population-based cohort: The rochester diabetic neuropathy study. Neurology 1993;43:817–24.

47. Drummond K, Mauer M. The early natural history of nephropathy in type 1 diabetes: II. Early renal structural changes in type 1 diabetes. Diabetes 2002;51:1580–7.

48. Laakso M. Hyperglycemia and cardiovascular disease in type 2 diabetes. Diabetes 1999;48:937–42.

49. Libby P, Buring JE, Badimon L, Hansson GK, Deanfield J, Bittencourt MS, et al. Atherosclerosis. Nat Rev Dis Prim 2019;5:56.

50. Lim S, Meigs JB. Links between ectopic fat and vascular disease in humans. Arterioscler Thromb Vasc Biol 2014;34:1820–6.

51. Heni M, Machann J, Staiger H, Schwenzer NF, Peter A, Schick F, et al. Pancreatic fat is negatively associated with insulin secretion in individuals with impaired fasting glucose and/or impaired glucose tolerance: A nuclear magnetic resonance study. Diabetes Metab Res Rev 2010;26:200–5.

52. Tushuizen ME, Bunck MC, Pouwels PJ, Bontemps S, Van Waesberghe JHT, Schindhelm RK, et al. Pancreatic fat content and β-cell function in men with and without type 2 diabetes. Diabetes Care 2007;30:2916–21.

53. Hall KD, Guo J, Dore M, Chow CC. The progressive increase of food waste in America and its environmental impact. PLoS One 2009;4:e7940.

54. Popkin BM, Hawkes C. Sweetening of the global diet, particularly beverages: Patterns, trends, and policy responses. Lancet Diabetes Endocrinol 2016;4:174–86.

55. Hall KD, Ayuketah A, Brychta R, Cai H, Cassimatis T, Chen KY, et al. Ultra-

Processed Diets Cause Excess Calorie Intake and Weight Gain: An Inpatient Randomized Controlled Trial of Ad Libitum Food Intake. Cell Metab 2019;30:67-77.e3.

56. Wadden TA, Webb VL, Moran CH, Bailer BA. Lifestyle modification for obesity: New developments in diet, physical activity, and behavior therapy. Circulation 2012;125:1157–70.

57. Hruby A, Hu FB. The Epidemiology of Obesity: A Big Picture. Pharmacoeconomics 2015;33:673–89.

58. Church TS, Thomas DM, Tudor-Locke C, Katzmarzyk PT, Earnest CP, Rodarte RQ, et al. Trends over 5 decades in U.S. occupation-related physical activity and their associations with obesity. PLoS One 2011;6:e19657.

59. von Loeffelholz C, Birkenfeld A. The Role of Non-exercise Activity Thermogenesis in Human Obesity. Endotext 2000.

60. Galton Sir, F. Natural inheritance,. New York: Macmillan and co.; 1894.

61. Allison DB, Kaprio J, Korkeila M, Koskenvuo M, Neale MC, Hayakawa K. The heritability of body mass index among an international sample of monozygotic twins reared apart. Int J Obes Relat Metab Disord 1996;20:501–6.

62. Maes HHM, Neale MC, Eaves LJ. Genetic and environmental factors in relative body weight and human adiposity. Behav Genet 1997;27:325–51.

63. Zaitlen N, Kraft P, Patterson N, Pasaniuc B, Bhatia G, Pollack S, et al. Using Extended Genealogy to Estimate Components of Heritability for 23 Quantitative and Dichotomous Traits. PLoS Genet 2013;9:e1003520.

64. Silventoinen K, Magnusson PKE, Tynelius P, Kaprio J, Rasmussen F. Heritability of body size and muscle strength in young adulthood: A study of one million Swedish men. Genet Epidemiol 2008;32:341–9.

65. Bouchard C, Tremblay A, Després JP, Nadeau A, Lupien PJ, Thériault G, et al. The Response to Long-Term Overfeeding in Identical Twins. N Engl J Med 1990;322:1477–82.

66. Bouchard C, Tremblay A, Després JP, Nadeau A, Lupien PJ, Moorjani S, et al. Overfeeding in identical twins: 5-Year postoverfeeding results. Metabolism 1996;45:1042–50.

67. Pigeyre M, Yazdi FT, Kaur Y, Meyre D. Recent progress in genetics, epigenetics and metagenomics unveils the pathophysiology of human obesity. Clin Sci 2016;130:943–86.

68. Farooqi IS, Yeo GSH, Keogh JM, Aminian S, Jebb SA, Butler G, et al. Dominant and recessive inheritance of morbid obesity associate with melanocortin 4

receptor deficiency. J Clin Invest 2000;106:271–9.

69. Vaisse C, Clement K, Durand E, Hercberg S, Guy-Grand B, Froguel P. Melanocortin-4 receptor mutations are a frequent and heterogeneous cause of morbid obesity. J Clin Invest 2000;106:253–62.

70. Greely HT. The Uneasy Ethical and Legal Underpinnings of Large-Scale Genomic Biobanks. Annu Rev Genomics Hum Genet 2007;8:343–64.

71. Gibbs RA, Belmont JW, Hardenbol P, Willis TD, Yu F, Yang H, et al. The international HapMap project. Nature 2003.

72. Barroso I, McCarthy MI. The Genetic Basis of Metabolic Disease. Cell 2019;177:146–61.

73. Sladek R, Rocheleau G, Rung J, Dina C, Shen L, Serre D, et al. A genome-wide association study identifies novel risk loci for type 2 diabetes. Nature 2007;445:881–5.

74. Zeggini E, Weedon MN, Lindgren CM, Frayling TM, Elliott KS, Lango H, et al. Replication of genome-wide association signals in UK samples reveals risk loci for type 2 diabetes. Science (80-) 2007;316:1336–41.

75. Saxena R, Voight BF, Lyssenko V, Burtt NP, De Bakker PIW, Chen H, et al. Genome-wide association analysis identifies loci for type 2 diabetes and triglyceride levels. Science (80-) 2007;316:1331–6.

76. Scott LJ, Mohlke KL, Bonnycastle LL, Willer CJ, Li Y, Duren WL, et al. A genome-wide association study of type 2 diabetes in finns detects multiple susceptibility variants. Science (80-) 2007;316:1341–5.

77. Frayling TM, Timpson NJ, Weedon MN, Zeggini E, Freathy RM, Lindgren CM, et al. A common variant in the FTO gene is associated with body mass index and predisposes to childhood and adult obesity. Science (80-) 2007;316:889–94.

78. Scott RA, Lagou V, Welch RP, Wheeler E, Montasser ME, Luan J, et al. Large-scale association analyses identify new loci influencing glycemic traits and provide insight into the underlying biological pathways. Nat Genet 2012;44:991–1005.

79. Locke AE, Kahali B, Berndt SI, Justice AE, Pers TH, Day FR, et al. Genetic studies of body mass index yield new insights for obesity biology. Nature 2015;518:197–206.

80. Klarin D, Damrauer SM, Cho K, Sun Y V., Teslovich TM, Honerlaw J, et al. Genetics of blood lipids among ~300,000 multi-ethnic participants of the Million Veteran Program. Nat Genet 2018;50:1514–23.

81. Mahajan A, Taliun D, Thurner M, Robertson NR, Torres JM, Rayner NW, et al.

Fine-mapping type 2 diabetes loci to single-variant resolution using high-density imputation and islet-specific epigenome maps. Nat Genet 2018;50:1505–13.

82. Manolio TA, Collins FS, Cox NJ, Goldstein DB, Hindorff LA, Hunter DJ, et al. Finding the missing heritability of complex diseases. Nature 2009;461:747–53.

83. Lupski JR, Belmont JW, Boerwinkle E, Gibbs RA. Clan genomics and the complex architecture of human disease. Cell 2011;147:32–43.

84. Fuchsberger C, Flannick J, Teslovich TM, Mahajan A, Agarwala V, Gaulton KJ, et al. The genetic architecture of type 2 diabetes. Nature 2016;536:41–7.

85. Yang J, Bakshi A, Zhu Z, Hemani G, Vinkhuyzen AAE, Lee SH, et al. Genetic variance estimation with imputed variants finds negligible missing heritability for human height and body mass index. Nat Genet 2015;47:1114–20.

86. Califano A, Butte AJ, Friend S, Ideker T, Schadt E. Leveraging models of cell regulation and GWAS data in integrative network-based association studies. Nat Genet 2012;44:841–7.

87. Herman MA, Rosen ED. Making biological sense of GWAS data: Lessons from the FTO locus. Cell Metab 2015;22:538–9.

88. Mahajan A, Wessel J, Willems SM, Zhao W, Robertson NR, Chu AY, et al. Refining the accuracy of validated target identification through coding variant fine-mapping in type 2 diabetes article. Nat Genet 2018;50:559–71.

89. Consortium T 1000 GP, McVean GA, Altshuler (Co-Chair) DM, Durbin (Co-Chair) RM, Abecasis GR, Bentley DR, et al. An integrated map of genetic variation from 1,092 human genomes. Nature 2012;491:56–65.

90. Ragvin A, Moro E, Fredman D, Navratilova P, Drivenes O, Engstrom PG, et al. Long-range gene regulation links genomic type 2 diabetes and obesity risk regions to HHEX, SOX4, and IRX3. Proc Natl Acad Sci 2010;107:775–80.

91. Schoenfelder S, Fraser P. Long-range enhancer–promoter contacts in gene expression control. Nat Rev Genet 2019;20:437–55.

92. Mahajan A, Sim X, Ng HJ, Manning A, Rivas MA, Highland HM, et al. Identification and Functional Characterization of G6PC2 Coding Variants Influencing Glycemic Traits Define an Effector Transcript at the G6PC2-ABCB11 Locus. PLoS Genet 2015;11:e1004876.

93. Wessel J, Chu AY, Willems SM, Wang S, Yaghootkar H, Brody JA, et al. Low-frequency and rare exome chip variants associate with fasting glucose and type 2 diabetes susceptibility. Nat Commun 2015;6:5897.

94. Loos RJF, Yeo GSH. The bigger picture of FTO - The first GWAS-identified obesity gene. Nat Rev Endocrinol 2014;10:51–61.

95. Speliotes EK, Willer CJ, Berndt SI, Monda KL, Thorleifsson G, Jackson AU, et al. Association analyses of 249,796 individuals reveal 18 new loci associated with body mass index. Nat Genet 2010;42:937–48.

96. Tung YCL, Yeo GSH, O'Rahilly S, Coll AP. Obesity and FTO: Changing focus at a complex locus. Cell Metab 2014;20:710–8.

97. Dina C, Meyre D, Gallina S, Durand E, Körner A, Jacobson P, et al. Variation in FTO contributes to childhood obesity and severe adult obesity. Nat Genet 2007;39:724–6.

98. Scuteri A, Sanna S, Chen WM, Uda M, Albai G, Strait J, et al. Genome-wide association scan shows genetic variants in the FTO gene are associated with obesity-related traits. PLoS Genet 2007;3:e115.

99. Gerken T, Girard CA, Tung YCL, Webby CJ, Saudek V, Hewitson KS, et al. The obesity-associated FTO gene encodes a 2-oxoglutarate-dependent nucleic acid demethylase. Science (80-) 2007;318:1469–72.

100. Cecil JE, Tavendale R, Watt P, Hetherington MM, Palmer CNA. An obesity-associated FTO gene variant and increased energy intake in children. N Engl J Med 2008;359:2558–66.

101. Speakman JR, Rance KA, Johnstone AM. Polymorphisms of the FTO gene are associated with variation in energy intake, but not energy expenditure. Obesity 2008;16:1961–5.

102. Timpson NJ, Emmett PM, Frayling TM, Rogers I, Hattersley AT, McCarthy MI, et al. The fat mass- and obesity-associated locus and dietary intake in children. Am J Clin Nutr 2008;88:971–8.

103. Park SL, Cheng I, Pendergrass SA, Kucharska-Newton AM, Lim U, Ambite JL, et al. Association of the FTO obesity risk variant rs8050136 with percentage of energy intake from fat in multiple racial/ethnic populations. Am J Epidemiol 2013;178:780–90.

104. Sonestedt E, Roos C, Gullberg B, Ericson U, Wirfält E, Orho-Melander M. Fat and carbohydrate intake modify the association between genetic variation in the FTO genotype and obesity. Am J Clin Nutr 2009;90:1418–25.

105. Wardle J, Carnell S, Haworth CMA, Farooqi IS, O'Rahilly S, Plomin R. Obesity associated genetic variation in FTO is associated with diminished satiety. J Clin Endocrinol Metab 2008;93:3640–3.

106. Wardle J, Llewellyn C, Sanderson S, Plomin R. The FTO gene and measured food intake in children. Int J Obes 2009;33:42–5.

107. Church C, Moir L, McMurray F, Girard C, Banks GT, Teboul L, et al. Overexpression of Fto leads to increased food intake and results in obesity. Nat

Genet 2010;42:1086–92.

108. Fischer J, Koch L, Emmerling C, Vierkotten J, Peters T, Brüning JC, et al. Inactivation of the Fto gene protects from obesity. Nature 2009;458:894–8.

109. Gao X, Shin YH, Li M, Wang F, Tong Q, Zhang P. The fat mass and obesity associated gene FTO functions in the brain to regulate postnatal growth in mice. PLoS One 2010;5:e14005.

110. Boissel S, Reish O, Proulx K, Kawagoe-Takaki H, Sedgwick B, Yeo GSH, et al. Loss-of-Function Mutation in the Dioxygenase-Encoding FTO Gene Causes Severe Growth Retardation and Multiple Malformations. Am J Hum Genet 2009;85:106–11.

111. Stratigopoulos G, Padilla SL, LeDuc CA, Watson E, Hattersley AT, McCarthy MI, et al. Regulation of Fto/Ftm gene expression in mice and humans. Am J Physiol - Regul Integr Comp Physiol 2008;294:R1185-96.

112. Stratigopoulos G, LeDuc CA, Cremona ML, Chung WK, Leibel RL. Cut-like homeobox 1 (CUX1) regulates expression of the fat mass and obesity-associated and retinitis pigmentosa GTPase regulator-interacting protein-1-like (RPGRIP1L) genes and coordinates leptin receptor signaling. J Biol Chem 2011;286:2155–70.

113. Smemo S, Tena JJ, Kim K-H, Gamazon ER, Sakabe NJ, Gómez-Marín C, et al. Obesity-associated variants within FTO form long-range functional connections with IRX3. Nature 2014;507:371–5.

114. Shungin D, Winkler TW, Croteau-Chonka DC, Ferreira T, Locke AE, Mägi R, et al. New genetic loci link adipose and insulin biology to body fat distribution. Nature 2015;518:187–96.

115. Claussnitzer M, Dankel SN, Klocke B, Grallert H, Glunk V, Berulava T, et al. Leveraging cross-species transcription factor binding site patterns: From diabetes risk loci to disease mechanisms. Cell 2014;156:343–58.

116. Visel A, Taher L, Girgis H, May D, Golonzhka O, Hoch R V., et al. A high-resolution enhancer atlas of the developing telencephalon. Cell 2013;152:895–908.

117. Claussnitzer M, Dankel SN, Kim K-H, Quon G, Meuleman W, Haugen C, et al. *FTO* Obesity Variant Circuitry and Adipocyte Browning in Humans. N Engl J Med 2015;373:895–907.

118. Herman MA, Rosen ED. Making biological sense of GWAS data: Lessons from the FTO locus. Cell Metab 2015;22:538–9.

119. Harms M, Seale P. Brown and beige fat: Development, function and therapeutic potential. Nat Med 2013;19:1252–63.

120. Bartelt A, Bruns OT, Reimer R, Hohenberg H, Ittrich H, Peldschus K, et al. Brown adipose tissue activity controls triglyceride clearance. Nat Med 2011;17:200–5.

121. Cederberg A, Gronning LM, Ahrén B, Taskén K, Carlsson P, Enerbäck S. FOXC2 is a winged helix gene that counteracts obesity, hypertriglyceridemia, and diet-induced insulin resistance. Cell 2001;106:563–73.

122. Feldmann HM, Golozoubova V, Cannon B, Nedergaard J. UCP1 Ablation Induces Obesity and Abolishes Diet-Induced Thermogenesis in Mice Exempt from Thermal Stress by Living at Thermoneutrality. Cell Metab 2009;9:203–9.

123. Seale P, Conroe HM, Estall J, Kajimura S, Frontini A, Ishibashi J, et al. Prdm16 determines the thermogenic program of subcutaneous white adipose tissue in mice. J Clin Invest 2011;121:96–105.

124. Kopecky J, Clarke G, Enerbäck S, Spiegelman B, Kozak LP. Expression of the mitochondrial uncoupling protein gene from the aP2 gene promoter prevents genetic obesity. J Clin Invest 1995;96:2914–23.

125. Qiang L, Wang L, Kon N, Zhao W, Lee S, Zhang Y, et al. Brown remodeling of white adipose tissue by SirT1-dependent deacetylation of Pparγ. Cell 2012;150:620–32.

126. Boström P, Wu J, Jedrychowski MP, Korde A, Ye L, Lo JC, et al. A PGC1-α-dependent myokine that drives brown-fat-like development of white fat and thermogenesis. Nature 2012;481:463–8.

127. Collins S, Daniel KW, Petro AE, Surwit RS. Strain-specific response to β3-adrenergic receptor agonist treatment of diet-induced obesity in mice. Endocrinology 1997;138:405–13.

128. Guerra C, Koza RA, Yamashita H, Walsh K, Kozak LP. Emergence of brown adipocytes in white fat in mice is under genetic control effects on body weight and adiposity. J Clin Invest 1998;102:412–20.

129. Stanford KI, Middelbeek RJ, Townsend KL, An D, Nygaard EB, Hitchcox KM, et al. Brown adipose tissue regulates glucose homeostasis and insulin sensitivity. J Clin Invest 2013;123:215–23.

130. Lowell BB, S-Susulic V, Hamann A, Lawitts J a, Himms-Hagen J, Boyer BB, et al. Development of obesity in transgenic mice after genetic ablation of brown adipose tissue. Nature 1993;366:740–2.

131. Cypess AM, Lehman S, Williams G, Tal I, Rodman D, Goldfine AB, et al. Identification and Importance of Brown Adipose Tissue in Adult Humans. N Engl J Med 2009;360:1509–17.

132. van Marken Lichtenbelt WD, Vanhommerig JW, Smulders NM, Drossaerts

JMAFL, Kemerink GJ, Bouvy ND, et al. Cold-activated brown adipose tissue in healthy men. N Engl J Med 2009;360:1500–8.

133. Saito M, Okamatsu-ogura Y, Matsushita M, Watanabe K, Yoneshiro T, Nio-kobayashi J, et al. High Incidence of Metabolically Active Brown Adipose Effects of Cold Exposure and Adiposity. Diabetes 2009;58:1526–31.

134. Hany TF, Gharehpapagh E, Kamel EM, Buck A, Himms-Hagen J, Von Schulthess GK. Brown adipose tissue: A factor to consider in symmetrical tracer uptake in the neck and upper chest region. Eur J Nucl Med 2002;29:1393–8.

135. Virtanen KA, Lidell ME, Orava J, Heglind M, Westergren R, Niemi T, et al. Functional brown adipose tissue in healthy adults. N Engl J Med 2009;360:1518–25.

136. Shabalina IG, Petrovic N, DeJong JMA, Kalinovich A V., Cannon B, Nedergaard J. UCP1 in Brite/Beige adipose tissue mitochondria is functionally thermogenic. Cell Rep 2013;5:1196–203.

137. Wu J, Boström P, Sparks LM, Ye L, Choi JH, Giang AH, et al. Beige adipocytes are a distinct type of thermogenic fat cell in mouse and human. Cell 2012;150:366–76.

138. Chondronikola M, Volpi E, Børsheim E, Porter C, Annamalai P, Enerbäck S, et al. Brown adipose tissue improves whole-body glucose homeostasis and insulin sensitivity in humans. Diabetes 2014;63:4089–99.

139. Orava J, Nuutila P, Noponen T, Parkkola R, Viljanen T, Enerbäck S, et al. Blunted metabolic responses to cold and insulin stimulation in brown adipose tissue of obese humans. Obesity 2013;21:2279–87.

140. Ouellet V, Routhier-Labadie A, Bellemare W, Lakhal-Chaieb L, Turcotte E, Carpentier AC, et al. Outdoor temperature, age, sex, body mass index, and diabetic status determine the prevalence, mass, and glucose-uptake activity of18F-FDG-detected BAT in humans. J Clin Endocrinol Metab 2011;96:192–9.

141. Yoneshiro T, Aita S, Matsushita M, Kayahara T, Kameya T, Kawai Y, et al. Recruited brown adipose tissue as an antiobesity agent in humans. J Clin Invest 2013;123:3404–8.

142. Van Der Lans AAJJ, Hoeks J, Brans B, Vijgen GHEJ, Visser MGW, Vosselman MJ, et al. Cold acclimation recruits human brown fat and increases nonshivering thermogenesis. J Clin Invest 2013;123:3395–403.

143. Lee P, Smith S, Linderman J, Courville AB, Brychta RJ, Dieckmann W, et al. Temperature-acclimated brown adipose tissue modulates insulin sensitivity in humans. Diabetes 2014;63:3686–98.

144. Hanssen MJ, Hoeks J, Brans B, van der Lans AA, Schaart G, van den Driessche

JJ, et al. Short-term cold acclimation improves insulin sensitivity in patients with type 2 diabetes mellitus. Nat Med 2015;21:863–5.

145. Hanssen MJW, Van Der Lans AAJJ, Brans B, Hoeks J, Jardon KMC, Schaart G, et al. Short-term cold acclimation recruits brown adipose tissue in obese humans. Diabetes 2016;65:1179–89.

146. Lee P, Bova R, Schofield L, Bryant W, Dieckmann W, Slattery A, et al. Brown Adipose Tissue Exhibits a Glucose-Responsive Thermogenic Biorhythm in Humans. Cell Metab 2016;23:602–9.

147. Inagaki T, Sakai J, Kajimura S. Transcriptional and epigenetic control of brown and beige adipose cell fate and function. Nat Rev Mol Cell Biol 2016;17:480–95.

148. Seale P, Bjork B, Yang W, Kajimura S, Chin S, Kuang S, et al. PRDM16 controls a brown fat/skeletal muscle switch. Nature 2008;454:961–7.

149. Seale P, Kajimura S, Yang W, Chin S, Rohas LM, Uldry M, et al. Transcriptional Control of Brown Fat Determination by PRDM16. Cell Metab 2007;6:38–54.

150. Rosenwald M, Perdikari A, Rülicke T, Wolfrum C. Bi-directional interconversion of brite and white adipocytes. Nat Cell Biol 2013;15:659–67.

151. Wang QA, Tao C, Gupta RK, Scherer PE. Tracking adipogenesis during white adipose tissue development, expansion and regeneration. Nat Med 2013;19:1338–44.

152. Lee YH, Petkova AP, Mottillo EP, Granneman JG. In vivo identification of bipotential adipocyte progenitors recruited by β3-adrenoceptor activation and high-fat feeding. Cell Metab 2012;15:480–91.

153. Vitali A, Murano I, Zingaretti MC, Frontini A, Ricquier D, Cinti S. The adipose organ of obesity-prone C57BL/6J mice is composed of mixed white and brown adipocytes. J Lipid Res 2012;53:619–29.

154. Rosen ED, MacDougald OA. Adipocyte differentiation from the inside out. Nat Rev Mol Cell Biol 2006;7:885–96.

155. Garten A, Schuster S, Kiess W. The Insulin-Like Growth Factors in Adipogenesis and Obesity. Endocrinol Metab Clin North Am 2012;41:283–95.

156. Matsumura Y, Nakaki R, Inagaki T, Yoshida A, Kano Y, Kimura H, et al. H3K4/H3K9me3 Bivalent Chromatin Domains Targeted by Lineage-Specific DNA Methylation Pauses Adipocyte Differentiation. Mol Cell 2015;60:584–96.

157. Mikkelsen TS, Xu Z, Zhang X, Wang L, Gimble JM, Lander ES, et al. Comparative epigenomic analysis of murine and human adipogenesis. Cell 2010;103:156–69.

158. Rosen ED. The molecular control of adipogenesis, with special reference to lymphatic pathology. Ann. N. Y. Acad. Sci., 2002, p. 143–58, discussion 188-196.

159. Wu Z, Rosen ED, Brun R, Hauser S, Adelmant G, Troy AE, et al. Cross-regulation of C/EBP alpha and PPAR gamma controls the transcriptional pathway of adipogenesis and insulin sensitivity. Mol Cell 1999;3:151–8.

160. Park J, Scherer PE. Adipocyte-derived endotrophin promotes malignant tumor progression. J Clin Invest 2012;122:4243–56.

161. Rajakumari S, Wu J, Ishibashi J, Lim HW, Giang AH, Won KJ, et al. EBF2 determines and maintains brown adipocyte identity. Cell Metab 2013;17:562–74.

162. Siersbaek MS, Loft A, Aagaard MM, Nielsen R, Schmidt SF, Petrovic N, et al. Genome-Wide Profiling of Peroxisome Proliferator-Activated Receptor in Primary Epididymal, Inguinal, and Brown Adipocytes Reveals Depot-Selective Binding Correlated with Gene Expression. Mol Cell Biol 2012;32:3452–63.

163. Lefterova MI, Zhang Y, Steger DJ, Schupp M, Schug J, Cristancho A, et al. PPARγ and C/EBP factors orchestrate adipocyte biology via adjacent binding on a genome-wide scale. Genes Dev 2008;22:2941–52.

164. Lefterova MI, Steger DJ, Zhuo D, Qatanani M, Mullican SE, Tuteja G, et al. Cell-Specific Determinants of Peroxisome Proliferator-Activated Receptor Function in Adipocytes and Macrophages. Mol Cell Biol 2010;30:2078–89.

165. Ohno H, Shinoda K, Ohyama K, Sharp LZ, Kajimura S. EHMT1 controls brown adipose cell fate and thermogenesis through the PRDM16 complex. Nature 2013;504:163–7.

166. Giguère V. Transcriptional control of energy homeostasis by the estrogen-related receptors. Endocr Rev 2008;29:677–96.

167. Puigserver P, Spiegelman BM. Peroxisome proliferator-activated receptor-gamma coactivator 1 alpha (PGC-1 alpha): transcriptional coactivator and metabolic regulator. Endocr Rev 2003;24:78–90.

168. Puigserver P, Wu Z, Park CW, Graves R, Wright M, Spiegelman BM. A cold-inducible coactivator of nuclear receptors linked to adaptive thermogenesis. Cell 1998;92:829–39.

169. Tiraby C, Tavernier G, Lefort C, Larrouy D, Bouillaud F, Ricquier D, et al. Acquirement of brown fat cell features by human white adipocytes. J Biol Chem 2003;278:33370–6.

170. Uldry M, Yang W, St-Pierre J, Lin J, Seale P, Spiegelman BM. Complementary action of the PGC-1 coactivators in mitochondrial biogenesis and brown fat

differentiation. Cell Metab 2006;3:333–41.

171. Leone TC, Lehman JJ, Finck BN, Schaeffer PJ, Wende AR, Boudina S, et al. PGC-1α deficiency causes multi-system energy metabolic derangements: Muscle dysfunction, abnormal weight control and hepatic steatosis. PLoS Biol 2005;3:e101.

172. Kleiner S, Mepani RJ, Laznik D, Ye L, Jurczak MJ, Jornayvaz FR, et al. Development of insulin resistance in mice lacking PGC-1α in adipose tissues. Proc Natl Acad Sci U S A 2012;109:9635–40.

173. Lee P, Zhao JT, Swarbrick MM, Gracie G, Bova R, Greenfield JR, et al. High prevalence of brown adipose tissue in adult humans. J Clin Endocrinol Metab 2011;96:2450–5.

174. Ohno H, Shinoda K, Spiegelman BM, Kajimura S. PPARγ agonists induce a white-to-brown fat conversion through stabilization of PRDM16 protein. Cell Metab 2012;15:395–404.

175. Hondares E, Rosell M, Diaz-Delfin J, Olmos Y, Monsalve M, Iglesias R, et al. PPARα induces PGC-1α gene expression and contributes to the thermogenic activation of brown fat; involvement of PRDM16. J Biol Chem 2011;286:43112–22.

176. Kajimura S, Seale P, Kubota K, Lunsford E, Frangioni J V., Gygi SP, et al. Initiation of myoblast to brown fat switch by a PRDM16-C/EBP-β transcriptional complex. Nature 2009;460:1154–8.

177. Dankel SN, Fadnes DJ, Stavrum AK, Stansberg C, Holdhus R, Hoang T, et al. Switch from stress response to homeobox transcription factors in adipose tissue after profound fat loss. PLoS One 2010;5:e11033.

178. Bürglin TR, Affolter M. Homeodomain proteins: an update. Chromosoma 2016;125:497–521.

179. Gehring W. Homeodomain Proteins. Annu Rev Biochem 1994;63:487–526.

180. Burglin T. A comprehensive classification of homeobox genes. In: D.D., editor. Guideb. to Homeobox Genes, Oxford: Oxford University Press; 1994, p. 25–71.

181. Burglin T. Homeodomain proteins. Weinheim: Wiley-VCH Verlag GmbH & Co; 2005.

182. Holland PW, Booth HAF, Bruford EA. Classification and nomenclature of all human homeobox genes. BMC Biol 2007;5:47.

183. Apiou F, Flagiello D, Cillo C, Malfoy B, Poupon MF, Dutrillaux B. Fine mapping of human HOX gene clusters. Cytogenet Genome Res 1996;73:114–5.

184. Scott MP. Vertebrate homeobox gene nomenclature. Cell 1992;71:551–3.

185. Graham A, Papalopulu N, Krumlauf R. The murine and Drosophila homeobox gene complexes have common features of organization and expression. Cell 1989;57:367–78.

186. Dekker EJ, Pannese M, Houtzager E, Timmermans A, Boncinelli E, Durston A. Xenopus Hox-2 genes are expressed sequentially after the onset of gastrulation and are differentially inducible by retinoic acid. Development 1992:195–202.

187. Mortlock DP, Innis JW. Mutation of HOXA13 in hand-foot-genital syndrome. Nat Genet 1997;15:179–80.

188. Nakamura T, Largaespada DA, Lee MP, Johnson LA, Ohyashiki K, Toyama K, et al. Fusion of the nucleoporin gene NUP98 to HOXA9 by the chromosome translocation t(7;11)(p15;p15) in human myeloid leukaemia. Nat Genet 1996;12:154–8.

189. Cillo C, Cantile M, Faiella A, Boncinelli E. Homeobox genes in normal and malignant cells. J Cell Physiol 2001;188:161–9.

190. Ferber S, Halkin A, Cohen H, Ber I, Einav Y, Goldberg I, et al. Pancreatic and duodenal homeobox gene 1 induces expression of insulin genes in liver and ameliorates streptozotocin-induced hyperglycemia. Nat Med 2000;6:568–72.

191. Kroll TG, Sarraf P, Pecciarini L, Chen CJ, Mueller E, Spiegelman BM, et al. PAX8-PPARγ1 fusion in oncogene human thyroid carcinoma. Science (80-) 2000;289:1357–60.

192. Cantile M, Procino A, D'Armiento M, Cindolo L, Cillo C. HOX gene network is involved in the transcriptional regulation of in vivo human adipogenesis. J Cell Physiol 2003;194:225–36.

193. Gesta S, Blüher M, Yamamoto Y, Norris AW, Berndt J, Kralisch S, et al. Evidence for a role of developmental genes in the origin of obesity and body fat distribution. Proc Natl Acad Sci U S A 2006;103:6676–81.

194. Yamamoto Y, Gesta S, Lee KY, Tran TT, Saadatirad P, Kahn RC. Adipose depots possess unique developmental gene signatures. Obesity 2010;18:872–8.

195. Vohl MC, Sladek R, Robitaille J, Gurd S, Marceau P, Richard D, et al. A survey of genes differentially expressed in subcutaneous and visceral adipose tissue in men. Obes Res 2004;12:1217–22.

196. Karastergiou K, Fried SK, Xie H, Lee MJ, Divoux A, Rosencrantz MA, et al. Distinct developmental signatures of human abdominal and gluteal subcutaneous adipose tissue depots. J Clin Endocrinol Metab 2013;98:362–71.

197. Nakagami H. The mechanism of white and brown adipocyte differentiation.

Diabetes Metab J 2013;37:85–90.

198. Brune JE, Kern M, Kunath A, Flehmig G, Schön MR, Lohmann T, et al. Fat depot-specific expression of HOXC9 and HOXC10 may contribute to adverse fat distribution and related metabolic traits. Obesity 2016;24:51–9.

199. Bürglin TR. Analysis of TALE superclass homeobox genes (MEIS, PBC, KNOX, Iroquois, TGIF) reveals a novel domain conserved between plants and animals. Nucleic Acids Res 1997;25:4173–80.

200. Bürglin TR. Homeodomain subtypes and functional diversity. Subcell Biochem 2011;52:95–122.

201. Cavodeassi F, Modolell J, Gómez-Skarmeta JL. The Iroquois family of genes: from body building to neural patterning. Development 2001;128:2847–55.

202. McNeill H, Yang CH, Brodsky M, Ungos J, Simon MA. Mirror encodes a novel PBX-class homeoprotein that functions in the definition of the dorsal-ventral border in the Drosophila eye. Genes Dev 1997;11:1073–82.

203. Barrios N, Campuzano S. Expanding the Iroquois genes repertoire: a non-transcriptional function in cell cycle progression. Fly (Austin) 2015;9:126–31.

204. Bonnard C, Strobl AC, Shboul M, Lee H, Merriman B, Nelson SF, et al. Mutations in IRX5 impair craniofacial development and germ cell migration via SDF1. Nat Genet 2012;44:709–13.

205. Bilioni A, Craig G, Hill C, McNeill H. Iroquois transcription factors recognize a unique motif to mediate transcriptional repression in vivo. Proc Natl Acad Sci U S A 2005;102:14671–6.

206. Perovic S, Schroder HC, Sudek S, Grebenjuk VA, Batel R, Stifanic M, et al. Expression of one sponge Iroquois homeobox gene in primmorphs from Suberites domuncula during canal formation. Evol Dev 2003;5:240–50.

207. Bosse A, Stoykova A, Nieselt-Struwe K, Chowdhury K, Copeland NG, Jenkins NA, et al. Identification of a novel mouse iroquois homeobox gene, Irx5, and chromosomal localisation of all members of the mouse iroquois gene family. Dev Dyn 2000;218:160–74.

208. Bosse A, Zülch A, Becker MB, Torres M, Gómez-Skarmeta JL, Modolell J, et al. Identification of the vertebrate Iroquois homeobox gene family with overlapping expression during early development of the nervous system. Mech Dev 1997:169–81.

209. Kudoh T, Dawid IB. Role of the iroquois3 homeobox gene in organizer formation. Proc Natl Acad Sci 2001;98:7852–7.

210. Bellefroid EJ, Kobbe A, Gruss P, Pieler T, Gurdon JB, Papalopulu N. Xiro3

encodes a xenopus homolog of the Drosophila Iroquois genes and functions in neural specification. EMBO J 1998;17:191–203.

211. Gomez-Skarmeta JL. Xiro, a Xenopus homolog of the Drosophila Iroquois complex genes, controls development at the neural plate. EMBO J 1998;17:181–90.

212. Bao Z. Regulation of Chamber-Specific Gene Expression in the Developing Heart by Irx4. Science (80-) 1999;283:1161–4.

213. Costantini DL, Arruda EP, Agarwal P, Kim K-H, Zhu Y, Zhu W, et al. The homeodomain transcription factor Irx5 establishes the mouse cardiac ventricular repolarization gradient. Cell 2005;123:347–58.

214. Gaborit N, Sakuma R, Wylie JN, Kim K-H, Zhang S-S, Hui C-C, et al. Cooperative and antagonistic roles for Irx3 and Irx5 in cardiac morphogenesis and postnatal physiology. Development 2012;139:4007–19.

215. Cheng Z, Wang J, Su D, Pan H, Huang G, Li X, et al. Two novel mutations of the IRX4 gene in patients with congenital heart disease. Hum Genet 2011;130:657–62.

216. Bruneau BG, Bao ZZ, Tanaka M, Schott JJ, Izumo S, Cepko CL, et al. Cardiac expression of the ventricle-specific homeobox gene Irx4 is modulated by Nkx2-5 and dHand. Dev Biol 2000;217:266–77.

217. Bruneau BG, Bao Z-Z, Fatkin D, Xavier-Neto J, Georgakopoulos D, Maguire CT, et al. Cardiomyopathy in Irx4-Deficient Mice Is Preceded by Abnormal Ventricular Gene Expression. Mol Cell Biol 2001.

218. Wang GF, Nikovits W, Bao ZZ, Stockdale FE. Irx4 Forms an Inhibitory Complex with the Vitamin D and Retinoic X Receptors to Regulate Cardiac Chamber-specific slow MyHC3 Expression. J Biol Chem 2001;276:28835–41.

219. Reggiani L, Raciti D, Airik R, Kispert A, Brändli AW. The prepattern transcription factor Irx3 directs nephron segment identity. Genes Dev 2007;21:2358-70.

220. Dominguez M, de Celis JF. A dorsal/ventral boundary established by Notch controls growth and polarity in the Drosophila eye. Nature 1998;396:276–8.

221. Cho K-O, Choi K-W. Fringe is essential for mirror symmetry and morphogenesis in the Drosophila eye. Nature 1998;396:272–6.

222. Cavodeassi F, Diez Del Corral R, Campuzano S, Domínguez M. Compartments and organising boundaries in the Drosophila eye: The role of the homeodomain Iroquois proteins. Development 1999;126:4933–42.

223. Yang CH, Simon MA, McNeill H. mirror controls planar polarity and equator

formation through repression of fringe expression and through control of cell affinities. Development 1999;126:5857–66.

224. Cheng CW, Chow RL, Lebel M, Sakuma R, Cheung HOL, Thanabalasingham V, et al. The Iroquois homeobox gene, Irx5, is required for retinal cone bipolar cell development. Dev Biol 2005;287:48–60.

225. Jordan KC, Clegg NJ, Blasi JA, Morimoto AM, Sen J, Stein D, et al. The homeobox gene mirror links EGF signalling to embryonic dorso-ventral axis formation through Notch activation. Nat Genet 2000;24:429–33.

226. Jin Z. Irx4-mediated regulation of Slit1 expression contributes to the definition of early axonal paths inside the retina. Development 2003;130:1037–48.

227. Hueber SD, Lohmann I. Shaping segments: Hox gene function in the genomic age. BioEssays 2008;30:965–79.

228. Gómez-Skarmeta J, de La Calle-Mustienes E, Modolell J. The Wnt-activated Xiro1 gene encodes a repressor that is essential for neural development and downregulates Bmp4. Development 2001;128:551–60.

229. Itoh M, Kudoh T, Dedekian M, Kim C-H, Chitnis AB. A role for iro1 and iro7 in the establishment of an anteroposterior compartment of the ectoderm adjacent to the midbrain-hindbrain boundary. Development 2002;129:2317–27.

230. Matsumoto K, Nishihara S, Kamimura M, Shiraishi T, Otoguro T, Uehara M, et al. The prepattern transcription factor Irx2, a target of the FGF8/MAP kinase cascade, is involved in cerebellum formation. Nat Neurosci 2004;7:605–12.

231. Costantini DL, Arruda EP, Agarwal P, Kim K-H, Zhu Y, Zhu W, et al. The Homeodomain Transcription Factor Irx5 Establishes the Mouse Cardiac Ventricular Repolarization Gradient. Cell 2005;123:347–58.

232. Zhang S-S, Kim K-H, Rosen A, Smyth JW, Sakuma R, Delgado-Olguin P, et al. Iroquois homeobox gene 3 establishes fast conduction in the cardiac His-Purkinje network. Proc Natl Acad Sci 2011;108:13576–81.

233. Kim KH, Rosen A, Hussein SMI, Puviindran V, Korogyi AS, Chiarello C, et al. Irx3 is required for postnatal maturation of the mouse ventricular conduction system. Sci Rep 2016;6:19197.

234. Koizumi A, Sasano T, Kimura W, Miyamoto Y, Aiba T, Ishikawa T, et al. Genetic defects in a His-Purkinje system transcription factor, IRX3, cause lethal cardiac arrhythmias. Eur Heart J 2016;37:1469–75.

235. Myrthue A, Rademacher BLS, Pittsenbarger J, Kutyba-Brooks B, Gantner M, Qian DZ, et al. The iroquois homeobox gene 5 is regulated by 1,25-dihydroxyvitamin D3 in human prostate cancer and regulates apoptosis and the cell cycle in LNCaP prostate cancer cells. Clin Cancer Res 2008;14:3562–70.

236. Liu D, Pattabiraman V, Bacanamwo M, Anderson LM. Iroquois homeobox transcription factor (*Irx5*) promotes G 1 /S-phase transition in vascular smooth muscle cells by CDK2-dependent activation. Am J Physiol - Cell Physiol 2016;311:C179–89.

237. Somerville TDD, Simeoni F, Chadwick JA, Williams EL, Spencer GJ, Boros K, et al. Derepression of the Iroquois Homeodomain Transcription Factor Gene IRX3 Confers Differentiation Block in Acute Leukemia. Cell Rep 2018;22:638–52.

238. Scarlett K, Pattabiraman V, Barnett P, Liu D, Anderson LM. The proangiogenic effect of iroquois homeobox transcription factor Irx3 in human microvascular endothelial cells. J Biol Chem 2015;290:6303–15.

239. Landgraf K, Scholz M, Kovacs P, Kiess W, Körner A. FTO obesity risk variants are linked to adipocyte IRX3 expression and BMI of children - Relevance of FTO variants to defend body weight in lean children? PLoS One 2016;11:1–10.

240. Neel J V. Diabetes Mellitus: A "Thrifty" Genotype Rendered Detrimental by "Progress"? Am J Hum Genet 1962;14:353-62.

241. de Araujo TM, Razolli DS, Correa-da-Silva F, de Lima-Junior JC, Gaspar RS, Sidarta-Oliveira D, et al. The partial inhibition of hypothalamic IRX3 exacerbates obesity. EBioMedicine 2019;39:448–160.

242. Zou Y, Lu P, Shi J, Liu W, Yang M, Zhao S, et al. IRX3 Promotes the Browning of White Adipocytes and Its Rare Variants are Associated with Human Obesity Risk. EBioMedicine 2017;24:64–75.

243. Inagaki T. Regulations of Adipocyte Phenotype and Obesity by IRX3. Positive or Negative? EBioMedicine 2017;24:7–8.

244. Nagy A, Rossant J, Nagy R, Abramow-Newerly W, Roder JC. Derivation of completely cell culture-derived mice from early-passage embryonic stem cells. Proc Natl Acad Sci U S A 1993;90:8424–8.

245. Church CD, Berry R, Rodeheffer MS. Isolation and study of adipocyte precursors. Methods Enzymol 2014;537:31–46.

246. Veum VL, Dankel SN, Gjerde J, Nielsen HJ, Solsvik MH, Haugen C, et al. The nuclear receptors NUR77, NURR1 and NOR1 in obesity and during fat loss. Int J Obes 2012;36:1195–202.

247. Lonowski LA, Narimatsu Y, Riaz A, Delay CE, Yang Z, Niola F, et al. Genome editing using FACS enrichment of nuclease-expressing cells and indel detection by amplicon analysis. Nat Protoc 2017;12:581–603.

248. Bhaya D, Davison M, Barrangou R. CRISPR-Cas Systems in Bacteria and Archaea: Versatile Small RNAs for Adaptive Defense and Regulation. Annu Rev

Genet 2011;45:273–97.

249. Deltcheva E, Chylinski K, Sharma CM, Gonzales K, Chao Y, Pirzada ZA, et al. CRISPR RNA maturation by trans-encoded small RNA and host factor RNase III. Nature 2011;471:602–7.

250. Jinek M, Chylinski K, Fonfara I, Hauer M, Doudna JA, Charpentier E. A programmable dual-RNA-guided DNA endonuclease in adaptive bacterial immunity. Science (80-) 2012;337:816–21.

251. Montague TG, Cruz JM, Gagnon JA, Church GM, Valen E. CHOPCHOP: A CRISPR/Cas9 and TALEN web tool for genome editing. Nucleic Acids Res 2014;42:W401-7.

252. Labun K, Montague TG, Gagnon JA, Thyme SB, Valen E. CHOPCHOP v2: a web tool for the next generation of CRISPR genome engineering. Nucleic Acids Res 2016;44:W272-6.

253. Labun K, Montague TG, Krause M, Torres Cleuren YN, Tjeldnes H, Valen E. CHOPCHOP v3: expanding the CRISPR web toolbox beyond genome editing. Nucleic Acids Res 2019;47:W171-W174.

254. Altschul SF, Madden TL, Schäffer AA, Zhang J, Zhang Z, Miller W, et al. Gapped BLAST and PSI-BLAST: A new generation of protein database search programs. Nucleic Acids Res 1997;25:3389–402.

255. de Jonge HJM, Fehrmann RSN, de Bont ESJM, Hofstra RMW, Gerbens F, Kamps WA, et al. Evidence Based Selection of Housekeeping Genes. PLoS One 2007;2:e898.

256. Schena M. Genome analysis with gene expression microarrays. BioEssays 1996;18:427–31.

257. Wang Z, Gerstein M, Snyder M. RNA-Seq: A revolutionary tool for transcriptomics. Nat Rev Genet 2009;10:57–63.

258. Park PJ. ChIP–seq: advantages and challenges of a maturing technology. Nat Rev Genet 2009;10:669–80.

259. Selkoe D. Cell Biology of the Alzheimer's Disease 1994:373–403.

260. Mattson MP. Pathways towards and away from Alzheimer's disease. Nature 2004;430:631–9.

261. Bloom GS. Amyloid-β and Tau. JAMA Neurol 2014;71:505.

262. Balakrishnan K, Verdile G, Mehta PD, Beilby J, Nolan D, Galvão DA, et al. Plasma Aβ42 correlates positively with increased body fat in healthy individuals. J Alzheimers Dis 2005;8:269–82.

263. Lee Y-H, Tharp WG, Maple RL, Nair S, Permana PA, Pratley RE. Amyloid Precursor Protein Expression Is Upregulated in Adipocytes in Obesity. Obesity 2008;16:1493–500.

264. Ghanim H, Monte S V, Sia CL, Abuaysheh S, Green K, Caruana J a, et al. Reduction in inflammation and the expression of amyloid precursor protein and other proteins related to Alzheimer's disease following gastric bypass surgery. J Clin Endocrinol Metab 2012;97:E1197-201.

265. Lee Y-H, Martin JM, Maple RL, Tharp WG, Pratley RE. Plasma amyloid-beta peptide levels correlate with adipocyte amyloid precursor protein gene expression in obese individuals. Neuroendocrinology 2009;90:383–90.

266. Puig KL, Floden AM, Adhikari R, Golovko MY, Combs CK. Amyloid precursor protein and proinflammatory changes are regulated in brain and adipose tissue in a murine model of high fat diet-induced obesity. PLoS One 2012;7:e30378.

267. Sommer G, Kralisch S, Lipfert J, Weise S, Krause K, Jessnitzer B, et al. Amyloid precursor protein expression is induced by tumor necrosis factor alpha in 3T3-L1 adipocytes. J Cell Biochem 2009;108:1418–22.

268. Mody N, Agouni A, Mcilroy GD, Platt B, Delibegovic M. Susceptibility to diet-induced obesity and glucose intolerance in the APP SWE/PSEN1 A246E mouse model of Alzheimer's disease is associated with increased brain levels of protein tyrosine phosphatase 1B (PTP1B) and retinol-binding protein 4 (RBP4), and bas. Diabetologia 2011;54:2143–51.

269. Freeman LR, Zhang L, Dasuri K, Fernandez-Kim SO, Bruce-Keller AJ, Keller JN. Mutant Amyloid precursor protein differentially alters adipose biology under obesogenic and non-obesogenic conditions. PLoS One 2012;7.

270. Puig KL, Brose SA, Zhou X, Sens MA, Combs GF, Jensen MD, et al. Amyloid precursor protein modulates macrophage phenotype and diet-dependent weight gain. Sci Rep 2017;7:43725.

271. Anandatheerthavarada HK, Devi L. Amyloid Precursor Protein and Mitochondrial Dysfunction in Alzheimer's Disease. Neurosci 2007;13:626–38.

272. Shi C, Zhu XM, Wang J, Long D. Intromitochondrial IκB/NF-κB signaling pathway is involved in amyloid β peptide-induced mitochondrial dysfunction. J Bioenerg Biomembr 2014;46:371–6.

273. Chen JX, Yan S Du. Amyloid-beta-induced mitochondrial dysfunction. J Alzheimers Dis 2007;12:177–84.

274. Canevari L, Clark JB, Bates TE. β-Amyloid fragment 25-35 selectively decreases complex IV activity in isolated mitochondria. FEBS Lett 1999;457:131–4.

275. Parks JK, Smith TS, Trimmer PA, Bennett JP, Davis Parker WJ. Neurotoxic Aβ peptides increase oxidative stress in vivo through NMDA-receptor and nitric-oxide-synthase mechanisms, and inhibit complex IV activity and induce a mitochondrial permeability transition in vitro. J Neurochem 2001;76:1050–6.

276. Boczonadi V, Horvath R. Amyloid-β in mitochondrial disease: mutation in a human metallopeptidase links amyloidotic neurodegeneration with mitochondrial processing. EMBO Mol Med 2016;8:1–3.

277. Brunetti D, Torsvik J, Dallabona C, Teixeira P, Sztromwasser P, Fernandez-Vizarra E, et al. Defective PITRM1 mitochondrial peptidase is associated with Aβ amyloidotic neurodegeneration. EMBO Mol Med 2015;8:1–15.

278. Moreira PI, Santos MS, Moreno A, Rego a C, Oliveira C. Effect of amyloid beta-peptide on permeability transition pore: a comparative study. J Neurosci Res 2002;69:257–67.

279. Abramov AY. -Amyloid Peptides Induce Mitochondrial Dysfunction and Oxidative Stress in Astrocytes and Death of Neurons through Activation of NADPH Oxidase. J Neurosci 2004;24:565–75.

280. Chiarini A, Armato U, Liu D, Dal Prà I. Calcium-sensing receptors of human neural cells play crucial roles in Alzheimer's disease. Front Physiol 2016;7:1–21.

281. He YH, He Y, Liao XL, Niu YC, Wang G, Zhao C, et al. The calcium-sensing receptor promotes adipocyte differentiation and adipogenesis through PPAR?? pathway. Mol Cell Biochem 2011:1–8.

282. Villarroel P, Reyes M, Fuentes C, Segovia MP, Tobar N, Villalobos E, et al. Adipogenic effect of calcium sensing receptor activation. Mol Cell Biochem 2013;384:139–45.

283. Anandatheerthavarada HK, Biswas G, Robin MA, Avadhani NG. Mitochondrial targeting and a novel transmembrane arrest of Alzheimer's amyloid precursor protein impairs mitochondrial function in neuronal cells. J Cell Biol 2003;161:41–54.

284. An YA, Crewe C, Asterholm IW, Sun K, Chen S, Zhang F, et al. Dysregulation of amyloid precursor protein impairs adipose tissue mitochondrial function and promotes obesity. Nat Metab 2019;1:1243–57.

285. Hansen JB, Jørgensen C, Petersen RK, Hallenborg P, De Matteis R, Bøye HA, et al. Retinoblastoma protein functions as a molecular switch determining white versus brown adipocyte differentiation. Proc Natl Acad Sci U S A 2004;101:4112–7.

286. Hakim-Weber R, Krogsdam A-M, Jørgensen C, Fischer M, Prokesch A, Bogner-

Strauss JG, et al. Transcriptional regulatory program in wild-type and retinoblastoma gene-deficient mouse embryonic fibroblasts during adipocyte differentiation. BMC Res Notes 2011;4:157.

287. Bjune J-I, Dyer L, Røsland G V, Tronstad KJ, Njolstad PR, Sagen J V, et al. The homeobox factor Irx3 maintains adipogenic identity. Metabolism 2019:154014.

288. Merkestein M, Laber S, McMurray F, Andrew D, Sachse G, Sanderson J, et al. FTO influences adipogenesis by regulating mitotic clonal expansion. Nat Commun 2015.

289. Bjune JI, Haugen C, Gudbrandsen O, Nordbø OP, Nielsen HJ, Våge V, et al. IRX5 regulates adipocyte amyloid precursor protein and mitochondrial respiration in obesity. Int J Obes 2019;43:2151–62.

290. Barrios N, Campuzano S. Expanding the Iroquois genes repertoire: a non-transcriptional function in cell cycle progression. Fly (Austin) 2015;9:126–31.

291. Lam DD, de Souza FSJ, Nasif S, Yamashita M, López-Leal R, Otero-Corchon V, et al. Partially Redundant Enhancers Cooperatively Maintain Mammalian Pomc Expression Above a Critical Functional Threshold. PLoS Genet 2015;11:e1004935.

292. Goto T, Macdonald P, Maniatis T. Early and late periodic patterns of even skipped expression are controlled by distinct regulatory elements that respond to different spatial cues. Cell 1989;57:431–422.

293. Yuh CH, Davidson EH. Modular cis-regulatory organization of Endo16, a gut-specific gene of the sea urchin embryo. Development 1996;122:1069–82.

294. Jeong Y, El-Jaick K, Roessler E, Muenke M, Epstein DJ. A functional screen for sonic hedgehog regulatory elements across a 1 Mb interval identifies long-range ventral forebrain enhancers. Development 2006;133:761–72.

295. Werner T, Hammer A, Wahlbuhl M, Bösl MR, Wegner M. Multiple conserved regulatory elements with overlapping functions determine Sox10 expression in mouse embryogenesis. Nucleic Acids Res 2007;35:6526–38.

296. Bavelloni A, Piazzi M, Raffini M, Faenza I, Blalock WL. Prohibitin 2: At a communications crossroads. IUBMB Life 2015;67:239–54.

297. Thuaud F, Ribeiro N, Nebigil CG, Désaubry L. Prohibitin ligands in cell death and survival: Mode of action and therapeutic potential. Chem Biol 2013;20:316–31.

298. Kurtev V, Margueron R, Kroboth K, Ogris E, Cavailles V, Seiser C. Transcriptional regulation by the repressor of estrogen receptor activity via recruitment of histone deacetylases. J Biol Chem 2004;279:24834–43.

299. Hwang C, Giri VN, Wilkinson JC, Wright CW, Wilkinson AS, Cooney KA, et al. EZH2 regulates the transcription of estrogen-responsive genes through association with REA, an estrogen receptor corepressor. Breast Cancer Res Treat 2008;107:235–42.

300. Kasashima K, Ohta E, Kagawa Y, Endo H. Mitochondrial functions and estrogen receptor-dependent nuclear translocation of pleiotropic human prohibitin 2. J Biol Chem 2006;281:36401–10.

9. Appendix

Paper II

II

Metabolism Clinical and Experimental 103 (2020) 154014

Contents lists available at ScienceDirect

Metabolism Clinical and Experimental

journal homepage: www.metabolismjournal.com

The homeobox factor Irx3 maintains adipogenic identity

Jan-Inge Bjune [a,b,c], Laurence Dyer [a,c], Gro V. Røsland [d], Karl Johan Tronstad [d,e], Pål R. Njølstad [a,f], Jørn V. Sagen [a,c], Simon N. Dankel [a,b,c,*], Gunnar Mellgren [a,b,c,*]

[a] Center for Diabetes Research, Department of Clinical Science, University of Bergen, N-5020 Bergen, Norway
[b] Mohn Nutrition Research Laboratory, Department of Clinical Science, University of Bergen, N-5020 Bergen, Norway
[c] Hormone Laboratory, Haukeland University Hospital, N-5021 Bergen, Norway
[d] Department of Biomedicine, University of Bergen, N-5020 Bergen, Norway
[e] Department of Oncology and Medical Physics, Haukeland University Hospital, N-5021 Bergen, Norway
[f] Department of Pediatrics and Adolescents, Haukeland University Hospital, N-5021 Bergen, Norway

ARTICLE INFO

Article history:
Received 15 August 2019
Accepted 13 November 2019
Available online xxxx

Keywords:
Irx3
Beige adipocytes
Obesity
FTO
Adipogenesis

ABSTRACT

Background: Inhibition of Irx3 and Irx5 has been shown to reduce body weight and white adipose tissue (WAT) mass through cell-autonomous and sympathetic-induced increases in adipocyte beiging and thermogenesis in mice and humans. However, the underlying mechanisms of the Irx control over beiging are still largely unknown, as illustrated by recent reports showing divergent effects of Irx3 on adipocyte metabolism and function. Here, we investigated the role of Irx3 in controlling beige preadipocyte function and differentiation.

Methods: Stable knock out of *Irx3* in ME3 mouse preadipocytes capable of beiging was performed using a CRISPR-Cas9 system, and the effect on cell differentiation was assessed by qPCR, RNA-seq, Oil-red-O lipid staining and Alcian Blue staining of proteoglycans. Changes in cell identities were validated using cell type enrichment analysis from RNA-seq data. Proliferation and cell cycle progression in undifferentiated cells were measured by WST-1 and flow cytometry, reactive oxygen species (ROS) generation was determined by fluorescence spectrometry and mitochondrial respiration was investigated by Seahorse assay.

Results: Irx3 was found to be essential for the identity, function and adipogenic differentiation of beige adipocyte precursors. *Irx3*-KO impaired proliferation, ROS generation and mitochondrial respiration in the preadipocytes. We further observed profound changes in numerous genes during both early and late stages of adipogenic differentiation, including genes important for adipocyte differentiation, cell cycle progression, oxidative phosphorylation (OXPHOS) and morphogenesis. Irx3-KO cells failed to accumulate lipids following adipogenic stimuli, and cell enrichment analysis revealed a loss of preadipocyte identity and a gain of chondrocyte-like identity in *Irx3*-KO cells during early differentiation. Finally, unlike the control cells, the *Irx3*-KO cells readily responded to chondrogenic stimuli.

Conclusions: Irx3 is required for preadipocyte identity and differentiation capacity. Our findings suggest that, while inhibition of Irx3 may be beneficial during later developmental stages to modulate adipogenesis in the beige direction, constitutive and complete absence of Irx3 in the embryonic fibroblast stage leads to detrimental loss of adipogenic differentiation capacity.

1. Introduction

Obesity has a strong genetic component that accounts for up to 70–80% of variations in BMI [1–3]. Progressive elevations in BMI associate with an exponential increase in mortality risk [4–6], and so identifying causal genes has long been an important focus in medical genetics. However, obesity is a complex disease whose underlying metabolic traits are influenced by thousands of common risk variants with moderate to diminishing allele effects [7]. Moreover, 95% of these variants are located in putative regulatory rather than coding regions, typically found in high linkage disequilibrium with nearby SNPs and interacting with genes up to several millions of base pairs away [7]. Thus, understanding the functional importance of these trait-associated loci has been challenging.

Recently, Claussnitzer et al. were able to pinpoint a causal SNP in the first intron of the *FTO* gene [8], the common variant locus most strongly

Abbreviations: DEG, differentially expressed gene; DN, dominant-negative; ECM, extracellular matrix; GAG, glycosaminoglycan; GO, gene ontology; ICC, immunocytochemistry; ISO, isoproterenol; MEF, mouse embryonic fibroblast; OXPHOS, oxidative phosphorylation; ROS, reactive oxygen species; WAT, white adipose tissue.

* Corresponding authors at: Center for Diabetes Research, Department of Clinical Science, University of Bergen, N-5020 Bergen, Norway.
E-mail addresses: simon.dankel@uib.no (S.N. Dankel), gunnar.mellgren@uib.no (G. Mellgren).

https://doi.org/10.1016/j.metabol.2019.154014
0026-0495/

associated with obesity [9–12], which has been previously linked to the distal genes *Irx3* and *Irx5* through long range enhancer-promoter interactions [13,14]. Moreover, in humans this variant locus was most active in mesenchymal cells, particularly in adipose tissue, where the risk variant increased the expression of IRX3/IRX5, which in turn inhibited beiging and thermogenesis, promoting white adipogenesis and fat storage [8]. Beige adipocytes are now well established to be present in human adults, where they are active during cold exposure and positively associate with reduced BMI, improved whole-body metabolism and increased insulin sensitivity [15–18]. Therefore, inhibition of IRX3/IRX5 to promote beiging has emerged as a possible intervention against obesity. In support of this mechanism, *Irx3*-KO mice, as well as mice with adipocyte-specific transgenic expression of dominant-negative (DN) Irx3, were resistant to weight gain and displayed increased energy expenditure [8,14]. We recently also demonstrated a similar protection from obesity in global *Irx5*-KO mice [19].

However, the mechanisms of Irx action in adipocyte development are far from fully delineated. For example, *IRX3* shows a significant influence over body weight through the hypothalamus [14], where its function may be independent of the *FTO* locus variants which show little activity in the brain [8]. Further, in contrast to DN *Irx3* mutants in either the brain or adipose tissue, lentiviral-mediated knock-down of *Irx3* in either tissue had the opposite effect and promoted obesity [20,21]. The reasons for this discrepancy are unknown, although it has been speculated that DN mutant proteins may retain some function in complexes with other proteins [22], highlighting the need for elucidating the transcriptional mechanisms of Irx3 action in adipose tissue using alternative methods. Here, we completely knocked out *Irx3* in beiging-competent preadipocytes using a CRISPR-Cas9 system, and found Irx3 to be critical for both preadipocyte identity and adipogenic potential.

2. Materials and methods

2.1. Mouse cells

Mouse embryonic fibroblast $Rb^{-/-}$ Line 3 (ME3) cells were previously generated [23] and characterized to be a model of beige/brown adipocytes [24,25]. Cells were grown in AmnioMAX-C100 medium supplemented with 7.5% FBS, 7.5% C100 (all from Thermo Fisher Scientific, Waltham, MA, USA), 1% penicillin-streptomycin (PEST) (Sigma, St. Louis, MO, USA) and 2 mM L-glutamine (Sigma) at 37 °C and 5% CO_2. Adipogenic differentiation was initiated three days post confluency (day 0) by induction medium containing 5 μg/mL Insulin (INS) (Sigma), 1 μM Dexamethasone (DEX) (Sigma), 0.5 mM isobutyl methylxanthine (IBMX) (Sigma) and 1 μM Rosiglitazone (ROSI) (Cayman Chemical, Ann Arbor, MI, USA). From day 2 to day 4 only insulin was added to the basal medium and from day 4 to 7 cells were grown in the basal medium. Stable knockout (KO) of *Irx3* in ME3 cells was performed by CRISPR-Cas9 as described before [19,26] using guide RNA MM0000204919 (CCGTCCCAAGAACGCCACCCGG) (Sigma). A non-targeting guide RNA (Sigma) was used as negative control. Due to reduced proliferation rate in *Irx3*-KO compared to control cells, differentiation was initiated three days after observed confluence in controls. This ensured the lagging *Irx3*-KO cells to be confluent for at least two days, thereby matching confluency between the two cell lines before induction of differentiation, to limit a confounding effect on differentiation. Chondrogenic micromass cultures were generated by seeding 80,000 cells in 5 μL droplets. The micromass cultures were incubated for 2 h in a CO_2 incubator before addition of StemPro osteocyte/chondrocyte differentiation basal medium with 10% StemPro chondrogenesis supplement (both from Thermo Fisher Scientific) and 1% PEST (Sigma).

2.2. Human cells

Primary human cells were derived from the stromovascular fraction (SVF) of liposuction material from patients undergoing plastic surgery. All patients gave written informed consent and the study was approved by the Regional committee for Medical and Health Research Ethics, Western Norway (REK Vest) (approval number 2010/502). The SVF fraction was isolated by collagenase treatment, sieving and centrifugation as previously described [27] and cultured in adipogenic basal medium (DMEM/F-12 GlutaMax (Invitrogen, Carlsbad, CA, USA) in 10% FBS and 50 μg/mL gentamicin (Sigma). Differentiation was induced by addition of 100 nM cortisol, 66 nM insulin, 10 μg/mL transferring, 33 μM biotin, 17 μM pantothenate, 1 nM T3 (all from Sigma) and 10 μM ROSI. Cells were treated with siRNA against IRX3 (Origene, Rockville, MD, USA) from day 0–2 before lysis and RNA purification.

2.3. Oil-red-O lipid staining

Cells were fixated in 4% formaldehyde (Sigma) prepared in PBS for 5 min followed by another 2 h in fresh fixation solution. Cells were subsequently washed twice with water and incubated in 60% isopropanol (Kemetyl, Trollåsen, Norway) for 5 min before incubation in freshly prepared working solution of Oil-red-O (Santa Cruz Biotechnology, Dallas, TX, USA) (1.8 mg/mL isopropanol) for 25 min. Cells were washed three times in water and examined under light-microscope. Quantification was performed spectrophotometrically at 500 nm by addition of 100% isopropanol.

2.4. Alcian Blue staining of proteoglycans

Cells were fixated in 4% formaldehyde/PBS for 1 h and washed twice in water before incubation in 1% Alcian Blue (Molekula, Darlington, UK) prepared in 0.1 N HCl for 30 min. Cells were washed three times in 0.1 N HCl before examination under light-microscope. Quantification was performed by incubation in 6 M Guanidine-HCl solution (Sigma) over night at 4 °C before reading absorbance at 600 nm.

2.5. Immunocytochemistry

ME3 cells were grown on coverslips coated with 0.1% gelatin and fixated by 4% PFA (Sigma) for 15 min. The coverslips were washed in TBS, blocked in 5% BSA/TBST for 30 min and incubated with rabbit anti-Irx3 (ab25703, Abcam, Cambridge, UK) and/or mouse anti-ATPB (ab5452, Abcam) diluted 1:500 in 5% BSA/TBST for 1 h at room temperature (RT). After washing with TBS, the coverslips were incubated with goat Alexa 546 anti-rabbit and/or goat Alexa 647 anti-mouse (Molecular Probes, Eugene, OR, USA) diluted 1:500 in 5% BSA/TBST for 1 h before mounting with Prolong Diamond antifade with DAPI (Thermo Fisher Scientific).

2.6. Mitochondrial isolation and western blotting

Mitochondria were isolated from ME3 cells using the reagent-based method of the Mitochondrial isolation kit for cultured cells (Thermo Scientific). Whole cells, as well as isolated mitochondria, were lysed in 1X RIPA buffer supplemented with 1X cOmplete Mini protease inhibitor cocktail (Roche) and analyzed by western blotting using 12 μg of lysate. The following antibodies were used: rabbit anti-Irx3 (ab25703, Abcam) 1:800, rabbit anti-Ucp1 (U6382, Sigma) 1:1000 and goat anti-rabbit IgG HRP (31,460, Thermo Scientific) 1:7500. Blots were detected with Femto substrate (Thermo Scientific) on a ChemiDoc XRS imager (Bio-Rad).

2.7. RNA isolation, cDNA synthesis and real-time qPCR analyses

Cells were lysed in RLT buffer (Qiagen, Hilden, Germany), homogenized by centrifugation on QIAShredder columns (Qiagen) and snap-frozen in liquid nitrogen. RNA was isolated using the RNeasy Mini kit (Qiagen) with on-column DNaseI-treatment, and RNA integrity was validated by the RNA 6000 Nano kit on the 2100 Bioanalyzer (Agilent,

Santa Clara, USA). cDNA was made from 100 ng RNA input with the High-Capacity cDNA Reverse Transcription kit (Applied Biosystems, Waltham, MA, USA). Real-time qPCR was performed using the LightCycler 480 system (Roche) and the delta-delta Ct method relative to reference gene *Rps13*. Data was plotted in GraphPad Prism 7 using backbone tracing. Primers were designed using either the Universal ProbeLibrary Assay Design Center (Roche) or Primer-BLAST softwares. Primer sequences shown in Table 1.

2.8. Global gene expression analyses

2.8.1. ME3 cells differentiation time course (RNA-seq)

ME3 cells were differentiated and lysed on days 0, 1, 2, 4 and 7 followed by RNA purification and quality control as described above. Library preparation and 2x75bp paired-end mRNA sequencing of 400 ng input RNA was performed using the TruSeq Stranded mRNA kit (Illumina, Sand Diego, CA, USA) and the HiSeq4000 instrument (Illumina). Reads were aligned to GRCm38.p5/mm10 reference genome using HISAT2 2.0.5, and then submitted to featureCounts in R, resulting in a raw read count matrix. RPKM normalization was then used for visualization purposes, and TMM normalization was used for statistical analysis. A regression analysis performed via the R package maSigPro version 1.54.0 [28] was used to analyze and cluster genes with similar expression profiles.

2.8.2. ME3 control versus Irx3-KO cells (RNA-seq)

RNA from ME3 control and *Irx3*-KO cells on day 1 and day 7 of differentiation was purified and subjected to RNA-sequencing as described above, with 300 ng input. Read alignment and counting was performed as before. The raw read count matrix was then submitted to DESeq2 (Version 1.24.0), normalized and filtered by expression. Differentially expressed genes (DEGs) were then identified and selected using a BH-adjusted p-value <.1 and an absolute log2 fold change >1. These gene sets were then separated into up- and down-regulated categories and submitted to gene ontology (GO) analysis.

2.8.3. Gene ontology analysis

Lists of genes that were differentially expressed over time, or between *Irx3*-KO and control cells, were subjected to GO analyses using publicly available databases of known gene function (PANTHER (pantherdb.org) and KEGG PATHWAY (genome.jp/kegg/pathway.html). KEGG was accessed via the R package clusterProfiler.

These analyses allowed identification of biological processes and pathways that were enriched with genes in the submitted gene lists.

2.8.4. silRX3 in human SVF (microarray)

Global gene expression in human primary SVF-derived cells was measured by microarray, using the Illumina TotalPrep RNA Amplification Kit (Applied Biosystems/Ambion, USA) with 400 ng input. Biotin-labelled cRNA was hybridized to the HumanHT-12 V4 Expression BeadChip and detected using the Illumina iScan Reader. A quantile-normalized intensity matrix was created and subsequently converted into log2 values, filtered for low intensity genes and the R package limma (Version 3.40.2) was then used to identify DEGs. Genes with an adjusted p-value <0.1 and an absolute log fold change >1 were used for downstream analysis.

2.9. Cell type enrichment analysis

Global gene expression profiles of control and *Irx3*-KO cells were compared with gene signatures of thousands of samples from pure cell types, using the xCell software [29]. Briefly, the software integrated gene expression profiles from six public databases, including ENCODE and FANTOM5, to make consolidated gene signatures for 64 cell types. These signatures were then compared with our submitted gene expression data, and an adjusted cell type enrichment score was calculated. This method allows characterization of cell identity based on activity of biological processes, reflecting coordinated changes in expression of multiple genes rather than the expression level of single genes.

2.10. Seahorse assay

Cellular mitochondrial respiration was assessed by oxygen consumption rate (OCR) using the Seahorse XF Cell Mito Stress Test kit as previously described [19] with the following modifications: Cells were seeded at 7500 cells/well and assayed either before reaching confluence (undifferentiated), or on day 1 of differentiation. Assay media glucose levels were 25 mM, and the concentration of CCCP, rotenone and antimycin was 2 μM each. Data was normalized to cell count by Hoechst stained nuclei.

2.11. ROS assay

Production of reactive oxygen species (ROS) was measured in control and *Irx3*-KO cells using the CM-H_2DCFDA fluorescent probe (Thermo Fisher Scientific). On the day of assay, culture media was replaced with PBS containing 5 μM ROS probe for 30 min. Cells were subsequently washed twice with Krebs Ringer Buffer (KRB) and assayed in KRB using a Spectramax fluorescence plate reader (Excitation 488 nm/Emission 538 nm) for 3 h with 10 min read intervals.

2.12. Proliferation assays

Non-synchronously proliferating cells were seeded at 5000 cells/well in 96 well plates, left to grow for 72 h and assayed with WST-1 for 1 h using the Quick Cell Proliferation Assay Kit II (Abcam) in 12 replicates. For 2D cell cycle analysis, non-synchronously proliferating cells were grown for 48 h post seeding, pulse-labelled for 1 h with 30 μM BrdU (Abcam) and left to grow for 6 h in BrdU-free medium before fixation in 70% ethanol, denaturing by 2 N HCl and neutralization by 0.1 M NaB4O7 (pH 8.5). Cells were incubated o/n with 1:100 dilutions of anti-BrdU (ab6326) or negative control IgG (ab171870) at 4 °C, followed by a

Table 1
Primer sequences.

Target gene	Forward primer	Reverse primer
Irx3	5′-AAAAGTTACTCAAGACAGCTTTCCA-3′	5′-CGATTTAAAAATGGTTGAAAAGTTAAG-3′
Fabp4	5′-ATCACCGCAGACGACAGG-3′	5′-TCATAACACATTCCACCACCA-3′
Pparg2	5′-TTATAGCTGTCATTATTCTCAGTGGAG-3′	5′-GACTCTGGGTGATTCAGCTTG-3′
Pgc-1α	5′-AATTTTTCAAGTCTAACTATGCAGACC-3′	5′-AAAATCCAGAGAGTCATACTTGCTC-3′
Cidea	5′-TCCTCGGCTGTCTCAATG-3′	5′-TGGCTGCTCTTCTGTATCG-3′
Ucp1	5′-GGGCATTCAGAGGCAAATCAG-3′	5′-TTTCCGAGAGAGGCAGGTGTTT-3′
Pparα	5′-CGGGAAAGACCAGCAACA-3′	5′-GAATCGGACCTCTGCCTCT-3′
Leptin	5′-CTGTGTCGGTTCCTGTGGCT-3′	5′-GTGACCCTCTGCTTGGCGG-3′
Cpt1b	5′-GACCCAAAACAGTATCCCAATC-3′	5′-AGACCCCGTAGCCATCATC-3′
Tbx1	5′-CCAAGGCAGGCAGACGAATGT-3′	5′-GTCATCTACGGGCACAAAGTCCA-3′

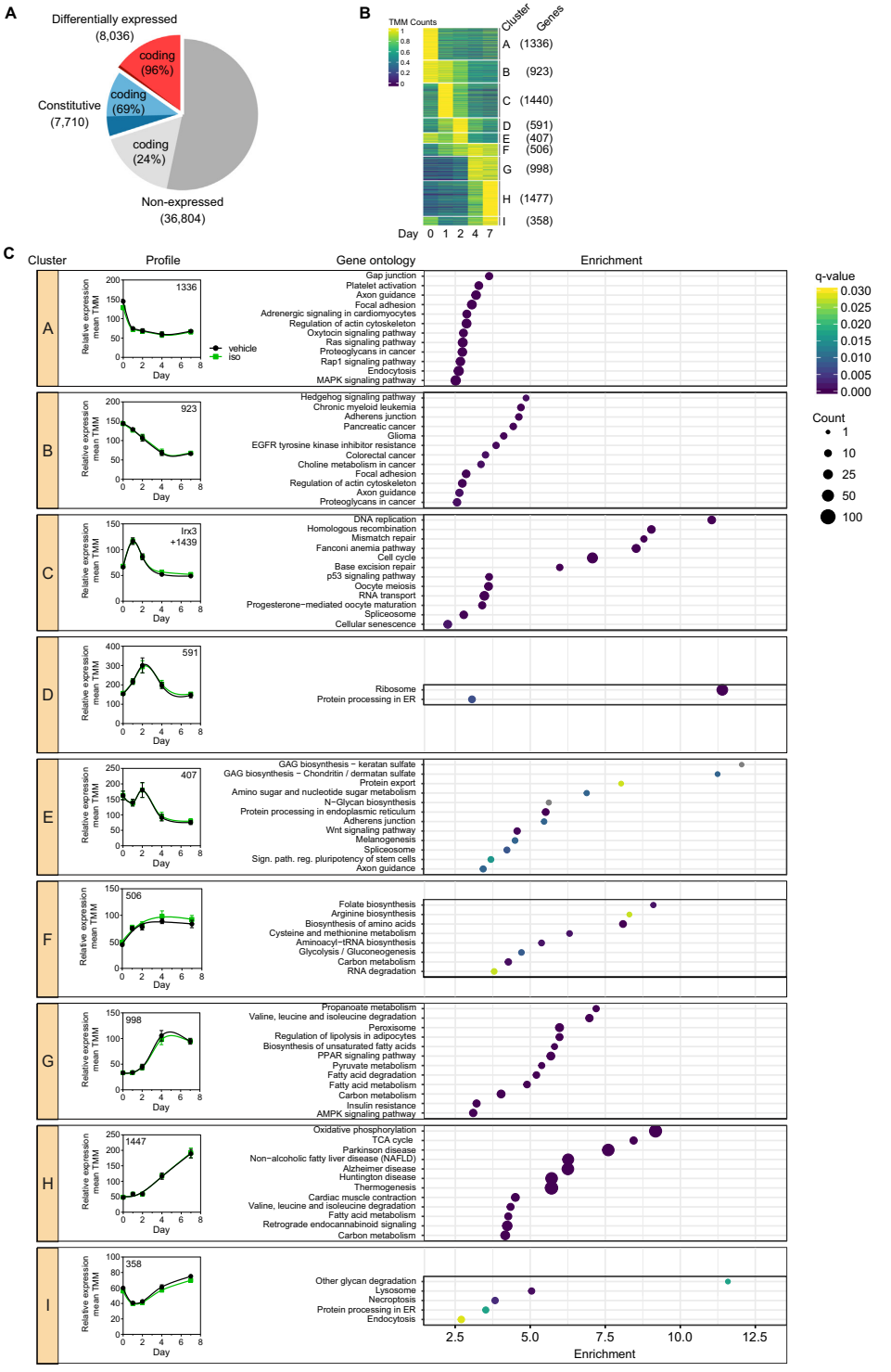
A
Differentially expressed
(8,036)
coding
(96%)
Constitutive
(7,710)
coding
(69%)
coding
(24%)
Non-expressed
(36,804)
B
TMM Counts
1
0.8
0.6
0.4
0.2
0
Cluster
Genes
A (1336)
B (923)
C (1440)
D (591)
E (407)
F (506)
G (998)
H (1477)
I (358)
Day 0 1 2 4 7
C
Cluster
Profile
Gene ontology
Enrichment
Relative expression mean TMM
Day
vehicle
iso
1336
Gap junction
Platelet activation
Axon guidance
Focal adhesion
Adrenergic signaling in cardiomyocytes
Regulation of actin cytoskeleton
Oxytocin signaling pathway
Ras signaling pathway
Proteoglycans in cancer
Rap1 signaling pathway
Endocytosis
MAPK signaling pathway
923
Hedgehog signaling pathway
Chronic myeloid leukemia
Adherens junction
Pancreatic cancer
Glioma
EGFR tyrosine kinase inhibitor resistance
Colorectal cancer
Choline metabolism in cancer
Focal adhesion
Regulation of actin cytoskeleton
Axon guidance
Proteoglycans in cancer
Irx3
+1439
DNA replication
Homologous recombination
Mismatch repair
Fanconi anemia pathway
Cell cycle
Base excision repair
p53 signaling pathway
Oocyte meiosis
RNA transport
Progesterone−mediated oocyte maturation
Spliceosome
Cellular senescence
591
Ribosome
Protein processing in ER
407
GAG biosynthesis − keratan sulfate
GAG biosynthesis − Chondritin / dermatan sulfate
Protein export
Amino sugar and nucleotide sugar metabolism
N−Glycan biosynthesis
Protein processing in endoplasmic reticulum
Adherens junction
Wnt signaling pathway
Melanogenesis
Spliceosome
Sign. path. reg. pluripotency of stem cells
Axon guidance
506
Folate biosynthesis
Arginine biosynthesis
Biosynthesis of amino acids
Cysteine and methionine metabolism
Aminoacyl−tRNA biosynthesis
Glycolysis / Gluconeogenesis
Carbon metabolism
RNA degradation
998
Propanoate metabolism
Valine, leucine and isoleucine degradation
Peroxisome
Regulation of lipolysis in adipocytes
Biosynthesis of unsaturated fatty acids
PPAR signaling pathway
Pyruvate metabolism
Fatty acid degradation
Fatty acid metabolism
Carbon metabolism
Insulin resistance
AMPK signaling pathway
1447
Oxidative phosphorylation
TCA cycle
Parkinson disease
Non−alcoholic fatty liver disease (NAFLD)
Alzheimer disease
Huntington disease
Thermogenesis
Cardiac muscle contraction
Valine, leucine and isoleucine degradation
Fatty acid metabolism
Retrograde endocannabinoid signaling
Carbon metabolism
358
Other glycan degradation
Lysosome
Necroptosis
Protein processing in ER
Endocytosis
2.5
5.0
7.5
10.0
12.5
Enrichment
q-value
0.030
0.025
0.020
0.015
0.010
0.005
0.000
Count
1
10
25
50
100

1:2000 dilution of anti-rat Alexa Fluor 488 (ab150157) for 30 min at RT. Counterstaining was performed with 50 μg/mL Propidium Iodide (PI) (Abcam) in the presence of 100 μg/mL RNase A in the dark at 37 °C for 30 and the cells were analyzed immediately after on a BD Accuri C6 flow cytometer according to manufacturer's instructions. Briefly, cell populations were gated with FSC-A vs SSC-A to eliminate debris and FL3-A vs FL3-H to exclude doublets. Live singlets were displayed as bivariate contour plots of DNA-content (PI/FL3) against BrdU staining (FL1) and gated for BrdU content and cell cycle stage.

2.13. Statistical analyses

Gene expression data were analyzed using R software [30] with indicated packages. Analysis of significance of all other data was performed in GraphPad Prism 8.1.0 using unpaired Student's t-test, one-way ANOVA or two-way repeated measures ANOVA with Holm-Sidak correction for multiple testing as indicated. Data were tested for normality using Shapiro-Wilk test and heteroscedasticity using Brown-Forsythe or Bartlett's test. Data shown as mean ± SD.

2.14. Data deposition

Global gene expression data have been deposited in the ArrayExpress database at EMBL-EBI (www.ebi.ac.uk/arrayexpress) under accession numbers E-MTAB-8200 (mouse differentiation time laps), E-MTAB-8209 (mouse control versus *Irx3*-KO) and E-MTAB-8183 (Human SVF with siIRX3).

3. Results

3.1. Irx3 is dynamically expressed during beige adipocyte differentiation

Due to the conflicting results reported on Irx3 function in beiging [8,14,30,31], we sought to investigate the transcriptional role of Irx3 during the differentiation of beige adipocytes. To this end, we employed ME3 cells, an immortalized mouse beiging-competent preadipocyte cell model (see Materials and methods). To validate the model, preadipocytes were differentiated for seven days and cell morphology was assessed. By day 7, cells developed into mature beige adipocytes with accumulation of multilocular lipid droplets (Fig. S1A) alongside mitochondrial remodeling and expansion (Fig. S1B). To verify the expression and subcellular localization of Irx3, we performed ICC, demonstrating that the Irx3 protein was predominately located in the nucleus, but is also detectable in the cytoplasm, where its concentration increases throughout differentiation (Fig. S1B).

To further characterize the cells, the gene expression of *Irx3*, as well as general and beige-specific adipocyte markers, was measured at days 0, 1, 2, 4 and 7 of differentiation (Fig. S1C). *Irx3* expression was found to peak on day 1, whereas the adipogenic master regulator *Pparγ2*, and the general mature adipocyte markers *Pparα*, *Fabp4* (also known as *Ap2*) and *Leptin* were all strongly induced on days 4–7. *Ucp1* is expressed at a high basal rate in brown adipocytes, and at a low basal rate, but with a potential for induction under β-adrenergic stimulation, in beige adipocytes [31,32]. As such, we treated the cells with either vehicle or 1 μM isoproterenol (ISO) for 4 h prior to lysis. Accordingly, *Ucp1* mRNA levels were low in the basal state and profoundly induced by ISO, indicating that ME3 cells more closely resemble beige than brown adipocytes. Moreover, the beige-specific markers *Tbx1*, *Pgc-1a* and *Cidea* and the mitochondrial marker *Cpt1b* were markedly increased throughout differentiation (Fig. S1C). In agreement with the reported gene expression data, Ucp1 protein levels were also strongly induced over the course of differentiation (Fig. S1D). Taken together, these results indicate that Irx3 is most highly expressed during early differentiation of the ME3 cells, a cell line that has the capacity to differentiate into beige-like adipocytes with a strong thermogenic capacity.

3.2. Irx3 and cell cycle genes are co-expressed

To identify genes co-expressed with Irx3 and to obtain a detailed view of the global transcriptional events during differentiation of ME3 cells, we performed RNA-sequencing of the cells at five timepoints during differentiation. DEGs were clustered according to expression profile similarity using unbiased linear regression (Fig. 1 and Supplementary file 1). About 3000 genes, including *C/ebpα* and *Pparγ* (Fig. S1E), were upregulated during differentiation (cluster F, G and H) and these were functionally enriched for gene ontology (GO) terms related to fundamental adipocytic processes such as differentiation (i.e. PPAR signaling pathways), insulin signaling and the metabolism of fatty acids, glucose and branched chain amino acids (BCAAs) (Fig. 1B-C). Conversely, genes in cluster A and B, which were downregulated over time, were enriched in adipogenic inhibitory pathways such as Hedgehog signaling (Fig. 1B-C). These data further indicate that the cells readily differentiated into highly metabolically active thermogenic adipocytes.

Consistent with qPCR analyses, *Irx3* peaked at day 1 and was found to cluster together with 1439 other genes (cluster C) with similar expression profiles. This cluster was found to be enriched in cell cycle related GOs (Fig. 1C) and included *C/ebpδ, an* early response gene well known to regulate mitotic clonal expansion and induce adipogenesis [33]. The closely related gene *C/ebpβ* was not assigned a cluster in the regression model, *but manual inspection revealed a peak expression on days 1–2* (Fig. S1E). These findings suggest that at least one round of cell division occurred and that this process is positively associated with the expression of Irx3.

3.3. Irx3 ablation impairs adipogenesis

Having established the basic characteristics of the beige cell model, we next set out to determine the effect of Irx3 depletion on global gene expression. A stable knock-out of Irx3 was generated, using a CRISPR-Cas9 system to introduce a frameshift mutation upstream of the HOX domain, resulting in the production of a truncated Irx3 protein, devoid of its DNA-binding and protein-interaction domains (Fig. 2A). Successful knockout was verified by Sanger DNA-sequencing and western blotting (WB) (Fig. 2B). Strikingly, *Irx3*-KO cells were largely unable to differentiate, as demonstrated by diminished lipid accumulation (Fig. 2C) and blunted adipocyte marker gene expression (Fig. 2D).

3.4. Irx3 inhibits adipogenesis independently of the clonal expansion

Because mitotic clonal expansion is often required for efficient adipocyte differentiation, and Irx3 expression coincided with this event, we hypothesized that loss of Irx3 could impair differentiation by perturbing cell cycle gene expression. To test this hypothesis, RNA-sequencing on days 1 and 7 of differentiation was performed in both the control and *Irx3*-KO cells. We observed a major impact on global gene expression during both early and late stages of differentiation,

Fig. 1. Irx3 and cell cycle genes are co-expressed. ME3 cells were grown to confluence and differentiated for 7 days in triplicates in 4 independent experiments. Cells were lysed at indicated days followed by RNA-purification and RNA-sequencing. (A) Distribution of DEGs, constitutive and unexpressed genes during differentiation. (B) Heatmap of the DEGs clustered according to similar expression profile by MaSigPro linear regression. Cluster name and number of genes in each cluster shown. Yellow color indicates highest expression. (C) Average expression profile, number of genes, gene ontology (GO) and enrichment of each cluster. Expression profiles were made from median expression of all genes in the cluster, mean median ± SD of the 4 experiments shown. Top enriched KEGG pathway GO shown for each cluster. Dot sizes represent number of genes in each category and color indicates level of statistical significance. (For interpretation of the references to color in this figure legend, the reader is referred to the web version of this article.)

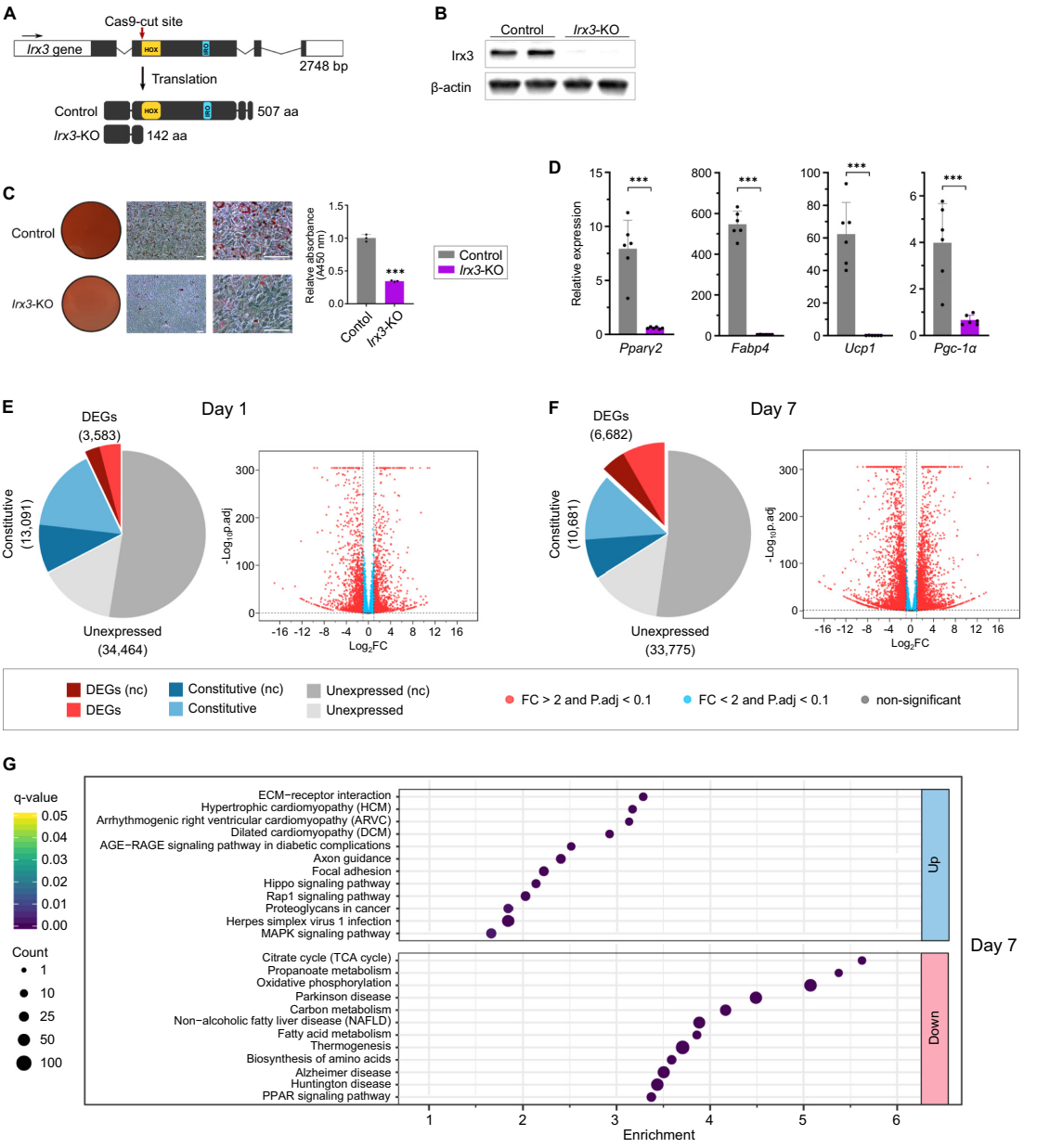

Fig. 2. Irx3 ablation impairs adipogenesis. (A) Schematic of CRISPR-Cas9 mediated KO of *Irx3*. Gene edit led to frameshift mutation and translation of truncated Irx3 protein. HOX, homeobox DNA-binding domain. IRO, Iroquois domain. Control, cells treated with non-targeting guide RNA. (B) *Irx3*-KO was verified on protein level by western blotting using antibodies recognizing the C-terminal of Irx3. β-actin was used as endogenous control. $n = 2$ replicate wells. Images were cut to remove lanes between control and *Irx3*-KO samples. (C) Oil-red-O lipid staining of control and *Irx3*-KO cells differentiated for 7 days. Representative of two independent experiments. Left panel, representative of $n = 3$ wells. Middle panels, representative images from brightfield microscope. Scale bars = 100 μm. Right panel, quantification of $n = 3$ wells. Individual values and mean ± SD shown. *** $p < 0.001$, Student's t-test. (D) Quantification of general and thermogenic adipocyte differentiation markers by RT-qPCR against reference gene *Rps13* in control and *Irx3*-KO cells on day 7, normalized to expression on day 1. Representative of two independent experiments with $n = 6$ replicate wells. Individual values and mean ± SD shown. *** $p < 0.001$, Student's t-test. (E-F) Distribution of differentially expressed genes (DEGs), constitutive and unexpressed genes between control and *Irx3*-KO cells on day 1 (E) and day 7 (F) of differentiation. From one experiment with $n = 6$ replicate wells. Log_2-fold change and adjusted *p*-value for each individual DEG shown as volcano plot. Nc, non-coding. (G) Top enriched KEGG pathways for up- and downregulated genes on day 7. Dot size represents number of genes in each category and color indicates level of statistical significance. See also Fig. S2 and Supplementary file 2 for complete GO information. (For interpretation of the references to color in this figure legend, the reader is referred to the web version of this article.)

with expression of 3000–6000 genes changing >2-fold and of 443 genes changing >100-fold (Fig. 2E–F and Supplementary file 2). GO of DEGs on day 7 confirmed the inability of *Irx3*-KO cells to undergo adipogenic differentiation (Fig. 2G). Unexpectedly, cell cycle related GO terms were significantly depleted among downregulated genes on day 1 (Fig. S2A and Supplementary file 2), and neither C/ebp isoform was changed on day 1 above the 2-fold threshold, suggesting that Irx3 regulates adipogenesis independently of the mitotic clonal expansion in these cells.

3.5. Loss of Irx3 alters morphogenic genes

Further interrogation of the global gene expression data revealed that upregulated genes in the *Irx3*-KO cells on day 1 were highly enriched for GO terms associated with regulation of extracellular matrix (ECM) and blood coagulation. Conversely, genes found to be downregulated on day 1 were enriched for GO terms ranging from interleukin-1 signaling and proliferation to patterning formation and other developmental-related processes (Fig. S2A and Supplementary file 2). Moreover, upregulated genes on day 7 were enriched in GO terms related to ECM, chondrocyte and osteoblasts differentiation and developmental processes such as morphogenesis of various cells and tissues including heart, bone, muscle and neurons (Top KEGG pathways shown in Fig. 2G, see also top enriched Panther GO in Fig. S2A and complete lists in Supplementary file 2). These data suggest that Irx3 control adipocyte differentiation through more fundamental processes controlling cell identities.

3.6. Irx3 deprivation reduces expression of adipocyte markers

To investigate the potential role of Irx3 in maintaining adipocyte identity, we searched for enrichment of Irx3-responsive genes among those found to change during differentiation. We identified highly significant enrichment in all nine clusters (Supplementary Table 1), supporting a hypothesis that one role of Irx3 lies in controlling genes that are dynamically expressed during differentiation, and thereby that Irx3 is an important factor in regulating adipocyte differentiation and function. For example, fundamental drivers and markers of adipocyte differentiation were downregulated on day 7 in KO cells, including *c/ebpα*, *Pparγ2*, *Fabp4*, *Plin2*, *Lpl*, *Mdh1*, *Gapdh* and *Fasn* (Fig. 3A and Fig. S2D). Moreover, expression of several other established [34–36] markers of pre-adipocytes, as well as general brown/beige and white adipocyte markers, was found to be altered in *Irx3*-KO cells on both day 1 and 7, and most of these were downregulated (Fig. 3A).

3.7. Irx3-KO cells lose adipocyte identity

Next, we addressed how *Irx3*-KO cells responded to adipogenic stimuli. Surprisingly, a high number of genes were altered in the *Irx3*-KO cells after seven days in adipogenic cocktail, but most of these were related to the cell cycle (Fig. 3B and Supplementary file 3). Genes that were uniquely differentially expressed over time in the control cells were enriched in GOs related to mitochondrial activity and adipocyte function. Moreover, not only were these genes unchanged in the KO cells; many genes involved in the same processes were in fact downregulated on day 7 as compared to day 1 (Fig. 3B and Supplementary file 3). Conversely, overlapping genes that were downregulated in the control cells, but upregulated in the *Irx3*-KO cells, were functionally enriched for the GO terms angiogenesis, regulation of cell migration, ECM organization and negative regulation of mesenchymal proliferation. These data show that *Irx3*-KO cells responded to mitogenic agents in the differentiation cocktail, and did change significantly over time, but not in the adipogenic direction.

To better understand the developmental identity of the *Irx3*-KO cells, we compared the global gene expression profile of both the control and *Irx3*-KO cells with gene signatures of 64 different cell types using cell type enrichment analysis [29]. As expected, the control cells were most significantly associated with mesenchymal stem cells, mouse embryonic fibroblasts (MEFs) and preadipocytes on day 1 and with adipocytes on day 7 (Fig. 3C). Strikingly, *Irx3*-KO cells lacked associations with any of these lineages, and were instead strongly associated with immune cells and chondrocytes on day 1 (Fig. 3C). We found the chondrocyte association to be particularly interesting because these cells share the same mesenchymal precursor as adipocytes. We therefore searched for differential expression of chondrocyte-related genes in KO versus control cells on day 1, and found strong upregulation of several markers, including *Has1* and *Prg4* (Fig. 3D). The former encodes an enzyme catalyzing the formation of hyaluronic acid, a glycosaminoglycan (GAG) and component of the ECM, whereas the latter encodes Lubricin, a proteoglycan produced specifically by chondrocytes [37].

To assess whether the *Irx3*-KO cells gained a more chondrocyte-like identity compared to controls in vitro, we quantified proteoglycans using Alcian Blue staining following either adipogenic or chondrogenic differentiation (Fig. 3E). The level of proteoglycans was negligible in either cell line before differentiation, and the levels remained low during adipogenic stimulation (Fig. 3E). Oil-red-O lipid staining was performed as a positive control of the adipogenic differentiation (Fig. 3F). In contrast, 19 days in chondrogenic medium raised proteoglycan levels 50-fold in *Irx3*-KO cells, while having little effect in control cells (Fig. 3E). These data show that, unlike the adipocyte-committed control cells, the *Irx3*-KO cells could be reprogramed to readily form chondrocytes, thereby supporting the gene expression data. Collectively, these data further support a crucial role of Irx3 in maintaining preadipocyte identity and thus permitting adipogenic differentiation.

3.8. Conserved roles of Irx3 in mouse ME3 cells and human primary cells

We next sought to compare the observed effects of Irx3 depletion on global gene expression between mouse and human preadipocytes. We therefore employed a microarray dataset where primary cells isolated from the stromovascular fraction (SVF) of liposuction material from patients with obesity were treated with siRNA against *IRX3* on day 0–2 of adipogenic differentiation. Most DEGs were upregulated (Fig. 4A and Supplementary file 4) and were functionally enriched for GO terms related to the immune response, extracellular matrix (ECM) assembly, focal adhesion, glycolysis, and the PI3K-Akt pathway (Fig. 4B and Supplementary file 4). Interestingly, downregulated genes were enriched for cell cycle related processes (Fig. 4B and Supplementary file 4). Because this dataset was derived from early stages of differentiation, we found it most relevant to be compared with DEGs on day 1 in mouse ME3.

We found 125 genes to overlap between mouse and human Irx3 depletion during early adipogenesis (day 1–2), with roughly half of the genes regulated in the same direction in both datasets (Fig. 4C–D and Supplementary Table 2). GO analysis of consistently upregulated genes revealed that the most enriched GO terms were involved in ECM organization, focal adhesion, PI3K-Akt signaling, bone morphogenesis and cholesterol synthesis (Fig. 4E and Supplementary table 3). Of note, ECM-related genes included Col1a2, which was among the most upregulated gene in the mouse KO dataset day 1, with an average fold change of 1616. Thus, both mouse and human cells with Irx3 deficiency displayed increased expression of genes related osteocytes and chondrocytes.

3.9. Knock-out of Irx3 impairs proliferation and mitochondrial respiration of preadipocytes

Since we found the loss of Irx3 to have a large impact on global gene expression already at day 1 of differentiation, with a loss of preadipocyte identity, we reasoned this would also be reflected in the cell phenotype prior to differentiation. Indeed, undifferentiated *Irx3*-KO cells displayed clear signs of mitochondrial dysfunction with reduced basal respiration and ATP production, and a strongly diminished maximal respiration and blunted spare capacity, as measured by Seahorse XF mito stress analyses (Fig. 5A).

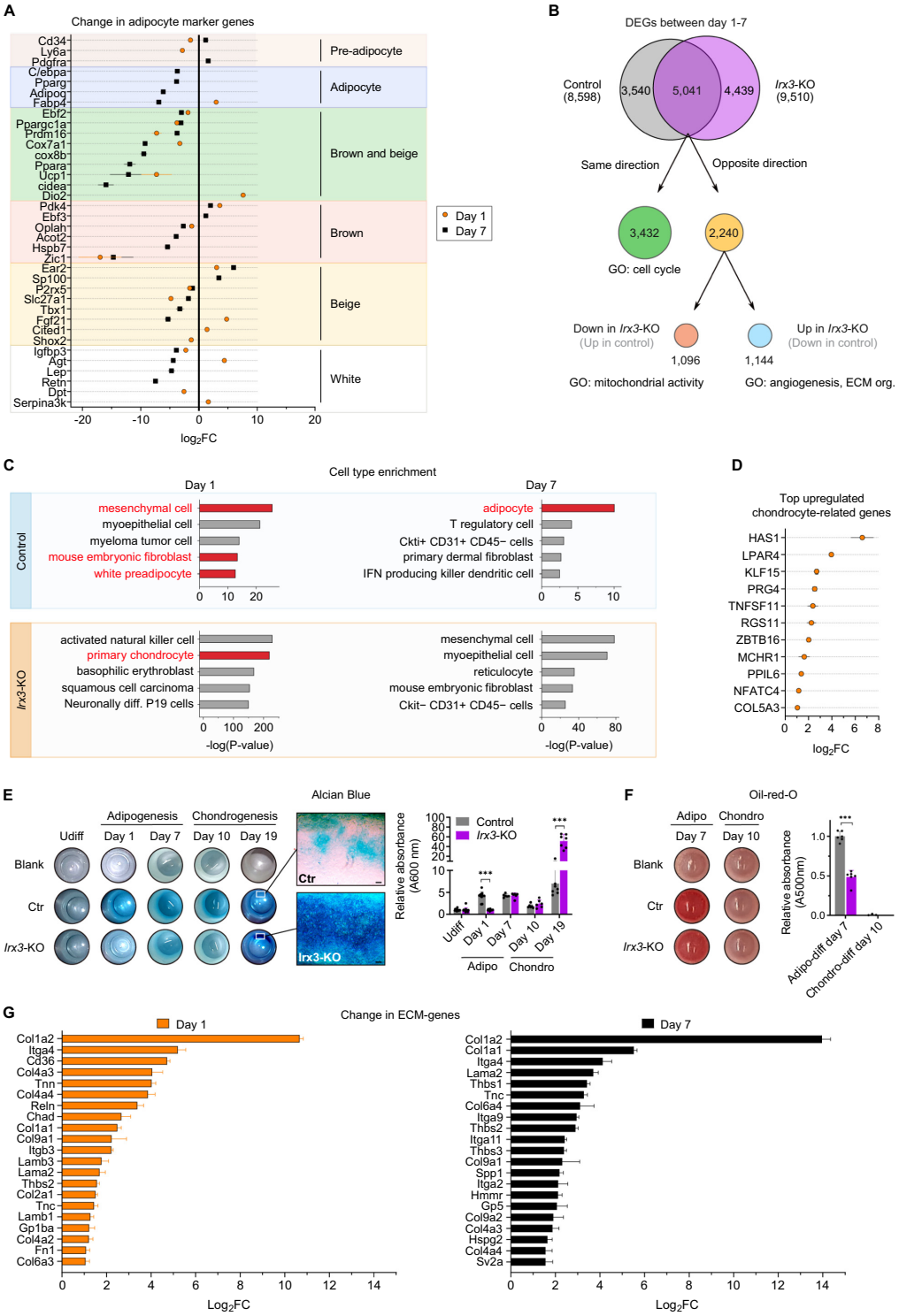
A
Change in adipocyte marker genes
Cd34
Ly6a
Pdgfra
C/ebpa
Pparg
Adipoq
Fabp4
Ebf2
Ppargc1a
Prdm16
Cox7a1
cox8b
Ppara
Ucp1
cidea
Dio2
Pdk4
Ebf3
Oplah
Acot2
Hspb7
Zic1
Ear2
Sp100
P2rx5
Slc27a1
Tbx1
Fgf21
Cited1
Shox2
Igfbp3
Agt
Lep
Retn
Dpt
Serpina3k
Pre-adipocyte
Adipocyte
Brown and beige
Brown
Beige
White
Day 1
Day 7
-20 -10 0 10 20
log2FC
B
DEGs between day 1-7
Control (8,598)
3,540
5,041
4,439
Irx3-KO (9,510)
Same direction
Opposite direction
3,432
2,240
GO: cell cycle
Down in Irx3-KO (Up in control)
Up in Irx3-KO (Down in control)
1,096
1,144
GO: mitochondrial activity
GO: angiogenesis, ECM org.
C
Cell type enrichment
Day 1
Day 7
Control
mesenchymal cell
myoepithelial cell
myeloma tumor cell
mouse embryonic fibroblast
white preadipocyte
adipocyte
T regulatory cell
Ckti+ CD31+ CD45− cells
primary dermal fibroblast
IFN producing killer dendritic cell
Irx3-KO
activated natural killer cell
primary chondrocyte
basophilic erythroblast
squamous cell carcinoma
Neuronally diff. P19 cells
mesenchymal cell
myoepithelial cell
reticulocyte
mouse embryonic fibroblast
Ckit− CD31+ CD45− cells
-log(P-value)
-log(P-value)
D
Top upregulated chondrocyte-related genes
HAS1
LPAR4
KLF15
PRG4
TNFSF11
RGS11
ZBTB16
MCHR1
PPIL6
NFATC4
COL5A3
log2FC
E
Alcian Blue
Adipogenesis
Chondrogenesis
Udiff
Day 1
Day 7
Day 10
Day 19
Blank
Ctr
Irx3-KO
Ctr
Irx3-KO
Relative absorbance (A600 nm)
Control
Irx3-KO
Udiff
Day 1
Day 7
Day 10
Day 19
Adipo
Chondro
F
Oil-red-O
Adipo
Chondro
Day 7
Day 10
Blank
Ctr
Irx3-KO
Relative absorbance (A500nm)
Adipo-diff day 7
Chondro-diff day 10
G
Change in ECM-genes
Day 1
Col1a2
Itga4
Cd36
Col4a3
Tnn
Col4a4
Reln
Chad
Col1a1
Col9a1
Itgb3
Lamb3
Lama2
Thbs2
Col2a1
Tnc
Lamb1
Gp1ba
Col4a2
Fn1
Col6a3
Log2FC
Day 7
Col1a2
Col1a1
Itga4
Lama2
Thbs1
Tnc
Col6a4
Itga9
Thbs2
Itga11
Thbs3
Col9a1
Spp1
Itga2
Hmmr
Gp5
Col9a2
Col4a3
Hspg2
Col4a4
Sv2a
Log2FC

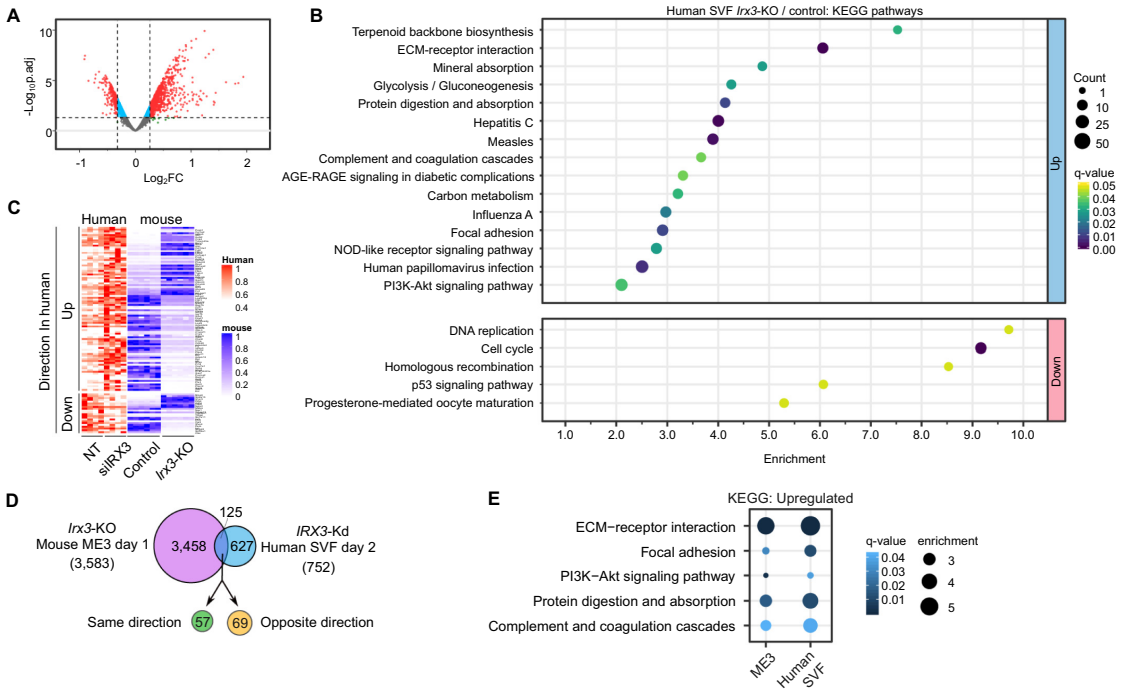

Fig. 4. Conserved roles of IRX3 in ME3 cells and human primary cells. (A) Volcano plot displaying changes in global gene expression following siRNA-mediated knockdown of *IRX3* in human primary SVF-derived preadipocytes on day 0–2 of differentiation. Log_2-fold change and adjusted *p*-value of individual genes shown. Red dots, FC > ±1.2 and adjusted p-value <0.1. Blue dots, FC < ±1.2 and adjusted *p*-value <0.1. Gray dots, not significant. (B) KEGG pathway analysis of DEGs after siIRX3 in human primary adipocytes. Dot size represents number of genes in each category and color indicates level of statistical significance. (C) Heatmap showing normalized expression levels of DEGs following *IRX3*-kd in human primary adipocytes day 2 compared to *Irx3*-KO in ME3 cells day 1. (D) Schematic Venn diagram of (C) showing the number of overlapping genes. (E) Overlapping KEGG pathways for upregulated genes in ME3 cells and human primary adipocytes after reduction of Irx3. Dot size represents enrichment and color indicates statistical significance. (For interpretation of the references to color in this figure legend, the reader is referred to the web version of this article.)

Reactive oxygen species (ROS) play important roles in regulating many preadipocyte processes, including proliferation and differentiation [38,39]. We therefore investigated the basal ROS levels in control and *Irx3*-KO cells, and found the KO-cells to produce significantly less ROS (Fig. 5B). Of note, overexpression of Irx3 in the KO cells completely restored ROS levels back to normal. Moreover, cell proliferation analysis by WST-1 revealed a strongly reduced proliferative ability in the *Irx3*-KO cells which could at least partially be rescued by overexpression of Irx3 (Fig. 5C). However, because the WST-1 assay relies on mitochondrial dehydrogenase activity, and the KO cells showed reduced mitochondrial activity in the Seahorse assays, we could not rule out the possibility that the observed differences in WST-1 formation may partially be due to altered mitochondrial activity rather than reduced proliferation. We therefore performed 2D-cell cycle analysis by flow cytometry to directly assess cell cycle progression in the control and *Irx3*-KO cells (Fig. 5D). Changes in DNA-content were quantified by Propidium Iodide (PI), whereas actively dividing S-phase cells were labelled with BrdU. BrdU incorporation was reduced by 45% in the *Irx3*-KO cells, with an accompanying 62% increase in cells retained in G_0 and G_1 phases (Fig. 5D). Moreover, the proportion of cells in $G_1{}^*$ phase was reduced by 49% in the KO cells. This population represents the cells that were in the S-phase during the 1-h BrdU pulse-labelling and that then, during the following 6 h progressed through the cell cycle to the G_1-phase. Taken together, these data demonstrate that lack of Irx3 in beige ME3 preadipocytes impairs fundamental functions including cell cycle and proliferation, respiration and ultimately differentiation.

Fig. 3. *Irx3*-KO cells lose adipocyte identity. (A) Log_2-fold changes in adipocyte markers in *Irx3*-KO cells compared to control on day 1 (orange) and day 7 (black). Data plotted as mean ± SD of $n = 6$ replicate wells. See also supplementary file 2. (B) Schematic illustrating overlap of DEGs over time (day 1 to 7) in control and *Irx3*-KO cells. Top panel, overlap between DEGs from day 1–7 of differentiation in control (gray) and *Irx3*-KO (purple) cells. Middle panel, overlapping DEGs stratified into genes changed in the same (green) or opposite (yellow) direction during differentiation. Bottom panel, overlapping DEGs with opposite direction in control/KO cells (yellow) further stratified according to direction in *Irx3*-KO cells during differentiation. Complete list of genes and GO terms shown in supplementary file 3. (C) Cell type enrichment analysis comparing the global gene expression on days 1 and 7 in control and *Irx3*-KO cells with gene signatures from 64 pure cell types, using the xCell software. The most significantly associated cell types are shown, with red bars indicating the most relevant hits. (D) Top upregulated genes in the xCell chondrocyte panel in *Irx3*-KO cells compared to controls on day 1. See supplementary file 2 for the entire panel. (E) Alcian Blue staining of proteoglycans and (F) Oil-red-O lipid staining following adipogenesis and chondrogenesis, $n = 6$–12 replicate wells. Left panels, image of one representative well shown. Middle panel, brightfield microscope image of cells after 19 days in chondrogenic medium. Scale bars = 100 μm. Right panel, quantification of all wells. *** $p < 0.001$, multiple t-test, with Holm-Sidak correction. (G) Log_2-fold changes of ECM-related genes in *Irx3*-KO compared to control cells. The genes comprised the KEGG pathway category ECM-receptor interaction, as described in Fig. 2 and Fig. S2. (For interpretation of the references to color in this figure legend, the reader is referred to the web version of this article.)

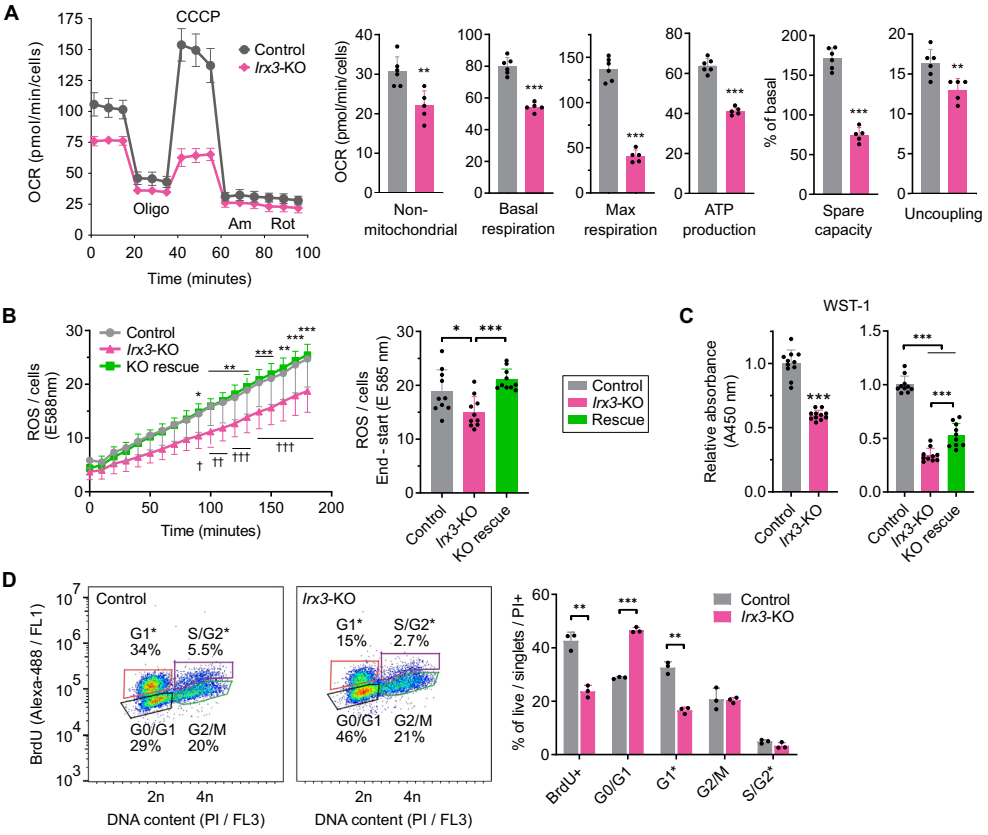

Fig. 5. Knock-out of Irx3 impairs proliferation and mitochondrial respiration in preadipocytes. (A) Real-time cellular oxygen consumption rate (OCR) measured by Seahorse mitochondrial stress tests. After establishing the basal respiration, inhibitors of mitochondrial respiration were added in the following order: Oligo, oligomycin, to block ATP synthase; CCCP, carbonyl cyanide m-chlorophenylhydrazone, to uncouple oxygen consumption from ATP production; Am, antimycin, to block complex III; Rot, rotenone, to block complex I. The effect of inhibitors enabled calculation of non-mitochondrial-, basal and max respiration, as well as spare capacity, ATP production and uncoupling, as shown with individual values and mean ± SD. ** $p < .01$, *** $p < .001$, Student's t-test. Representative of two independent experiments with $n = 6$ replicates, adjusted for cell number. (B) Real-time quantification of reactive oxygen species (ROS) in control and *Irx3*-KO cells transfected with empty plasmid, and *Irx3*-KO cells transfected with Irx3 plasmid (KO rescue). Data from one experiment with $n = 12$ replicates. Left panel, time course data shown with mean ± SD. * $p < 0.05$, ** $p < 0.01$, *** $p < 0.001$ comparing control to *Irx3*-KO. † $p < 0.05$, †† $p < 0.01$, ††† $p < 0.001$ comparing *Irx3*-KO to rescue. Two-way repeated measures Anova, with Holm-Sidak post hoc test. Right panel, delta end-start values with individual values and mean ± SD shown. * $p < 0.05$, *** $p < 0.001$, One-way Anova with Holm-Sidak post hoc test. (C) Quantification of proliferation by WST-1. Data representative of 4 independent experiments with $n = 12$ replicates. Individual values and mean ± SD shown. *** $p < .001$, Student's t-test or One-way Anova. (D) 2D cell cycle analysis. Actively dividing control and *Irx3*-KO cells were pulse-labeled with BrdU for 1 h and left to grow for 6 h in BrdU-free medium. Cells were fixed and stained with anti-BrdU conjugated to Alexa-488 (FITC) and counterstained with Propidium Iodide (PI). Representative of two independent experiments with $n = 3$ replicates. Left panel, representative bivariate contour plots of BrdU against DNA content (PI) on cell population pregated with FSC-A vs SSC-A to eliminate debris and FL3-A vs FL3-H to exclude doublets. Shown gates represent BrdU-negative cells in G_0/G_1 and G2/M phases, and BrdU-positive G_1* and S/G_2 phases. Right panel, gate summary statistics from three parallels, individual values and mean ± SD shown. ** $p < 0.01$, *** $p < 0.001$, multiple *t*-tests with Holm-Sidak correction.

4. Discussion

The present study shows that adipocyte precursor cells depend on Irx3 to maintain their identity and functions, most notably the ability to undergo adipogenic differentiation (Fig. 6). Complete and stable ablation of Irx3 in MEFs resulted in a loss of mesenchymal/preadipocyte gene signatures and a gain of chondrocyte-like and immune-cell related identities. Moreover, upregulated genes on day 7 in *Irx3*-KO cells were functionally enriched for pathways related to morphogenesis of a range of tissues whose development is known to be regulated by Irx3, including the heart [40–43], neurons [44] and blood vessels [45]. Additionally, we observed a clear enrichment and strong upregulation of collagen-encoding genes and other genes involved in ECM organization and focal adhesion. Consistently, these pathways were also upregulated in human primary SVF-derived cells treated with transient *Irx3* knockdown.

While Claussnitzer et al. reported effects on adipocyte white versus beige lineage determination during early mesenchymal differentiation, when the IRX-controlling enhancer in intron 1 of *FTO* is active [8], we show here that manipulating Irx3 in undifferentiated cells may greatly affect the adipocyte phenotype. Specifically, knocking out Irx3 profoundly inhibited mitochondrial respiration, reduced ROS formation and impaired proliferation, processes that all promote adipogenesis under appropriate cellular circumstances [46–48]. In agreement, mitochondrial gene expression and respiration remained low in *Irx3*-KO cells, even after treatment with differentiation-inducing stimuli (Fig. 2 and Fig. S3). Moreover, increase in ROS levels due to elevated mitochondrial activity has been shown to be required for adipocyte differentiation [38,39], where a delicate ROS balance is required for healthy adipocyte formation. We observed a significant reduction in ROS in *Irx3*-KO preadipocytes that could be completely rescued by

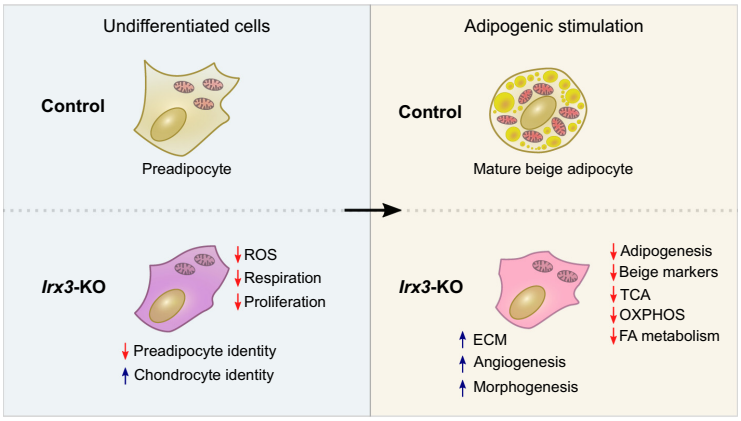

Fig. 6. Overall effect of Irx3 ablation in adipocyte precursor cells. In the undifferentiated state and first day of differentiation (left panel), *Irx3*-KO cells demonstrated profound changes in gene expression compared to controls, including downregulation of mesenchymal and preadipocyte markers and upregulation of genes promoting chondrocyte identity. Moreover, the *Irx3*-KO cells showed reduced ROS generation, impaired mitochondrial respiration and lower proliferation rates compared to control cells. After seven days of adipogenic stimulation (right panel), the control cells developed into mature beige adipocytes (top), whereas the *Irx3*-KO cells (bottom) completely blocked adipogenic differentiation and instead upregulated genes controlling morphogenesis towards other cells and tissues.

overexpression of Irx3, likely contributing to the inability of the KO cells to differentiate. Interestingly, *Ucp2*, which is known to limit ROS production (reviewed in [49]), was upregulated at day 1 in *Irx3*-KO cells, likely exacerbating the ROS deficiency.

The proliferation and differentiation of adipocytes are tightly linked processes [50]. We observed a clear reduction in proliferation rate and cell cycle progression in *Irx3*-KO preadipocytes. Moreover, although we observed no clear effect of Irx3 on mitotic clonal expansion in mouse cells, cell-cycle genes were highly enriched among DEGs in the human primary cells after siRNA knockdown of IRX3. Indeed, Irx family members have been reported to regulate cell cycle progression in other tissues and organisms [51–53]. Here we noted that one of the most consistently downregulated genes in *Irx3*-KO cells was *Appl2*, an essential gene for cell proliferation which interacts with the nucleosome remodeling and histone deacetylase complex NuRD/MeCP1 [54]. Moreover, *Nudt5*, was also found to be downregulated in the KO cells. This gene is utilized in breast cancer cells to produce energy in the nucleus to drive chromatin remodeling and gene expression, and inhibition of Nudt5 was shown to impair proliferation [55]. Taken together, these data indicate that Irx3 may impair proliferation and differentiation partially via processes involving chromatin remodeling.

Irx3 deficiency likely inhibits proliferation and differentiation via multiple pathways. For example, *Nmnat2* was found to be downregulated on day 1 in the *Irx3*-KO cells, and loss of this gene has previously been shown to inhibit adipogenesis through compartmentalized NAD^+ synthesis [56]. Moreover, *Gas1*, which was upregulated in response to Irx3 depletion in both the mouse and human dataset, is a cell cycle inhibitor, known to block entry into S-phase. Thus, derepression of Gas1 by Irx3 ablation may contribute to the observed G_1-phase retention and reduced S-phase progression observed in *Irx3*-KO cells (Fig. 5D). Furthermore, Gas1 is a coreceptor for Sonic Hedgehog (SHH) signaling [57], a pathway well known to suppress adipogenesis and promote osteogenesis [58,59], which could partially explain the observed loss of adipocyte identity in *Irx3*-KO cells with increased Gas1 expression/SHH signaling. Indeed, *Gli1*, a well-known marker of SHH pathway activation [60] was upregulated in *Irx3*-KO cells compared to control and also increased during differentiation.

Our observation that Irx3-deficient adipocyte precursor cells are unable to differentiate per se reconcile with *Irx3*-KO and adipo-Irx3DN mice having a reduced body weight and total fat mass, as reported by Smemo et al. and Claussnitzer et al., respectively [8,14]. However, whereas Irx3 ablation in those studies promoted adipocyte beiging at the expense of white adipogenesis, we found *Irx3*-KO to inhibit beige adipogenesis as well. This discrepancy can be explained at least in the case of adipo-Irx3DN mice, where the transgenic expression of mutant Irx3 was driven by *Fabp4* which is expressed primarily in mature adipocytes. Therefore, loss of functional Irx3 in these mice may have occurred primarily late in differentiation, thus leading to a transdifferentiation from white to beige cells in already differentiated adipocytes.

Interestingly, in contrast to the results by Smemo et al. and Claussnitzer et al., but in line with our report, lentiviral-mediated reduction of Irx3 in mouse SVF-derived beige cells reduced both lipid accumulation and inhibited expression of beige markers including *Ucp1*, *Pgc-1α* and *Cidea*, although apparently without affecting general adipocyte markers such as *Fabp4* or *Pparg* [21]. Thus, Irx3 may regulate lipid metabolism and whole body energy homeostasis through a yet undiscovered mechanism, in addition to its demonstrated control over thermogenesis and adipogenesis. Considering the conflicting effects on beiging reported for hypothalamic disruption of Irx3 [14,20], it becomes clear that differences in spatial, temporal and perhaps methodological repression of Irx3 function may all affect the outcome on adipocyte fate.

5. Conclusion

Complete loss of Irx3 in beiging-competent MEFs lead to reduced cell cycle progression, impaired mitochondrial respiration, loss of mesenchymal-like cell identity and an inability to undergo adipogenic differentiation. Therefore, the developmental stage, target cells and means of manipulation should be carefully considered when interpreting the role for Irx3 in adipose tissue, including effects on adipocyte beiging.

6. Limitations

Most of the data presented in this study were generated from mouse cell line experiments, and the CRISPR-Cas9 system introduced constitutive KO of *Irx3*.

Supplementary data to this article can be found online at https://doi.org/10.1016/j.metabol.2019.154014.

Acknowledgements

We thank the engineers at the Hormone Laboratory, particularly Carol Cook, Margit Solsvik, Alba Kaci and Maren Hoff Austgulen for their excellent technical assistance. We also thank Ole Petter Nordbø and Karen Toska for their valuable contributions in generating and sequencing CRISPR-Cas9 clones. Finally, we thank Rita Holdhus and Tomasz Stokowy at the Genomics Core Facility and Brith Bergum at the Flow Cytometry Core Facility, Department of Clinical Science, University of Bergen.

Author contributions

JIB, SND, PRN, JVS and GM conceived the study. JIB and SND designed the experiments. JIB performed the experiments, analyzed and graphed most data and wrote the manuscript. LD performed the bioinformatics analyses. GVR performed the ICC-assays and provided, together with KJT, invaluable help in establishing the Seahorse assay. All authors contributed to data interpretation and revision of the manuscript.

Funding

This work is supported by *Persontilpasset medisin for barn og voksne med diabetes mellitus* (PERSON-MED-DIA), the Western Norway Regional Health Authority, Meltzerfondet, University of Bergen and Trond Mohn Foundation. PRN was supported by the European Research Council (AdG #293574). The Genomics Core Facility (GCF) at the University of Bergen, which is a part of the NorSeq consortium, provided services on RNA-seq and microarray analyses; GCF is supported in part by major grants from the Research Council of Norway (grant no. 245979/F50) and Trond Mohn Stiftelse (grant no. BFS2016-genom).

Disclosures

The authors have nothing to disclose.

References

[1] Maes HHM, Neale MC, Eaves LJ. Genetic and environmental factors in relative body weight and human adiposity. Behav Genet 1997;27:325–51. https://doi.org/10.1023/A:1025635913927.
[2] Zaitlen N, Kraft P, Patterson N, Pasaniuc B, Bhatia G, Pollack S, et al. Using extended genealogy to estimate components of heritability for 23 quantitative and dichotomous traits. PLoS Genet 2013;9. https://doi.org/10.1371/journal.pgen.1003520.
[3] Allison DB, Kaprio J, Korkeila M, Koskenvuo M, Neale MC, Hayakawa K. The heritability of body mass index among an international sample of monozygotic twins reared apart. Int J Obes Relat Metab Disord 1996;20:501–6.
[4] Katzmarzyk PT, Janssen I, Ardern CI. Physical inactivity, excess adiposity and premature mortality. Obes Rev 2003;4:257–90. https://doi.org/10.1046/j.1467-789X.2003.00120.x.
[5] Adams KF, Schatzkin A, Harris TB, Kipnis V, Mouw T, Ballard-Barbash R, et al. Overweight, obesity, and mortality in a large prospective cohort of persons 50 to 71 years old. N Engl J Med 2006;355:763–78. https://doi.org/10.1056/NEJMoa055643.
[6] Global BMI Mortality Collaboration. Body-mass index and all-cause mortality: individual-participant-data meta-analysis of 239 prospective studies in four continents. Lancet 2016;388:776–86. https://doi.org/10.1016/S0140-6736(16)30175-1.
[7] Barroso I, McCarthy MI. The genetic basis of metabolic disease. Cell 2019;177:146–61. https://doi.org/10.1016/j.cell.2019.02.024.
[8] Claussnitzer M, Dankel SN, Kim K-H, Quon G, Meuleman W, Haugen C, et al. *FTO* obesity variant circuitry and adipocyte browning in humans. N Engl J Med 2015;373:895–907. https://doi.org/10.1056/NEJMoa1502214.
[9] Speliotes EK, Willer CJ, Berndt SI, Monda KL, Thorleifsson G, Jackson AU, et al. Association analyses of 249,796 individuals reveal 18 new loci associated with body mass index. Nat Genet 2010;42:937–48. https://doi.org/10.1038/ng.686.
[10] Tung YCL, Yeo GSH, O'Rahilly S, Coll AP. Obesity and FTO: changing focus at a complex locus. Cell Metab 2014;20:710–8. https://doi.org/10.1016/j.cmet.2014.09.010.
[11] Frayling TM, Timpson NJ, Weedon MN, Zeggini E, Freathy RM, Lindgren CM, et al. A common variant in the FTO gene is associated with body mass index and predisposes to childhood and adult obesity. Science 2007;316:889–94. https://doi.org/10.1126/science.1141634 (80-).
[12] Loos RJF, Yeo GSH. The bigger picture of FTO - the first GWAS-identified obesity gene. Nat Rev Endocrinol 2014;10:51–61. https://doi.org/10.1038/nrendo2013227.
[13] Ragvin A, Moro E, Fredman D, Navratilova P, Drivenes O, Engstrom PG, et al. Long-range gene regulation links genomic type 2 diabetes and obesity risk regions to HHEX, SOX4, and IRX3. Proc Natl Acad Sci 2010;107:775–80. https://doi.org/10.1073/pnas.0911591107.
[14] Smemo S, Tena JJ, Kim K-H, Gamazon ER, Sakabe NJ, Gómez-Marín C, et al. Obesity-associated variants within FTO form long-range functional connections with IRX3. Nature 2014;507:371–5. https://doi.org/10.1038/nature13138.
[15] Cypess AM, Lehman S, Williams G, Tal I, Rodman D, Goldfine AB, et al. Identification and importance of brown adipose tissue in adult humans. N Engl J Med 2009;360:1509–17. https://doi.org/10.1056/NEJMoa0810780.
[16] van Marken Lichtenbelt WD, Vanhommerig JW, Smulders NM, Drossaerts JMAFL, Kemerink GJ, Bouvy ND, et al. Cold-activated brown adipose tissue in healthy men. N Engl J Med 2009;360:1500–8. https://doi.org/10.1056/NEJMoa0808718.
[17] Virtanen KA, Lidell ME, Orava J, Heglind M, Westergren R, Niemi T, et al. Functional brown adipose tissue in healthy adults. N Engl J Med 2009;360:1518–25. https://doi.org/10.1056/NEJMoa0808949.
[18] Hanssen MJ, Hoeks J, Brans B, van der Lans AA, Schaart G, van den Driessche JJ, et al. Short-term cold acclimation improves insulin sensitivity in patients with type 2 diabetes mellitus. Nat Med 2015;21:863–5. https://doi.org/10.1038/nm.3891.
[19] Bjune JI, Haugen C, Gudbrandsen O, Nordbø OP, Nielsen HJ, Våge V, et al. IRX5 regulates adipocyte amyloid precursor protein and mitochondrial respiration in obesity. Int J Obes (Lond) 2018:1–12. https://doi.org/10.1038/s41366-018-0275-y.
[20] de Araujo TM, Razolli DS, Correa-da-Silva F, de Lima-Junior JC, Gaspar RS, Sidarta-Oliveira D, et al. The partial inhibition of hypothalamic IRX3 exacerbates obesity. EBioMedicine 2019;39. https://doi.org/10.1016/j.ebiom.2018.11.048 448–160.
[21] Zou Y, Lu P, Shi J, Liu W, Yang M, Zhao S, et al. IRX3 promotes the browning of white adipocytes and its rare variants are associated with human obesity risk. EBioMedicine 2017;24:64–75. https://doi.org/10.1016/j.ebiom.2017.09.010.
[22] Inagaki T. Regulations of adipocyte phenotype and obesity by IRX3. Positive or negative? EBioMedicine 2017;24:7–8. https://doi.org/10.1016/j.ebiom.2017.09.032.
[23] Lukas J, Bartkova J, Rohde M, Strauss M, Bartek J. Cyclin D1 is dispensable for G1 control in retinoblastoma gene-deficient cells independently of cdk4 activity. Mol Cell Biol 1995;15:2600–11. https://doi.org/10.1128/MCB.15.5.2600.
[24] Hansen JB, Jørgensen C, Petersen RK, Hallenborg P, De Matteis R, Bøye HA, et al. Retinoblastoma protein functions as a molecular switch determining white versus brown adipocyte differentiation. Proc Natl Acad Sci U S A 2004;101:4112–7. https://doi.org/10.1073/pnas.0301964101.
[25] Hakim-Weber R, Krogsdam A-M, Jørgensen C, Fischer M, Prokesch A, Bogner-Strauss JG, et al. Transcriptional regulatory program in wild-type and retinoblastoma gene-deficient mouse embryonic fibroblasts during adipocyte differentiation. BMC Res Notes 2011;4:157. https://doi.org/10.1186/1756-0500-4-157.
[26] Lonowski LA, Narimatsu Y, Riaz A, Delay CE, Yang Z, Niola F, et al. Genome editing using FACS enrichment of nuclease-expressing cells and indel detection by amplicon analysis. Nat Protoc 2017;12:581–603.
[27] Veum VL, Dankel SN, Gjerde J, Nielsen HJ, Solsvik MH, Haugen C, et al. The nuclear receptors NUR77, NURR1 and NOR1 in obesity and during fat loss. Int J Obes (Lond) 2012;36:1195–202. https://doi.org/10.1038/ijo.2011.240.
[28] Conesa A, Nueda MJ. maSigPro: significant gene expression profile differences in time course gene expression data. R Packag Version 2018:1520.
[29] Aran D, Hu Z, Butte AJ. xCell: digitally portraying the tissue cellular heterogeneity landscape. Genome Biol 2017;18:220. https://doi.org/10.1186/s13059-017-1349-1.
[30] R Development Core Team. R: a language and environment for statistical computing. R Found Stat Comput 2016. https://doi.org/10.1017/CBO9781107415324.004.
[31] Wu J, Boström P, Sparks LM, Ye L, Choi JH, Giang AH, et al. Beige adipocytes are a distinct type of thermogenic fat cell in mouse and human. Cell 2012;150:366–76. https://doi.org/10.1016/j.cell.2012.05.016.
[32] Qiu Y, Nguyen KD, Odegaard JI, Cui X, Tian X, Locksley RM, et al. Eosinophils and type 2 cytokine signaling in macrophages orchestrate development of functional beige fat. Cell 2014;157:1292–308. https://doi.org/10.1016/j.cell.2014.03.066.
[33] Cao Z, Umek RM, McKnight SL. Regulated expression of three C/EBP isoforms during adipose conversion of 3T3-L1 cells. Genes Dev 1991. https://doi.org/10.1101/gad.5.9.1538.
[34] Wang W, Seale P. Control of brown and beige fat development. Nat Rev Mol Cell Biol 2016;17:691–702. https://doi.org/10.1038/nrm.2016.96.
[35] Garcia RA, Roemmich JN, Claycombe KJ. Evaluation of markers of beige adipocytes in white adipose tissue of the mouse. Nutr Metab (Lond) 2016;13(24). https://doi.org/10.1186/s12986-016-0081-2.
[36] Siersbaek MS, Loft A, Aagaard MM, Nielsen R, Schmidt SF, Petrovic N, et al. Genome-wide profiling of peroxisome proliferator-activated receptor in primary epididymal, inguinal, and brown adipocytes reveals depot-selective binding correlated with gene expression. Mol Cell Biol 2012;32:3452–63. https://doi.org/10.1128/MCB.00526-12.
[37] Jay GD, Waller KA. The biology of lubricin: near frictionless joint motion. Matrix Biol 2014. https://doi.org/10.1016/j.matbio.2014.08.008.
[38] Tormos KV, Anso E, Hamanaka RB, Eisenbart J, Joseph J, Kalyanaraman B, et al. Mitochondrial complex III ROS regulate adipocyte differentiation. Cell Metab 2011;14:537–44. https://doi.org/10.1016/j.cmet.2011.08.007.
[39] Castro JP, Grune T, Speckmann B. The two faces of reactive oxygen species (ROS) in adipocyte function and dysfunction. Biol Chem 2016;397:709–24. https://doi.org/10.1515/hsz-2015-0305.
[40] Koizumi A, Sasano T, Kimura W, Miyamoto Y, Aiba T, Ishikawa T, et al. Genetic defects in a His-Purkinje system transcription factor, IRX3, cause lethal cardiac arrhythmias. Eur Heart J 2016;37:1469–75. https://doi.org/10.1093/eurheartj/ehv449.
[41] Christoffels VM, Keijser AG, Houweling AC, Clout DE, Moorman AF. Patterning the embryonic heart: identification of five mouse Iroquois homeobox genes in the developing heart. Dev Biol 2000;224:263–74. https://doi.org/10.1006/dbio.2000.9801.
[42] Zhang S-S, Kim K-H, Rosen A, Smyth JW, Sakuma R, Delgado-Olguin P, et al. Iroquois homeobox gene 3 establishes fast conduction in the cardiac His-Purkinje network. Proc Natl Acad Sci 2011;108:13576–81. https://doi.org/10.1073/pnas.1106911108.

[43] Kim KH, Rosen A, Hussein SMI, Puviindran V, Korogyi AS, Chiarello C, et al. Irx3 is required for postnatal maturation of the mouse ventricular conduction system. Sci Rep 2016;6:19197. https://doi.org/10.1038/srep19197.
[44] Bellefroid EJ, Kobbe A, Gruss P, Pieler T, Gurdon JB, Papalopulu N. Xiro3 encodes a xenopus homolog of the Drosophila Iroquois genes and functions in neural specification. EMBO J 1998;17:191–203. https://doi.org/10.1093/emboj/17.1.191.
[45] Scarlett K, Pattabiraman V, Barnett P, Liu D, Anderson LM. The proangiogenic effect of iroquois homeobox transcription factor Irx3 in human microvascular endothelial cells. J Biol Chem 2015;290:6303–15. https://doi.org/10.1074/jbc.M114.601146.
[46] Zhang Y, Marsboom G, Toth PT, Rehman J. Mitochondrial respiration regulates adipogenic differentiation of human mesenchymal stem cells. PLoS One 2013;8:e77077. https://doi.org/10.1371/journal.pone.0077077.
[47] Shi X, Burkart A, Nicoloro SM, Czech MP, Straubhaar J, Corvera S. Paradoxical effect of mitochondrial respiratory chain impairment on insulin signaling and glucose transport in adipose cells. J Biol Chem 2008;283:30658–67. https://doi.org/10.1074/jbc.M800510200.
[48] Green CR, Wallace M, Divakaruni AS, Phillips SA, Murphy AN, Ciaraldi TP, et al. Branched-chain amino acid catabolism fuels adipocyte differentiation and lipogenesis. Nat Chem Biol 2015;12:15–21. https://doi.org/10.1038/nchembio.1961.
[49] De Pauw A, Tejerina S, Raes M, Keijer J, Arnould T. Mitochondrial (dys)function in adipocyte (de)differentiation and systemic metabolic alterations. Am J Pathol 2009;175:927–39. https://doi.org/10.2353/ajpath.2009.081155.
[50] Hausman DB, DiGirolamo M, Bartness TJ, Hausman GJ, Martin RJ. The biology of white adipocyte proliferation. Obes Rev 2001;2:239–54. https://doi.org/10.1046/j.1467-789X.2001.00042.x.
[51] Myrthue A, Rademacher BLS, Pittsenbarger J, Kutyba-Brooks B, Gantner M, Qian DZ, et al. The iroquois homeobox gene 5 is regulated by 1,25-dihydroxyvitamin D3 in human prostate cancer and regulates apoptosis and the cell cycle in LNCaP prostate cancer cells. Clin Cancer Res 2008;14:3562–70. https://doi.org/10.1158/1078-0432.CCR-07-4649.
[52] Liu D, Pattabiraman V, Bacanamwo M, Anderson LM. Iroquois homeobox transcription factor (*Irx5*) promotes G_1/S-phase transition in vascular smooth muscle cells by CDK2-dependent activation. Am J Physiol - Cell Physiol 2016;311:C179–89. https://doi.org/10.1152/ajpcell.00293.2015.
[53] Barrios N, Campuzano S. Expanding the Iroquois genes repertoire: a non-transcriptional function in cell cycle progression. Fly (Austin) 2015;9:126–31. https://doi.org/10.1080/19336934.2016.1139654.
[54] Miaczynska M, Christoforidis S, Giner A, Shevchenko A, Uttenweiler-Joseph S, Habermann B, et al. APPL proteins link Rab5 to nuclear signal transduction via an endosomal compartment. Cell 2004;116:445–56. https://doi.org/10.1016/S0092-8674(04)00117-5.
[55] Page BDG, Valerie NCK, Wright RHG, Wallner O, Isaksson R, Carter M, et al. Targeted NUDT5 inhibitors block hormone signaling in breast cancer cells. Nat Commun 2018;9:250. https://doi.org/10.1038/s41467-017-02293-7.
[56] Ryu KW, Nandu T, Kim J, Challa S, DeBerardinis RJ, Lee Kraus W. Metabolic regulation of transcription through compartmentalized NAD + biosynthesis. Science 2018;360. https://doi.org/10.1126/science.aan5780 (80-).
[57] Lee HJ, Jo SB, Romer AI, Lim HJ, Kim MJ, Koo SH, et al. Overweight in mice and enhanced adipogenesis in vitro are associated with lack of the hedgehog coreceptor BOC. Diabetes 2015;64:2092–103. https://doi.org/10.2337/db14-1017.
[58] James AW, Leucht P, Levi B, Carre AL, Xu Y, Helms JA, et al. Sonic hedgehog influences the balance of osteogenesis and adipogenesis in mouse adipose-derived stromal cells. Tissue Eng Part A 2010;16:2605–16. https://doi.org/10.1089/ten.tea.2010.0048.
[59] Suh JM, Gao X, McKay J, McKay R, Salo Z, Graff JM. Hedgehog signaling plays a conserved role in inhibiting fat formation. Cell Metab 2006;3:25–34. https://doi.org/10.1016/j.cmet.2005.11.012.
[60] Cousin W, Fontaine C, Dani C, Peraldi P. Hedgehog and adipogenesis: fat and fiction. Biochimie 2007. https://doi.org/10.1016/j.biochi.2007.08.012.

Errata

Page 5 Misspelling: “Nordby” – corrected to “Nordbø”

Page 9 Ectopic word: “followed by of RNA” – corrected to “followed by RNA”

Page 23 Missing character: “48” – corrected to “≥ 48”

Page 26 Misspelling: “account” – corrected to “accounts”

Page 30 Misspelling: “for” – corrected to “of”

Page 41 Misspelling: “follow up-study” – corrected to “follow-up study”

Page 41 Missing word: “specific binding” – corrected to “specific abolished binding”

Page 42 Switched words: “shift from white to beige adipogenesis” – corrected to “shift from beige to white adipogenesis”

Page 45 Missing word: “by opposite findings other studies” – corrected to “by opposite findings in other studies”

Page 54 Missing word: “most often TF” – corrected to “most often a TF”

Page 54 Misspelling: “reveals whether the IRX proteins transcriptionally regulates the given promoter or not.“ – corrected to “reveal whether the IRX proteins transcriptionally regulate the given promoter or not.”

Page 56 Misspelling: “adipocyte” – corrected to “adipocytes”

Page 57 Switched word: “downregulated with *Irx5*-KO” – corrected to “upregulated with *Irx5*-KO”

Page 63 Missing words: “adipocyte-specific *Irx3*-DN mice actually” – corrected to “adipocyte-specific *Irx3*-DN mice reported by Claussnitzer et al. actually

Graphic design: Communication Division, UiB / Print: Skipnes Kommunikasjon AS

uib.no

ISBN: 9788230866986 (print)
9788230848630 (PDF)